UNIVERSITY OF CALIFORNIA SANTA CRUZ

The duration of mitosis and daughter cell size are modulated by nutrients in budding yeast

A dissertation submitted in partial satisfaction
of the requirements for the degree of

DOCTOR OF PHILOSOPHY

In

MOLECULAR, CELL AND DEVELOPMENTAL BIOLOGY

by

Ricardo Leitao

March 2016

The Dissertation of Ricardo Leitão
is approved:

_____

Professor Douglas Kellogg, chair

_____

Professor Susan Strome

_____

Professor Bill Sullivan

_____

Tyrus Miller
Vice Provost and Dean of Graduate Studies

TABLE OF CONTENTS

LIST OF FIGURES

LIST OF TABLES

THE DURATION OF MITOSIS AND DAUGHTER CELL SIZE ARE MODULATED BY NUTRIENTS IN BUDDING YEAST

RICARDO LEITÃO

ABSTRACT

It is virtually impossible to think of cell division without thinking of cellular growth. If cells would divide without growing an adult organism would be as big as the cells that it originated from. Growth must, therefore, be coupled with cellular division with a precision so great that all cells of a given tissue maintain, as we know, remarkably little variation in size.

Maintaining cell size homeostasis is critical for life. Not only is cellular hypertrophy known as an adaptive mechanism in response to metabolic demand, loss of size control is also commonly associated with malignancy.

Coordination of cell size and division is achieved via cell size checkpoints which ensure that a cell has grown enough before it progresses through the cell cycle. Cell size checkpoints are best known in yeast where a sole checkpoint is believed to regulate cell size. Such checkpoint has been described to occur at the G1/S transition. In this thesis I revisit old concepts at the light of new techniques and present results that support the hypothesis that significant cell size regulation occurs during mitosis. In addition I will provide evidence that suggest that mitotic cell size regulation is achieved through coordination of the phosphatase $PP2A^{Rts1}$ and the kinase Gin4. Cooperatively they control Swe1 activity in response to nutrients, allowing for nutrient modulation of cell size.

DEDICATION AND ACKNOWLEDGMENTS

I dedicate this dissertation to my partner, Barry Fitzgerald, a key support throughout my Ph.D. Barry gave me the time needed to complete this arduous task, cooking numerous meals when fatigue was the dominating feeling. Barry has also been my morning barista, and my evening bartender. In these past 6 years Barry has prepared over 4000 morning cappuccinos, ensuring I am functional at work, and always welcomed me home with an evening *aperitif*. In the midst of it all I managed to teach him science. In addition to his extensive knowledge he now "phosphorylates" every so often.

This dissertation would not be possible without the contribution of many others. First, I would like to thank my advisor, Douglas Kellogg, for welcoming me to his lab and providing unlimited support throughout my Ph.D. Your constant availability and positive attitude were key for completion of this work. In addition, I would like to thank all members of the Kellogg lab. Your help with experiments and engaging scientific discussion have been important for my work and education. But, most of all, the atmosphere you all created in the Kellogg lab managed to dissipate any hardship at work. Days went by quickly and it was always fun to come back.

I would like to specially thank Bob Sommer, a great friend and colleague. Bob has also been my gym buddy in the last few years at UCSC. I am not sure if a visit to the gym was work or a workout as we always spent as much time discussing science as we did exercising. Regardless, it was always fun! I love that you did never complain about my constant visits to your bay and were always free to interpret results and discuss science. Finally, thank you for proofreading this dissertation in such a short notice. And, by the way, "you made the best coffee!"

A great thank you to Ben Abrams, Facilities Manager for the UCSC Life Sciences Microscopy Center for support and mentoring with all microscopy related techniques, and the Aldea lab for sharing BudJ: an ImageJ plugin to analyze images of budding yeast cells (http://www.ibmb.csic.es/home/maldea). In addition I thank Andreas Rechtsteiner for helping me through my quest to learn "R". Without him I would not have been able to solve major programming hurdles.

Finally I thank the "Fundação para a Ciência e a Tecnologia" (FCT) for their financial contribution. Without an FCT fellowship I would not be here today. This fellowship (SFRH/BD/75004/2010) was funded by the "Programa Operacional Potencial Humano/ Fundo Social Europeu" (POPH/FSE). In addition, this work was supported by National Institutes of Health Grant R01-GM053959.

The text of this dissertation includes excerpts from the following previously published material: *Leitao, R. M., Pham, A., & Kellogg, D. R. (2016, October 12). The duration of mitosis and daughter cell size are modulated by nutrients in budding yeast. http://doi.org/10.1101/080648.* Doug Kellogg, a co-author listed in this publication, directed and supervised the research which forms the basis for this dissertation. Annie Pham, participated in the characterization of *rts1-AID* and *swe1Δ* mutants. She contributed to figure 2.8 and the supplemental figure S2.3.

INTRODUCTION

This body of work explores a fundamental question in cell biology: what are the mechanisms by which cell size regulation and homeostasis occurs?

The quest to understand cell size control started nearly a century ago (Bayne-Jones & Adolph, 1932; Haldane, 1926; Hartmann, 1926). It wasn't, however, until the late 70s when yeast biologists made striking advances in the quest to understand cell size (Fantes & Nurse, 1977; Hartwell & Unger, 1977; Johnston, Pringle, & Hartwell, 1977; Young & Fantes, 1987). Their discoveries have empowered the field with great insights, yet today cell size regulation is an unanswered aspect of cell biology and one of fundamental importance. Cell size regulation is not only key for development but its failure is associated with an array of diseases.

Whether and how cells regulate cell size have puzzled scientists for decades, as technical challenges have hampered the attainment of solid answers. First, measuring individual living cells is difficult. Second, understanding how growth correlates with cell cycle progression was simply not possible, with most conclusions extrapolated from complex correlations. With the discovery of fluorescent proteins and the development of high resolution microscopy a new world of possibilities have emerged. Here we revisit old questions pertinent to cell size control and explore them using modern techniques to test how they stand through time.

This thesis is divided into three chapters. In *Chapter I*, I conduct a brief overview on cell size regulation and the physiological consequences of cell size changes. In *Chapter II*, I present newly published data where we summarize key experiments and findings regarding cell size control. The data presented is disruptive as it describes a new mechanism for cell size control. In *Chapter III*, I lay

down additional unpublished-experiments that in some way support or add to the findings described in *Chapter II*.

CHAPTER I:
OVERVIEW

"The back of the human eye… is composed of a mosaic of "rods and cones" whose diameter is little more than a length of an average light wave. Each eye has about a half a million, and for two objects to be distinguishable their images must fall on separate rods or cones. It is obvious that with fewer but larger rods and cones we should see less distinctly. If they were twice as broad two points would have to be twice as far apart before we could distinguish them at a given distance. But if their size were diminished and their number increased we should see no better. For it is impossible to form a definite image smaller than a wave-length of light. Hence a mouse's eye is not a small-scale model of a human eye. Its rods and cones are not much smaller than ours, and therefore there are far fewer of them. A mouse could not distinguish one human face from another six feet away. In order that they should be of any use at all the eyes of small animals have to be much larger in proportion to their bodies than our own."

(Haldane, 1926)

Early evidence of cell size control

The question of size regulation is one that have puzzled biologists for decades. Do cells control their size or is size the result of physical constraints? What are the contributions of cell size to organ size and physiology? These and other questions have been central to this conundrum. Although I can not fully answer these questions I will discuss them and other subjects in the pages to come.

Early biologists observed an intriguing phenomena: organs orthotopically transplanted between animals of different sizes accommodate to match the size of the recipient's body. While livers transplanted to dogs of equal size retained their size post-transplantation, those transplanted to a dog of a larger size rapidly resumed growth and grew to the size characteristic of a liver of a bigger dog (Francavilla et al., 1988; Kam et al., 1987). This feature is unlikely to be specific to the liver. Although baby rat kidneys transplanted to adult rats grew with similar dynamics characteristic of baby rats, they ultimately reached the size of an adult kidney (Silber, 1976). These findings have multiple implications. For one, they suggest that the size of an organ is controlled externally by the environment so that it grows to match the demands of the body into which it was transplanted. On the other hand, the observations that organs adjust to the body of an older recipient's just as they do in the young donor, reveals the possibility that growth is controlled autonomously by intrinsic factors while responding to extrinsic stimuli. The mechanisms that underlie the adaptive response of an organ's size are unknown but they must require alterations in cell proliferation, cell death and/or cell size. A change to either of these parameters would culminate in the change of an organ's size.

The notion that organ size is determined by a balance between proliferation and cell size isn't new. Early studies have demonstrated that pentaploid

salamanders maintain the same body and organ size as haploid salamanders (Fankhauser, 1945) despite the fact that higher ploidy leads to increased cell size (Mortimer, 1958). For example, the diameter of pronephric tubules and the size of the epithelium of an eye-lens remains unchanged despite an increase of cell size as ploidy increases. In some instances the pronephric tubules, normally surrounded by multiple cells, are enveloped by a single cell that wraps around the entire tubular structure. These studies have demonstrated that alterations in cell number and shape can compensate for cell size changes, while fully maintaining organ structure. The existence of compensatory mechanisms that ensure a fixed organ/body size also reinforces the idea that homeostatic organ size must be critical for its physiology. An alternative interpretation derived from these observations is that changes in cell size and shape do not affect an organ's anatomical and physiological properties. While these data favors the control or organ size as opposed to cell size, other studies contradict such ideas.

While cell size has little impact on the shape of a salamander's pronephric tubules, salamanders with smaller sized cells have increased brain complexity (Roth, Blanke, & Wake, 1994). In addition, between salamanders of equally sized cells, those who possess bigger brains have a more complex tacta (Roth et al., 1994). It is plausible, therefore, that the size of a cell has organ-specific consequences. This observation adds to the complexity obscuring a complete understanding of the importance of changes in cell size. Furthermore, these studies also fail to address how an increase in cell size affects organ physiology — what are the consequences of a less complex tacta for the life of a salamander? In the next section I will convey evidence that support the effects of cell size on organ size and physiology.

The advantages and consequences of cell size changes

The histological observation of stained tissues highlights a striking evidence: the cells that constitute them are greatly uniform. In addition, loss of such uniformity has early been identified as a sign of malignancy (DF, 1966; Kufe & Frei, 2003). These observations support the idea that cell size and physiology are intrinsically related.

In 1966, Donald Gleason, a Minneapolis pathologist, depicted a standardized pathological testing scheme to measure the development and aggressiveness of prostatic adenocarcinomas. The “Gleason Score”, simple yet comprehensive, is largely based on the levels of cytologic atypia (abnormal size, shape and cellular content), where states of larger atypia are associated with increased aggressiveness (Amin, 2004; Brimo et al., 2012; DF, 1966; Majno & Joris, 2004). Despite the advances of medical tests that aid in the diagnosis of prostatic cancers, the “Gleason Score” is still widely used and remains greatly unchanged (Epstein et al., 2005; Trpkov, 2015). Such cellular changes aren’t uniquely characteristic of prostatic tissues and are used by pathologists in a variety of cancers with different etiological origins (Kufe & Frei, 2003; Majno & Joris, 2004). The correlation of cellular atypia with malignancy goes beyond the basic observations that patients with higher atypia are often associated with a worse prognosis. When cells grown in culture were heterotransplanted into mice cheek only those with high cytologic atypia proliferated and were capable of inducing tumors (Caspersson, Lomakka, Killander, & Foley, 1963).

While the association between cancer malignancy and cell size has been universally observed, it is highly controversial whether cell size is causative or simply a consequence of the characteristic polyploidy of cancer cells. Nevertheless, the observation that cancer is often associated with anaplasia is remarkable, and

supports the possibility that drugs that affect cellular growth might be of use in the treatment of cancer.

In addition to cancer, the physiological impact of cell size changes is observed in a variety of human health and diseases states. When it comes to cell size, the kidney is likely one of the most plastic organs in the body. Ciliated kidney cells sense fluid flow and, in response, reduce their size (Boehlke et al., 2010). Increases in cell size are, however, seen as a common response to multiple nephropathies. During diabetic nephropathy (DN) kidney enlargement by cellular hypertrophy occurs as an adaptive response to the loss of nephrons (J.-K. Chen, Chen, Thomas, Kozma, & Harris, 2009; Lieberthal & Levine, 2012; Sakaguchi et al., 2006). While initially beneficial, the persistence of kidney hypertrophy will contribute to podocyte injury and ultimately loss of renal function (Lieberthal & Levine, 2012). One other remarkable observation is kidney hypertrophy after uninephrectomy (the surgical removal of one kidney) (J.-K. Chen et al., 2009; Rubin & Reisner, 2009). Studies in mice have demonstrated that after removal of one kidney, the remaining kidney will increase in size by about 40%, a feat solely achieved by cell growth (J.-K. Chen et al., 2009; J.-K. Chen, Chen, Neilson, & Harris, 2005). Interestingly, upon necrotic or apoptotic cell loss kidneys regenerate by proliferation. What influences the decision to undergo hyperplasia *vs* hypertrophy is not understood but these observations suggest that in some instances hyperplasia is preferred over cell hypertrophy. Cell hypertrophy is not, therefore, a universal response to loss of function but instead likely to confer an adaptive mechanism triggered as response to specific stimuli.

One other organ of particular interest when it comes to cell size changes is the pancreas. In order to cope with increasing dietary demands the weight of the pancreas increases from early development to adult life in a manner proportional to

body weight. While in early infant rats, beta cell proliferation is key for the increased cell mass of the pancreas, it is cell hypertrophy that mostly contributes for the mass increase observed throughout adult life (Montanya, Nacher, Biarnés, & Soler, 2000). Such changes in cell size allow for a dynamic response of the pancreas in maintaining normoglycemia, despite changes in metabolic demand (Montanya et al., 2000). Mutant mice incapable of cellular hypertrophy, but containing normal number of beta cells, suffer a 40-50% reduction in circulating insulin and, in response, become hyperglycemic when faced with increased levels of dietary glucose (Lingohr, Buettner, & Rhodes, 2002; Pende et al., 2000). Increased cell size is equally observed during pregnancy as the beta cell mass increases through the combined result of hyperplasia and hypertrophy. In pregnant mice over 50% of beta cells undergo a size increase that surpasses 3 fold the size of normal beta cells (Rieck & Kaestner, 2010; Rieck et al., 2009). While mice with abnormally big induced beta cells are hyperinsulinemic, the amount of secreted insulin does not, however, increase linearly proportional to cell size (Bernal-Mizrachi, Wen, Stahlhut, Welling, & Permutt, 2001). The combined effect of cellular replication and increased cell size is likely to be required for an efficient response to the increased insulin demands during pregnancy (Dhawan, Georgia, & Bhushan, 2007). Together, these studies suggest a direct link between cell size and homeostatic physiology.

While a combination of cellular hypertrophy and hyperplasia contributes to organ size in a variety of instances, certain organs, such as those made uniquely of terminally differentiated cells, can only undergo cellular hypertrophy. While hypertrophy is often associated with natural health situations (such as the result of exercise), pathological myocardial hypertrophy is almost always associated with apoptosis and, ultimately, heart failure (Rubin & Reisner, 2009).

Why a persistent increase in cell size is, at instances, associated with organ failure is not well understood. Recent modeling studies might have, however, answered such conundrum. In 2013, Pissadaki and Bolam, sought to understand why Parkinson's disease, which affects 10 million humans worldwide but is unknown to other mammals, primarily affects the dopamine neurons of the susbtancia nigra compacta (SNc). Why are dopamine neurons of the SNc more susceptible to death than other dopamine neurons? By creating a model that reproduced many characteristics of dopamine neurons and inferring on the cost of action potential propagation they determined that dopamine neurons of the SNc are orders of magnitude longer than less susceptible neurons. In addition, dopamine neurons of the SNc are likely to produce ten times the number of synapses of other neurons. Such magnitude, combined with the lack of myelinated axons, results in high energy demand which exponentially increases with the level of axon branching (Pissadaki & Bolam, 2013). It is possible that the high cost of action potential propagation through complex neurons places them at higher risk of energy imbalance. These cells would possibly fail to cope with cases of mitochondrial disfunction or oxidative stress, leading to ever increasing cellular stresses. Ultimately, cells would fail to deal with protein turnover and suffer of impaired autophagy, factors known to contribute to cell death during Parkinson's disease (Pissadaki & Bolam, 2013). The prediction that action potential propagation in human dopamine neurons of the SNc have energetic costs an order of magnitude greater than those of rat neurons could also explain why PD is uniquely a human disease (Pissadaki & Bolam, 2013).

What are the mechanisms that control cell size?

Cell size checkpoints: coordination between growth and cell cycle progression in G1

So far we have analyzed some of the physiological consequences of cell size. But what controls cell size and size uniformity? A plausible possibility is that uniformity of cell size is simply regulated by contact inhibition, due to the spacial restrictions of cells within a given tissue. While this hypothesis could explain many scenarios, many others would be left unexplained. How would spatial restriction explain the hypertrophic growth of the adult kidney? How would pancreatic beta cells share the same spacial restrictions as the surrounding acinar cells, but differ in size and shape? How would beta cells undergo hypertrophy during pregnancy and obesity? Finally, how would unicellular organisms maintain a relatively constant size when grown in liquid culture?

The quest to understand cell size regulation and the mechanisms underlying it emerged nearly a century ago (Bayne-Jones & Adolph, 1932). Yet, many questions remain unanswered and are a key aspect of active cell biology research.

Although the mechanisms of cell size control are still greatly unknown they must impinge on the mechanisms that control cell cycle progression. If cell division would occur without cellular growth, cells would become infinitely small. Continued growth without division would, on the other hand, result in cells with great energetic demands. In order to maintain a confined range of cell sizes growth must be tightly coupled with cellular division. Aiming to test such dependency, Prescott experimentally amputated growing amoeba to test if a reduction in size would affect cellular division. The results were striking, repeated cytoplasmic amputations

prevented amoeba division indefinitely (Prescott, 1956). The evidence that growth mediates progression through the cell cycle has now been investigated in a variety of species (Fantes & Nurse, 1977; Johnston et al., 1977; Killander & Zetterberg, 1965). Studies in yeast and human cells demonstrate that cell size variations are smallest at the initiation of DNA synthesis and highest at completion of mitosis (Johnston et al., 1977; Killander & Zetterberg, 1965). These observations argue that entry into the cell cycle requires attainment of a critical size while its completion does not. It is now known that coordination between cell growth and cell cycle progression is achieved by cell size checkpoints, which delay key cell cycle transitions until an appropriate amount of growth has occurred.

Cell size checkpoints are best understood in yeast. Budding yeast cell division is asymmetric, yielding a large mother cell and a small daughter cell. The small daughter cell spends more time undergoing cell growth in G1 prior to cell cycle entry. In addition, when cells are switched between poor and rich media conditions, the duration and amount of growth in G1 is adjusted. Cells in richer conditions undergo cellular hypertrophy during G1, a phenomena known as nutrient modulation of cell size (Hartwell & Unger, 1977; Johnston et al., 1977). These observations led to the initial idea of a G1 cell size checkpoint that blocks cell cycle entry until sufficient growth has occurred. The checkpoint is thought to control G1 cyclin transcription because loss of the early G1 cyclins, that drive cell cycle entry, causes a delay in G1 phase (F. R. Cross, 1988; 1990; Nash, Tokiwa, Anand, Erickson, & Futcher, 1988; Richardson, Wittenberg, Cross, & Reed, 1989). Cell growth continues during the delay, leading to abnormally large cells (F. R. Cross, 1988). Conversely, overexpression of early G1 cyclins causes cell cycle entry at a reduced cell size (F. R. Cross, 1988; Nash et al., 1988).

The mTOR pathway facilitates cellular hypertrophy through modulation of the G1 cell size checkpoint

The evidence that cell cycle progression is triggered by cellular growth raises an intriguing question: how are cells, such as those from the pancreas and kidney, capable of undergoing hypertrophy without stimulating cellular division?

In a series of brilliant studies Johnston and colleagues first demonstrated that cells continue to grow even when prevented from progressing through the cell cycle (Johnston et al., 1977). These evidence suggest that uncoupling cell cycle progression from cellular growth could be the basis of cellular hypertrophy. In addition, when yeast cells grown under restrictive conditions were switched to more favorable conditions (such as increased sugar and nitrogen levels) they resumed further growth prior to committing to a new round of division (Fantes & Nurse, 1977; Johnston et al., 1977). These observations suggest that the mechanisms employed by yeast in response to nutritional changes are likely universal and might regulate hypertrophic growth in health and disease.

A plethora of recent studies analyze the question of cell hypertrophy in kidney and pancreas cells. Diabetic mice suffer from kidney hypertrophy. Hypertrophy results from continued growth without initiation of DNA synthesis, caused by increased expression of cyclin-dependent kinase inhibitors (CKIs) in the kidney of diabetic mice (Sakaguchi et al., 2006). In response to the increased levels of CKIs, early G1 cyclins are activated without a subsequent engagement of late G1/S cyclins, resulting in a late G1 cell cycle arrest (J.-K. Chen et al., 2005; B. Liu & Preisig, 1999). In addition to the cell cycle arrest, growth is stimulated due to increased phosphorylation of the ribosomal protein S6 kinase (S6K), a target of mTOR. Treatment of diabetic mice with rapamycin, unlike in normal mice, reduces

S6K phosphorylation and reduction of kidney weight, while slowing down progression of DN (Lieberthal & Levine, 2012; Sakaguchi et al., 2006).

Activation of mTOR is equally responsible for the observed hypertrophy after unilateral nephrectomy (UNX). Upon UNX the level of ribosomal protein S6 (rpS6) phosphorylation in the contralateral kidney increases. Loss of S6K, or treatment of mice with rapamycin after surgery, prevents rpS6 phosphorylation and highly reduces hypertrophy (J.-K. Chen et al., 2005; 2009). This observation is likely to account for the increased protein production in the remaining kidney, observed as an increase in the polysome profile (J.-K. Chen et al., 2005).

Environmental sensing and modulation of cell size in kidney cells is achieved through cilia movement. In response to fluid flow, ciliated cells reduce in size. Loss of cilia results in increased activation of mTOR and, consequently, cellular hypertrophy (Boehlke et al., 2010). During fluid flow cilia movement induces Lkb1 activity, an inhibitor of mTOR. In addition, increased phosphorylation of mTOR in mice leads to polycystic kidney disease (PKD) and is a common feature of human PKD (Lieberthal & Levine, 2012). Loss of function of PC1, a cilia plasma membrane receptor responsible to bind the mTOR inhibitor tuberin, is likely to cause the onset of PKD due to a deficit of cells to sense mechanical and chemical cues (Lieberthal & Levine, 2012). Inhibition of mTOR with rapamycin reduces cyst formation (Boehlke et al., 2010). In addition, loss of primary cilia is also a key characteristic of premalignant lesions of the breast as well as in invasive breast cancers (Basten & Giles, 2013; Menzl et al., 2014)

Why kidney cells reduce cell size in response to fluid flow is not clearly understood. Studies performed in either adipocytes and pancreatic cells have, however, revealed an intriguing relationship: smaller cells have higher insulin sensitivity (Mezza et al., 2014; Nestel, Austin, & Foxman, 1969; Salans, Knittle, &

Hirsch, 1968). Whether this phenomena is universal across different tissue types is unclear. It is however intriguing that S6K mutant mice, which secrete 40-50% less insulin due to a reduction in beta cell size, are normoglycemic during fasting (Pende et al., 2000). These observations suggest that S6K mutant mice are more sensitive to insulin (Pende et al., 2000). In addition, continued activation of mTOR is know to be associated with insulin resistance (Laplante & Sabatini, 2012). Together these evidence suggest that inactivation of mTOR and reduction of cell size by kidney tubular cells in response to fluid flow, might ensure optional insulin sensitivity to match dietary demands.

The mechanisms controlling hypertrophy of kidney cells are likely the same mechanisms controlling hypertrophy in a variety of tissues. Mice lacking S6K have reduced pancreas size, accounted uniquely to a reduction of beta cell size. As a consequence they become hypoinsulinaemic and are incapable of coping with increased insulin demand (Lingohr et al., 2002; Pende et al., 2000; Ruvinsky et al., 2005). Inhibition of S6K using rapamycin in adulthood, when cells have grown to the size characteristic of an adult pancreas, has little affect on insulin secretion (Pende et al., 2000). Loss of S6K is not, therefore, impacting insulin production by means other than cell size control. In addition, these mechanisms seem conserved throughout species. Loss of Sch9, the budding yeast homologue of S6K, leads to reduced cell size and failure of cells to adjust their size to nutrient availability, a feature characteristic of a variety of cells (Fantes & Nurse, 1977; Johnston et al., 1977; Jorgensen, 2002; Jorgensen et al., 2004; Kimball & Vogt-Köhne, 1961; Weisz, 1954; Young & Fantes, 1987).

The full mechanisms by which mTOR senses the environment and controls cell size are still, at best, weakly understood.

Cell size checkpoints beyond G1

Although significant cell size control occurs in G1 phase, there is evidence that important size control occurs at other phases in the cell cycle in budding yeast. For example, cells lacking all known regulators of the G1 cell size checkpoint show robust nutrient modulation of cell size, a feat believed to be controlled solely during G1 (Jorgensen et al., 2004). This could be explained by the existence of additional G1 cell size control mechanisms that have yet to be discovered, but it could also suggest that normal nutrient modulation of cell size requires checkpoints that work outside of G1 phase. More evidence comes from the observation that daughter cells complete mitosis at a significantly smaller size in poor nutrients than in rich nutrients (Johnston et al., 1977). This suggests the existence of a checkpoint that operates after G1, during bud growth, to control the size at which daughter cells are born. This possibility has not received significant attention because early work suggested that the duration of daughter bud growth is invariant and independent of nutrients (Hartwell & Unger, 1977). As a result, it has been thought that birth of small daughter cells in poor nutrients is a simple consequence of their reduced growth rate, rather than active size control. However, this has not been tested by directly measuring the duration of daughter cell growth in rich and poor nutrients, so it remains possible that checkpoints actively modulate the extent of daughter cell growth to control cell size at completion of mitosis.

Further evidence for size control outside of G1 phase has come from analysis of nutrient modulation of cell size. Protein phosphatase 2A associated with the Rts1 regulatory subunit ($PP2A^{Rts1}$) is required for nutrient modulation of cell size (Artiles, Anastasia, McCusker, & Kellogg, 2009). Proteome-wide analysis of targets of $PP2A^{Rts1}$ revealed that it controls critical components of both the G1 and mitotic cell size checkpoints, as well as several additional key regulators of mitotic progression

(Zapata et al., 2014). The fact that $PP2A^{Rts1}$ is required for nutrient modulation of cell size, while regulators of the G1 checkpoint are not, could be explained by a model in which $PP2A^{Rts1}$ controls mitotic cell size checkpoints that play an important role in nutrient modulation of cell size.

Closing remarks

The observations outlined through the course of this chapter emphasize the importance of cell size regulation. Given the vast array of consequences derived from cell size changes, understanding cell size regulation and the biochemical pathways that control it is, therefore, of utter importance.

Saccharomyces cerevisiae is a unique model system for the comprehension of cell size. It's characteristic shape in combination with powerful genetics, makes yeast suitable for cell size studies. Furthermore, yeast cells do not suffer from the same spatial constrains that mammalian cells do, aiding in result interpretation. Finally, just like kidney and pancreatic cells, yeast cells are capable of cellular size changes in response to environmental cues.

In the following chapters I will expose our recent findings and report on the mechanisms that allow yeast cells to adapt to local changes in sugar availability. We set out to determine whether nutrient modulation of cell size occurs solely at the G1 checkpoint, or whether it occurs at other times during the cell cycle. In addition, I will expose new molecular mechanisms by which cell size is controlled beyond G1.

CHAPTER II [PUBLISHED RESULTS]: The duration of mitosis and daughter cell size are modulated by nutrients in budding yeast

In the following pages I will describe our published results that support the hypothesis of cell size regulation during mitosis. In addition I will describe key players involved in this new checkpoint.

The duration of mitosis is modulated by nutrients

Previous work suggested that the cell cycle events that occur after bud emergence have a constant duration that is independent of the growth rate set by nutrients (Hartwell and Unger, 1977). However, the limited tools available at the time meant that the duration of cell cycle events had to be inferred from indirect measurements. To more directly address this question, we first grew cells in a rich carbon source (2% dextrose) or a poor carbon source (2% glycerol + 2% ethanol) and determined the duration of mitosis by assaying levels of the mitotic cyclin Clb2 in synchronized cells. Clb2 persisted for a longer interval in cells growing in poor nutrients, which suggested that the duration of mitosis is increased (**Figure 2.1A**).

We next asked whether cells already in mitosis were sensitive to a shift from rich to poor carbon. Cells growing in rich carbon were synchronized and shifted to poor carbon when Clb2 reached peak levels and most cells had short mitotic spindles, indicating that they were in metaphase. A shift to poor carbon at this point in mitosis caused a prolonged metaphase delay, as well as delayed destruction of Clb2 (**Figures 1.1B,C**). In contrast, if cells were switched to poor carbon slightly later in mitosis, when cells were in anaphase, there was no delay in destruction of Clb2 or in completion of anaphase (**Figures 1.1D,E**). The insensitivity of anaphase

cells to carbon source suggests that the metaphase delay is not due simply to a starvation response.

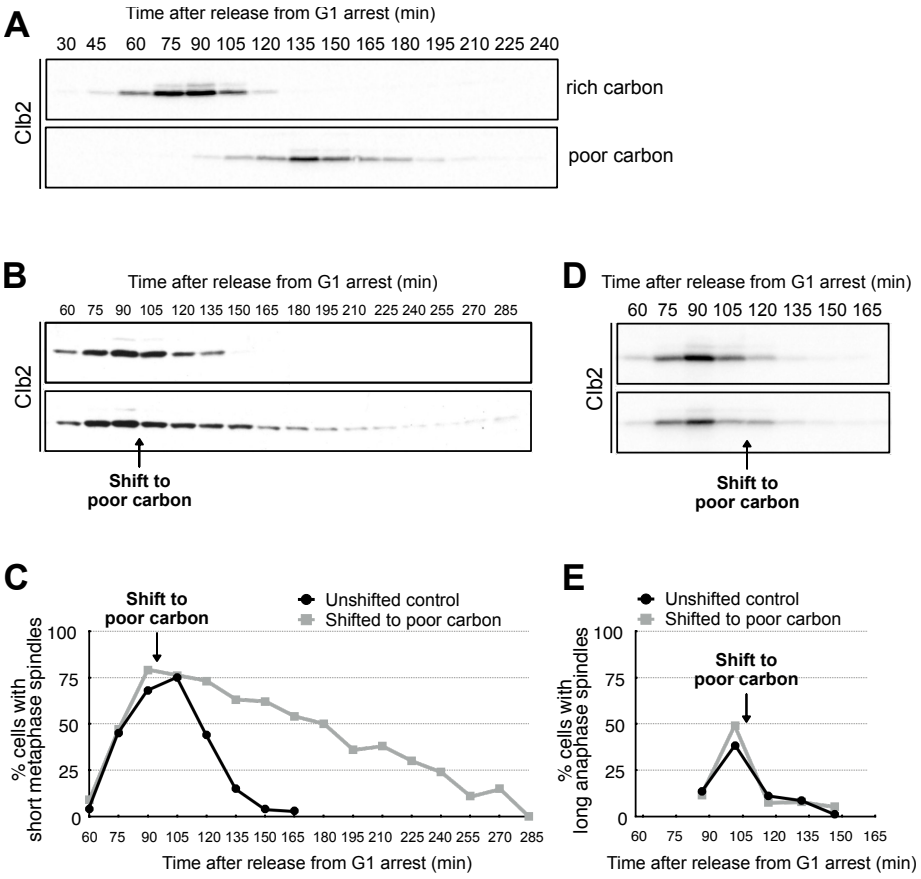

Figure 2.1. The duration of mitosis is modulated by nutrients

(A) *Wild type* cells growing in YPD (rich carbon) or YPGE (poor carbon) were arrested in G1 phase by addition of mating pheromone. The cells were released from the arrest and levels of the mitotic cyclin Clb2 were assayed by western blot. (B,C) Cells growing in YPD were released from a G1 arrest. At 90 minutes, the culture was split and one half was washed into YPD and the other half was washed into YPGE. Levels of the mitotic cyclin Clb2 were assayed by western blot and short metaphase spindles were assayed by immunofluorescence. (D,E) Cells growing in YPD were released from a G1 arrest. At 105 minutes, the culture was split and one half was washed into YPD the other half was washed into YPGE. Levels of the

mitotic cyclin Clb2 were assayed by western blot and long anaphase spindles were assayed by immunofluorescence.

To further investigate the effects of nutrients, we used a combination of fluorescence and bright field microscopy to simultaneously monitor daughter bud growth and mitotic events in living cells. Bud growth was monitored by plotting daughter bud volume as a function of time. The duration of mitotic events was monitored by marking mitotic spindle poles with spc42-GFP and plotting the distance between poles as a function of time. Initiation of metaphase corresponds to the initial separation of spindle poles, while the duration of metaphase corresponds to the interval when spindle poles remain separated by 1-2 microns within the mother cell (Lianga et al., 2013; Winey & O'Toole, 2001). Initiation of anaphase is detected when spindle poles begin to move further apart and one pole migrates into the daughter cell. We defined the duration of anaphase as the interval between anaphase initiation and the time when the spindle poles reached their maximum distance apart. GFP-tagged myosin was used to detect completion of cytokinesis, which is marked by disappearance of the myosin ring (Lippincott & Li, 1998). In addition to the stages of mitosis, we defined an S/G2 interval as the time from bud emergence to spindle pole separation, and G1 phase as the time from when the daughter cell completes cytokinesis to the time that it initiates formation of a new daughter bud.

Daughter cell growth was monitored for one complete bud growth cycle, from the time the bud emerged from the mother cell to the time that it initiated formation of a new bud at the end of the next G1 phase. Representative data for a cell growing in rich carbon are shown in **Figure 2.2A**, and data for a cell growing in poor carbon in **Figure 2.2B**. Examples of cell images taken during the course of bud growth are

shown in **Figure 2.2C**. At least 25 cells were analyzed under each condition (See **Figure 2.S1** for individual growth curves).

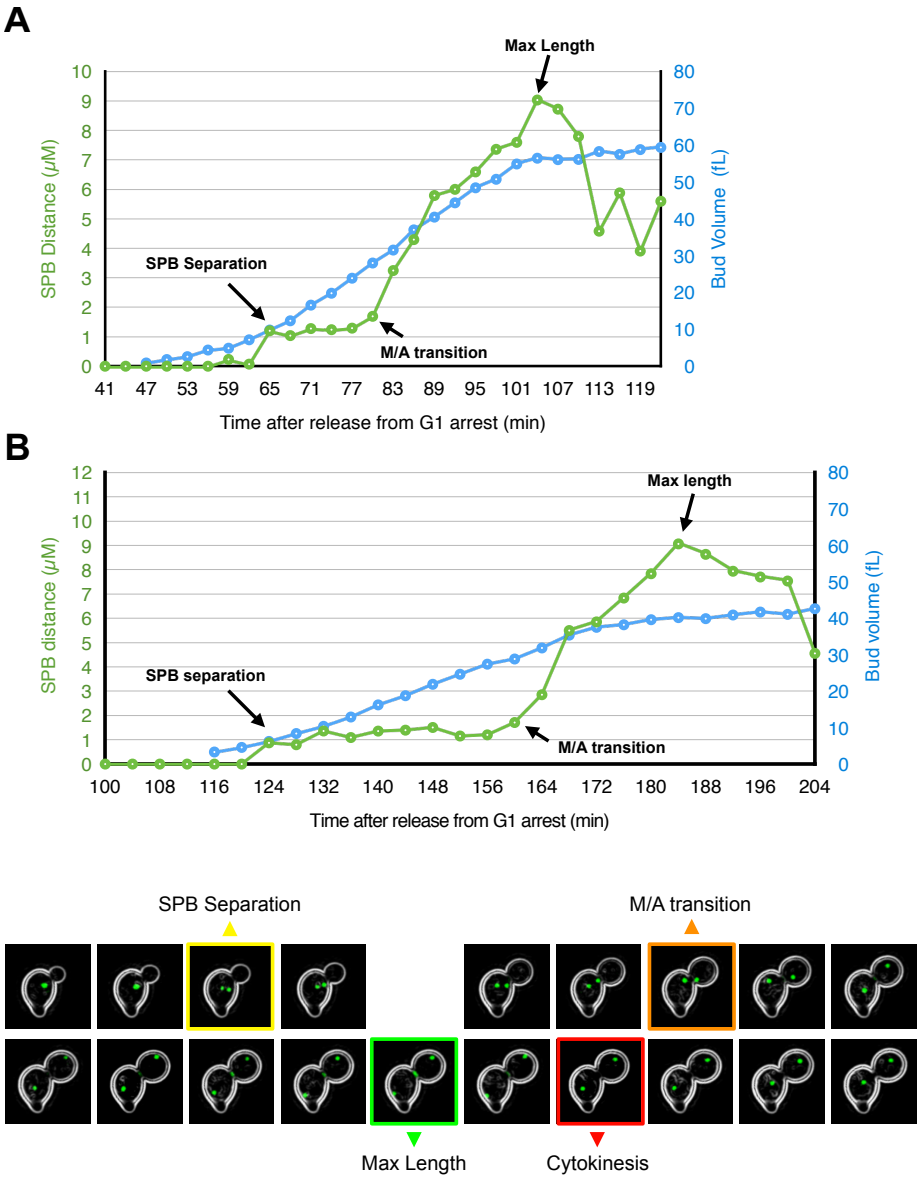

Figure 2.2. Simultaneous imaging of bud growth and mitotic spindle dynamics in living single cells

(A,B) Representative growth curves for cells growing in rich carbon (A) or poor carbon (B). The volume of the daughter bud is plotted in blue and the distance

between spindle poles in green. (C) Contrast enhanced images of a representative growing bud with GFP tagged spindle poles (Spc42-GFP) and myosin ring (Myo1-GFP). Key transitions are highlighted. Images taken in metaphase that were omitted so that all key transition points could be shown are indicate with ■■■ .

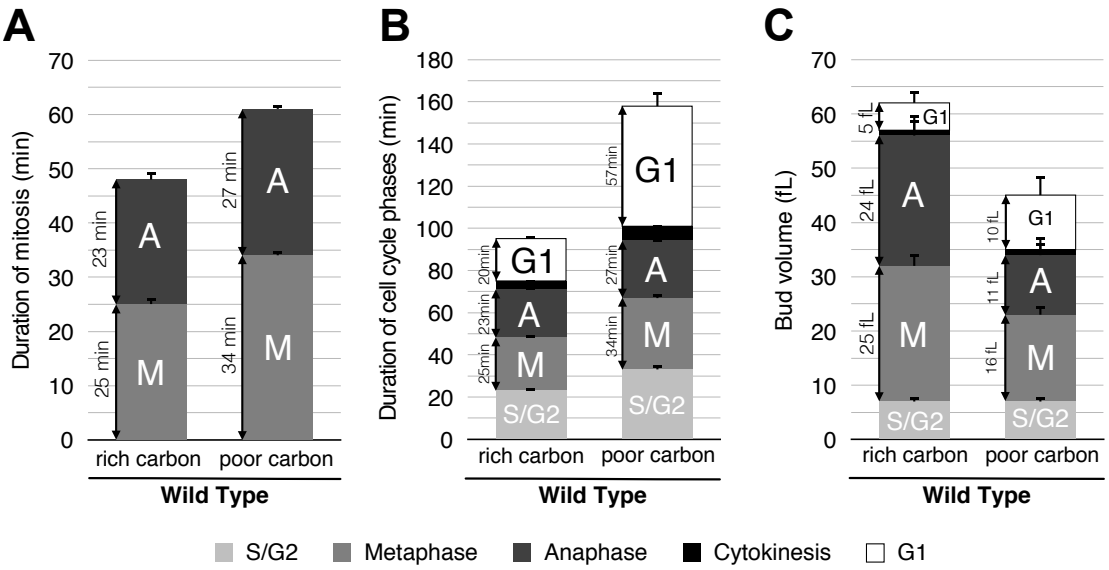

Figure 2.3. The duration of mitosis and bud volume are modulated by nutrients

(A) A plot showing the average durations of metaphase and anaphase for cells growing in rich or poor carbon. (B) A plot showing the average durations of all cell cycle stages for cells growing in rich or poor carbon. (C) A plot showing the average growth in volume during all phases of the cell cycle for cells growing in rich or poor carbon. Error bars represent standard error of the mean.

Growth of the daughter bud occurred throughout mitosis (**Figure 2.2**). To focus on the effects of carbon source on the duration of mitosis, we first plotted the average duration of each stage of mitosis for cells growing in rich or poor carbon (**Figure 2.3A**; see **Figure 2.S2A** for scatter plots and p-values). The durations of

both metaphase and anaphase were significantly increased in poor carbon, although the greatest increase was observed for metaphase. The overall duration of mitosis, from the beginning of metaphase to cytokinesis was 52 minutes in rich carbon, and 68 minutes in poor carbon.

The durations of all cell cycle stages comprising a complete bud growth cycle in rich and poor carbon are shown in **Figure 2.3B** (see **Figure 2.S2A** for scatter plots and p-values). This revealed that the fraction of the growth cycle that occurs in G1 phase increased in poor carbon, as previously reported (Hartwell and Unger, 1977).

Daughter cells complete mitosis at a smaller size in poor nutrients

We next plotted bud size at completion of each cell cycle stage (**Figure 2.3C;** see **Figure 2.S2B** for scatter plots and p values). Metaphase was initiated at the same daughter cell size in both carbon sources (7 fL). Cells in poor carbon, however, completed each stage of mitosis at a significantly smaller size. Overall, cells in rich carbon completed cytokinesis at a volume of 57 fL, whereas cells in poor carbon completed mitosis at a volume of 35 fL. Cells in rich carbon underwent the same amount of growth in metaphase as in anaphase (25 fL vs 24 fL), while cells in poor carbon grew more in metaphase than in anaphase (16 fL vs 10fL).

Together, the data indicate that the duration of both metaphase and anaphase is increased in poor carbon, while daughter cell size at each mitotic transition is reduced. Thus, the data are inconsistent with a model in which cells complete mitosis at a reduced size in poor nutrients simply because their growth rate is reduced, while the duration of mitotic events is unchanged. Rather, the duration of mitosis and cell size at completion of mitosis are modulated in response to changes in carbon source that cause large changes in growth rate.

Most cell growth occurs during mitosis

Analysis of the data in **Figure 2.3C** shows that most growth occurs during mitosis**.** Thus, in rich carbon, 80% of the volume of a daughter cell is achieved during mitosis; growth of the daughter cell during the subsequent G1 adds only 5 fL, or 8% of the final volume of the daughter cell before it becomes a mother cell. In poor carbon, these numbers are shifted: 61% of the volume of a cell growing in poor carbon is achieved during mitosis; growth during the subsequent G1 adds 10 fL, or 23% of the final volume. Fission yeast cells show a similar expansion of G1 phase when grown in poor nitrogen (Costello et al., 1986; Su et al., 1996).

Growth rate changes during the cell cycle and is modulated by nutrients

The growth curves in **Figure 2.2** suggest that the growth cycle is comprised of distinct phases characterized by different growth rates. Previous studies suggested that growth rate changes during the cell cycle, but did not include analysis of growth during specific stages of mitosis in unperturbed single cells (Mitchison, 1958; Goranov et al., 2009; Ferrezuelo et al., 2012). To extend these studies, we calculated growth rates at each stage of the cell cycle in rich and poor carbon (**Figures 1.4 A,B**). When the bud first emerges, growth is relatively slow. Entry into mitosis initiates a fast growing phase that lasts nearly the entire length of mitosis. As cells complete anaphase the growth rate slows. A slow rate of growth persists during G1 phase. Poor carbon reduced the rate of growth in mitosis by half, but caused significantly smaller reductions in growth rate during other stages of the growth cycle.

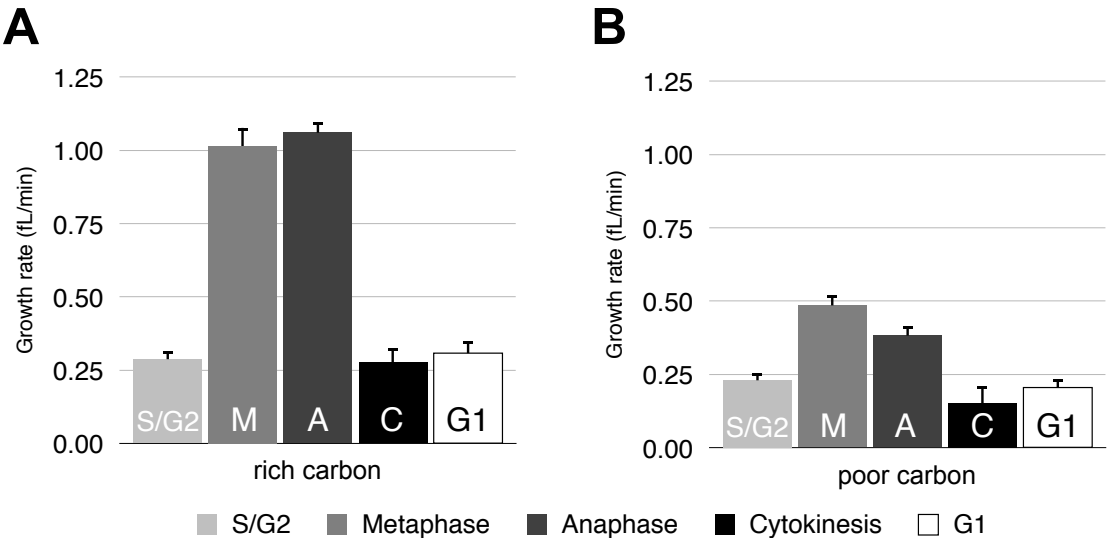

Figure 2.4. Growth rate changes during the cell cycle and is modulated by nutrients

The growth rate at each phase of the cell cycle was calculated as the average of individual cell growth rates during each cell cycle phase. The growth rate of each cell was calculated by dividing the volume increase of the cell during a phase by the time the cell spent in the phase. (A) Data for cells growing in rich carbon. (B) Data for cells growing in poor carbon. Error bars represent the standard error of the mean.

Previous work found that the bud initially grows in a polar manner, and that activation of mitotic Cdk1 triggers a switch to isotropic growth that occurs over the entire surface of the bud (Farkaš et al., 1974; Lew and Reed, 1993; Barral et al., 1995; McCusker et al., 2007). Thus, the data indicate that the polar and isotropic growth phases occur at significantly different rates.

The effects of carbon source on daughter cell size are not due solely to changes in mother cell size

Mother cell size influences daughter cell size: small mothers produce small daughters, and large mothers produce large daughters (Johnston et al., 1977; Schmoller et al., 2015). In addition, newborn daughter cells progress through the G1 cell size checkpoint at a smaller size in poor carbon, which means that they initiate bud emergence and become mother cells at a smaller size (Johnston et al., 1979; Lorincz and Carter, 1979; Jorgensen and Tyers, 2004). Thus, we considered the possibility that reduced daughter cell size in poor carbon is primarily a consequence of the reduced size of their mothers. In this model, mother cells become small in poor carbon because they pass the G1 cell size checkpoint at a reduced cell size, and they produce small daughters because they have a reduced biosynthetic capacity. This model does not explain the increased duration of mitosis in poor carbon, which suggests that decreased mother cell size is unlikely to be the sole factor influencing the size of daughter cells. Nevertheless, we analyzed the effects of mother cell size on daughter cell size and growth rate both within and between media conditions.

Growth rate was positively correlated with mother cell size in both rich and poor carbon (**Figure 2.5A**). Thus, daughters of large mothers grew faster than daughters of small mothers, consistent with the idea that mother cell size influences biosynthetic capacity. However, carbon source had a stronger influence on growth rate than mother cell size. This can be seen by the fact that mothers of similar size in rich and poor carbon had significantly different growth rates, which was true across the entire range of mother cell sizes (**Figure 2.5A**).

We also plotted daughter cell size at completion of cytokinesis versus mother cell size (**Figure 2.5B**). Daughter cell size was positively correlated with mother cell

size in both conditions. Again, however, the influence of carbon source was much stronger. Mother cells growing in poor carbon that were the same size as mother cells in rich carbon consistently produced much smaller daughter cells. Thus, the reduced size at which daughter cells complete mitosis in poor carbon cannot be explained simply by reduced mother cell size.

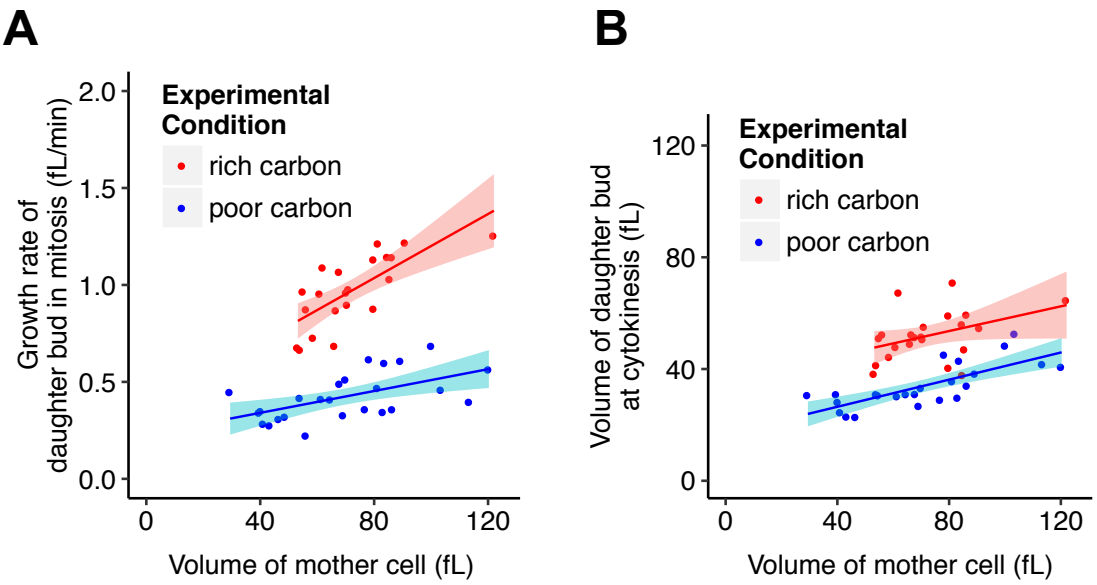

Figure 2.5. The growth rate and final volume of a daughter bud is influenced by the size of its mother cell

(A) The growth rate in mitosis of each daughter bud was plotted against the volume of its mother cell. (B) The volume of each daughter bud at cytokinesis was plotted against the size of its mother. Red dots represent cells in rich carbon. Blue dots represent cells in poor carbon. Smooth lines are logistic regressions of the data. Shaded areas represent 95% confidence interval.

Cell size at completion of mitosis is correlated with growth rate during mitosis

Previous studies found that cell size at the end of G1 phase is correlated with growth rate during G1 phase (Ferrezuelo et al., 2012; Johnston et al., 1979). The correlation held true when comparing cells growing in the same carbon source and when comparing cells growing in different carbon sources. To determine whether a similar relationship exists for growth during mitosis, we plotted daughter cell size at cytokinesis as a function of daughter bud growth rate during mitosis for cells growing in rich or poor carbon (**Figure 2.6**). Daughter cell size was strongly correlated with growth rate under both conditions.

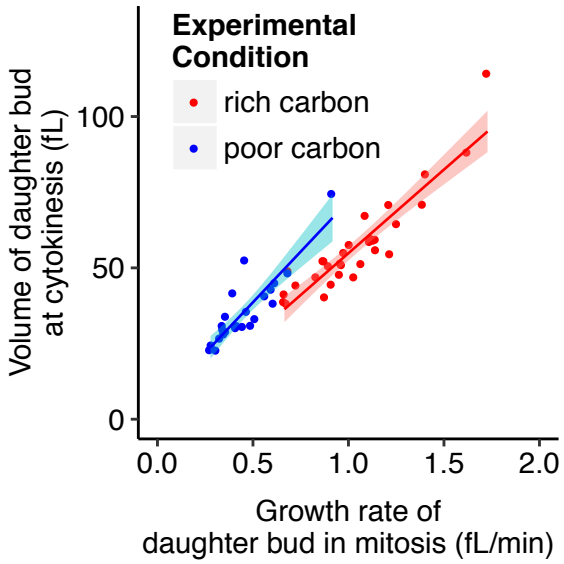

Figure 2.6. Cell size at cytokinesis is proportional to the growth rate during mitosis

The volume of daughter cells at cytokinesis was plotted against their growth rate during mitosis. Red dots represent cells in rich carbon. Blue dots represent cells in poor carbon. Smooth lines are logistic regressions of the data. Shaded areas represent 95% confidence interval.

PP2A^{Rts1} is required for normal control of mitotic duration and cell size at completion of mitosis

We next searched for signals that modulate the duration of mitosis and daughter cell size in response to nutrients. In previous work, we discovered that *rts1Δ* cells show a nearly complete failure in nutrient modulation of cell size, which suggested that PP2A^{Rts1} plays an important role (Artiles et al., 2009). We therefore tested the effects of a loss of function of Rts1 on mitotic duration and daughter cell size. Interpretation of results from *rts1Δ* cells would be complicated by the possibility that effects on bud growth and size could be a secondary consequence of pre-existing defects in mother cell size arising in previous generations. Therefore, we created an auxin-inducible degron version of Rts1 (*rts1-AID*), which allowed us to observe the immediate effects of inactivating PP2A^{Rts1} (Nishimura et al., 2009). In the absence of auxin, *rts1-AID* did not cause significant defects in cell size or cell cycle progression (**Figures 1.S3A,B**). Addition of auxin caused rapid destruction of rts1-AID protein within 15-30 minutes (**Figure 2.S3C**). Approximately 10% of the rts1-AID protein remained in the presence of auxin, and *rts1-AID* cells formed colonies more rapidly than *rts1Δ* cells at elevated temperatures (**Figure 2.S3D**). Together, these observations suggest that *rts1-AID* causes a partial loss of function. Nevertheless, we utilized *rts1-AID* because it allowed analysis of bud growth and mitotic duration without the complication of aberrant mother cell size.

rts1-AID cells were released from a G1 arrest and auxin was added shortly before bud emergence. Destruction of rts1-AID caused an approximately 3-fold increase in the average duration of metaphase in both rich and poor carbon (**Figures 1.7A,B;** see **Figures 1.S4A,B** for dot plots and p-values). The duration of anaphase was also increased, although not to the same extent. Destruction of rts1-AID caused a large increase in the variance of metaphase duration compared to *wild type* cells

(See dot plots in **Figure 2.S4A,B**). Moreover, although the duration of metaphase in *rts1-AID* cells was somewhat shorter in rich carbon compared to poor carbon, the difference was barely significant (p-value = 0.025). In contrast, the difference in metaphase duration between rich and poor carbon in *wild type* cells was highly significant (p-value = 0.000002) (**Figure 2.S2B**). Together, these observations suggest that *rts1-AID* caused defects in nutrient modulation of metaphase duration, despite the fact that *rts1-AID* caused only a partial loss of function. There was a statistically significant decrease in the duration of anaphase in rich carbon in *rts1-AID* cells, which could again be due to partial function of *rts1-AID* (**Figure 2.7A,B**).

rts1-AID caused a large increase in daughter bud size at all stages of mitosis in both rich and poor carbon (**Figures 1.7C,D**; see **Figures 1.S4C,D** for dot plots and p-values). The variance in size at the end of metaphase was much larger in *rts1-AID* cells compared to *wild type* cells. In addition, there was not a statistically significant difference in the size of *rts1-AID* cells in rich or poor carbon at the end of metaphase. By the end of anaphase, *rts1-AID* cells in rich carbon were slightly larger than their counterparts in poor carbon.

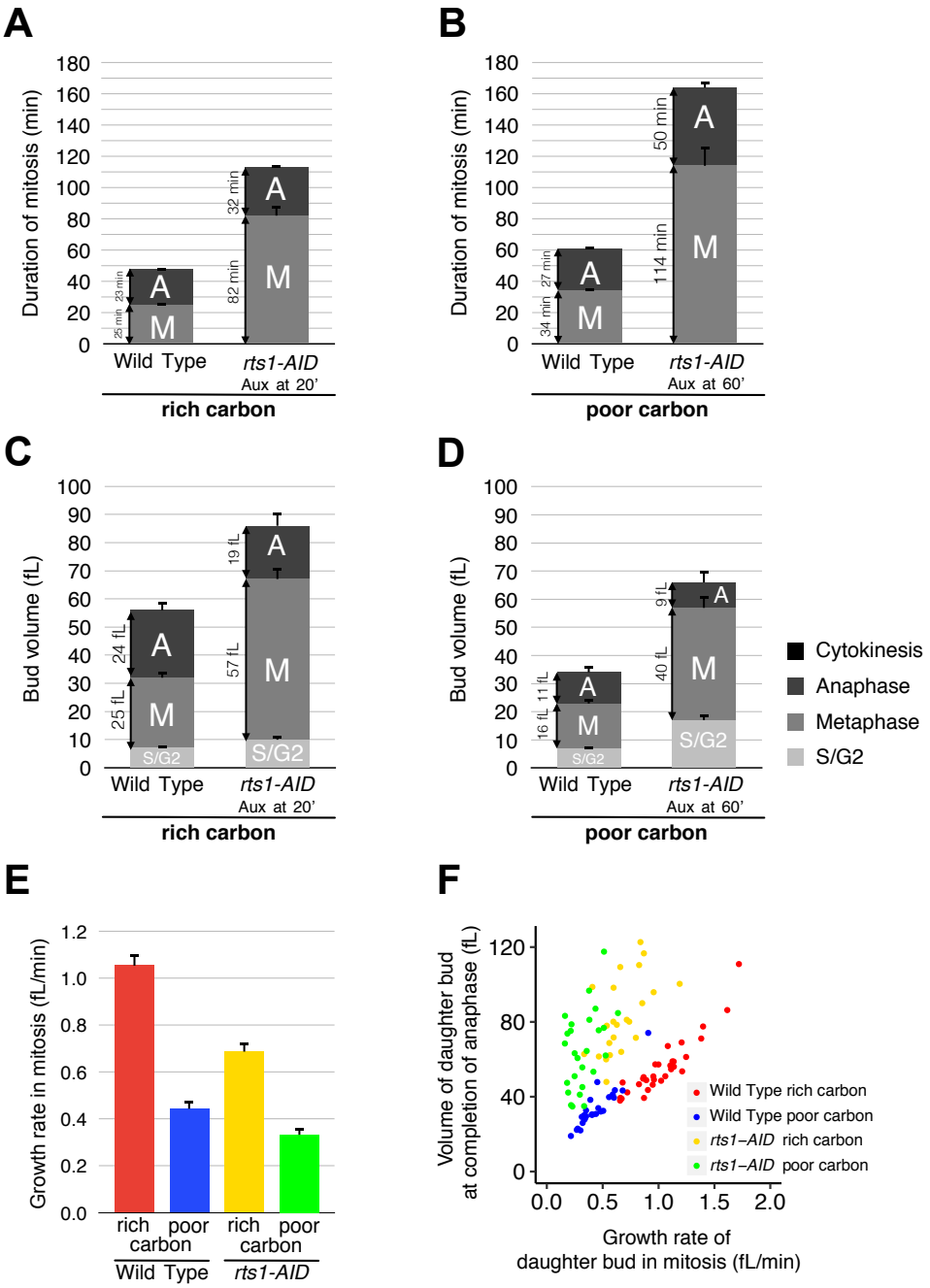

Figure 2.7. PP2A^{Rts1} is required for normal control of mitotic duration and cell size

(A,B) Plots showing the average durations of metaphase and anaphase for *wild type* and *rts1-AID* cells grown in rich or poor carbon. (C,D) The average growth in volume for all phases of the cell cycle except G1 is plotted for *wild type* and *rts1-AID* cells

grown in rich or poor carbon. Due to the extended length of the cell cycle in rts1-AID cells, only a few cells were followed through G1. For this reason, we omitted the limited data regarding G1 from these plots. (E) The growth rate during metaphase and anaphase was calculated as the average of individual cell growth rates. The growth rate of each cell was calculated by dividing its volume increase during metaphase and anaphase by the time it spent in these phases. (F) The volume of the daughter bud at completion of anaphase is plotted as a function of growth rate during metaphase plus anaphase. For panels C and D, red and blue represent *wild type* cells in rich and poor carbon, respectively. Similarly, yellow and green represents rts1-AID cells in rich and poor carbon. Error bars represent standard error of the mean.

Inactivation of PP2A^{Rts1} disrupts the normal relationship between growth rate and bud size

Destruction of rts1-AID reduced the growth rate by approximately 30% in both rich and poor carbon (**Figure 2.7E;** see **Figure 2.S4E** for dot plots and p-values). Under normal circumstances, a reduced growth rate causes a reduced cell size, whereas destruction of rts1-AID causes a reduced growth rate, but an increase in size. More importantly, the correlation between growth rate and daughter cell size was largely lost in *rts1-AID* cells (**Figure 2.7F**). Thus, buds with nearly identical growth rates completed mitosis at very different sizes. Together, these observations demonstrate that inactivation of PP2A^{Rts1} disrupts the normal relationship between growth rate and size.

The increased duration of mitosis in poor carbon is partially due to Cdk1 inhibitory phosphorylation

We next searched for targets of PP2A^{Rts1} that control mitotic duration and daughter cell size. In a previous study we identified candidate targets of PP2A^{Rts1} by

using proteome-wide mass spectrometry to search for proteins that are hyperphosphorylated in *rts1Δ* cells (Zapata et al., 2014). The analysis identified multiple proteins in a pathway that delays mitosis via inhibitory phosphorylation of Cdk1 (Cdk1-Y19℗). In this pathway, Swe1, the budding yeast homolog of Wee1, phosphorylates and inhibits Cdk1 (Gould and Nurse, 1989; Booher et al., 1993). The most strongly hyperphosphorylated site identified in *rts1Δ* cells was the inhibitory site on Cdk1 targeted by Swe1. The analysis also showed that multiple sites on Swe1 that play a role in its activation are hyperphosphorylated in *rts1Δ* cells, which suggests that Swe1 is hyperactive (Harvey et al., 2005; 2011). Finally, the analysis identified two related kinases, Gin4 and Hsl1, that inhibit Swe1 via poorly understood mechanisms (Ma et al., 1996; Barral et al., 1999; McMillan et al., 1999; Longtine et al., 2000). Thus, the mass spectrometry data established that $PP2A^{Rts1}$ works in a pathway that controls mitotic Cdk1 inhibitory phosphorylation.

Although inhibitory phosphorylation of Cdk1 was originally thought to control entry into mitosis, more recent work found that metaphase is shortened in *swe1Δ* cells (Lianga et al., 2013; Raspelli et al., 2014). Moreover, overexpression of Swe1, or inactivation of Gin4, causes cells to undergo prolonged delays in metaphase (Raspelli et al., 2014; Altman and Kellogg, 1997; Booher et al., 1993). Together, these observations suggest that inhibitory phosphorylation of Cdk1 influences the duration of mitotic events after entry into mitosis, which led us to hypothesize that lengthening of mitosis in poor carbon is due, at least in part, to inhibitory phosphorylation of Cdk1 by Swe1. To test this, we first used a phospho-specific antibody to determine whether Cdk1 inhibitory phosphorylation is prolonged in poor carbon. Cells growing in either rich or poor carbon were released from a G1 arrest and samples were taken at 15 minute intervals for western blot analysis with antibodies that detect Clb2 and Cdk1 inhibitory phosphorylation. Cdk1 inhibitory

phosphorylation was prolonged in poor carbon and closely paralleled Clb2 levels throughout most of mitosis (**Figures 2.1A** and **2.8A;** western blots in both Figures are from the same samples). These observations suggest that Cdk1 inhibitory phosphorylation can persist well beyond entry into mitosis, and that it could play a role in the lengthening of mitosis in poor nutrients.

We also analyzed the behavior of Swe1 during the cell cycle in rich and poor carbon. Swe1 passes through multiple phosphorylation states during mitosis that can be detected via electrophoretic mobility shifts; attainment of a fully hyperphosphorylated state is correlated with inactivation of Swe1 (Sreenivasan and Kellogg, 1999; McMillan et al., 2002; Raspelli et al., 2011; Harvey et al., 2011). In rich media, Swe1 reached full hyperphosphorylation and was degraded shortly thereafter (**Figure 2.8B**). In poor media, Swe1 was present throughout most of the prolonged mitosis. Moreover, Swe1 took longer to reach the fully hyperphosphorylated state, and it persisted in the partially hyperphosphorylated state that is thought to represent the active form of Swe1. These observations suggest that signals that control Swe1 could play a role in prolonging Cdk1 inhibitory phosphorylation in poor nutrients.

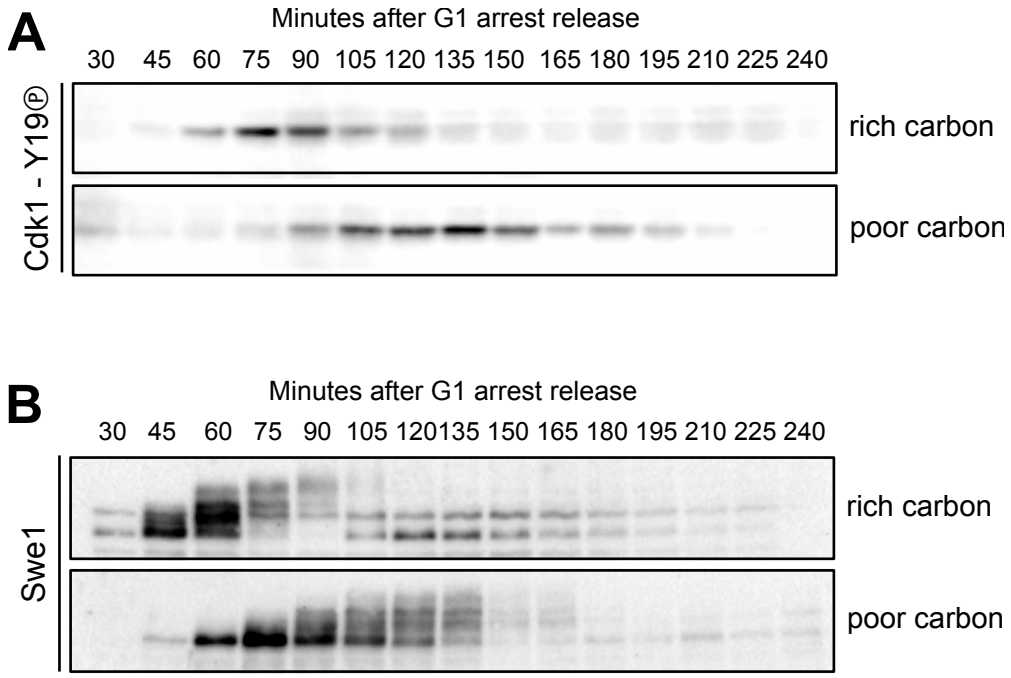

Figure 2.8. The increased duration of mitosis in poor carbon is partially due to Cdk1 inhibitory phosphorylation

(A,B) The same samples used for Figure 2.1A were probed for Cdk1-Y19 phosphorylation (A) and Swe1 (B) by western blot.

The role of Swe1 was further characterized by analyzing daughter cell growth and mitotic events in single cells. In rich carbon, *swe1Δ* caused a slight reduction in the average duration of metaphase, as previously described (**Figure 2.9A;** see **Figure 2.S5A** for dot plots and p-values). In poor carbon, *swe1Δ* caused a greater reduction in metaphase duration, from 34 minutes to 29 minutes (**Figure 2.9B**). Although *swe1Δ* reduced the duration of metaphase in poor carbon, it did not reduce it to the duration observed for *wild type* cells in rich carbon, which indicates that the mitotic delay in poor carbon is not due solely to inhibitory phosphorylation of Cdk1.

In both rich and poor carbon, *swe1Δ* caused a reduction in growth rate (**Figure 2.9C**). This, combined with the reduced duration of metaphase, caused

swe1Δ daughter buds to undergo each of the mitotic transitions at a significantly reduced size in both rich and poor carbon (**Figures 1.9D,E;** see **Figures 1.S5C,D** for dot plots and p-values). Together, the data demonstrate that Swe1 plays a role in the increased duration of mitosis in poor carbon and is required for normal control of daughter cell size at cytokinesis.

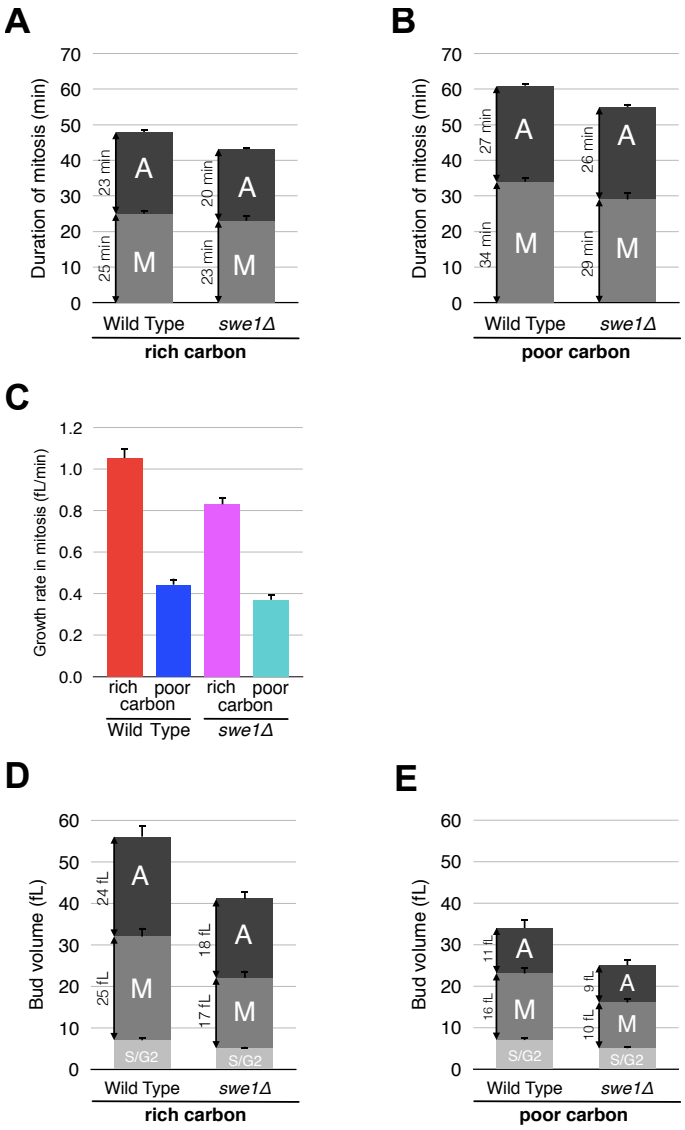

Figure 2.9. The increased duration of mitosis in poor carbon is partially due to Cdk1 inhibitory phosphorylation

(A) A plot showing the average durations of metaphase and anaphase for *wild type* and swe1Δ cells growing in rich carbon. (B) A plot showing the average durations of metaphase and anaphase for *wild type* and swe1Δ cells growing in poor carbon. (C) A plot showing the average growth rate during metaphase and anaphase in *wild type* or swe1Δ cells in rich or poor carbon. (D) A plot showing the average growth in volume during metaphase and anaphase for *wild type* or swe1Δ cells growing in rich carbon. (E) A plot showing the average growth in volume during metaphase and anaphase for *wild type* or swe1Δ cells growing in poor carbon. Error bars represent standard error of the mean.

$PP2A^{Rts1}$ controls the duration of mitosis by Swe1-dependent and Swe1-independent mechanisms

We next tested whether $PP2A^{Rts1}$ controls mitotic duration and daughter cell size via Swe1. Western blot assays confirmed that destruction of rts1-AID in synchronized cells caused a prolonged mitotic delay in both rich and poor carbon (**Figure 2.10A**). The delay was reduced, but not eliminated, by *swe1Δ*. We also found that *rts1Δ* caused a mitotic delay after release from a metaphase arrest that was largely reduced by *swe1Δ*, but not fully eliminated (**Figure 2.10B**).

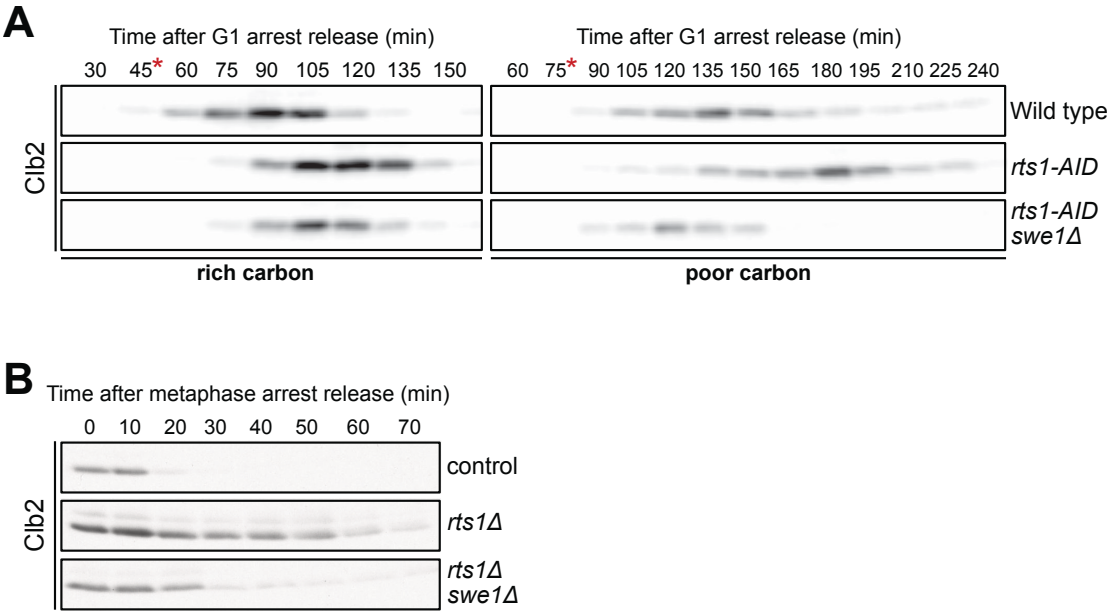

Figure 2.10. PP2A^{Rts1} controls the duration of mitosis by Swe1-dependent and Swe1-independent mechanisms [western blots]

(A) Cells of the indicated genotypes, grown in YPD or YPGE, were released from a G1 arrest and auxin was added at 45 min (YPD) or 75min (YPGE). Addition of auxin is denoted by *. Levels of the mitotic cyclin Clb2 were assayed by western blot. (B) Cells of the indicated genotypes were arrested in metaphase by depletion of Cdc20. After release from the arrest, levels of the mitotic cyclin Clb2 were assayed by western blot.

In single cell assays, the delays in metaphase caused by *rts1-AID* in rich and poor carbon were largely reduced by *swe1Δ*, but not fully eliminated (**Figures 1.11A,B;** see **Figures 1.S5E,F** for dot plots and p-values). The increased duration of anaphase caused by *rts1-AID* in rich and poor carbon was largely unaffected by *swe1Δ*. Although *swe1Δ* did not fully rescue the mitotic delay caused by *rts1-AID*, it caused *rts1-AID* cells to exit mitosis at a size similar to that of *swe1Δ* cells (**Figures 1.11C,D;** see **Figures 1.S5G,H** for dot plots and p-values). This was a combined

result of the reduction in mitotic duration and a decrease in growth rate in *rts1-AID swe1Δ* cells relative to *rts1-AID* or *swe1Δ* cells (**Figures 1.7C, 9C** and **11E**). Together, these observations demonstrate that PP2A^{Rts1} controls mitotic duration and daughter cell size via a Swe1-dependent pathway, as well as a Swe1-independent pathway.

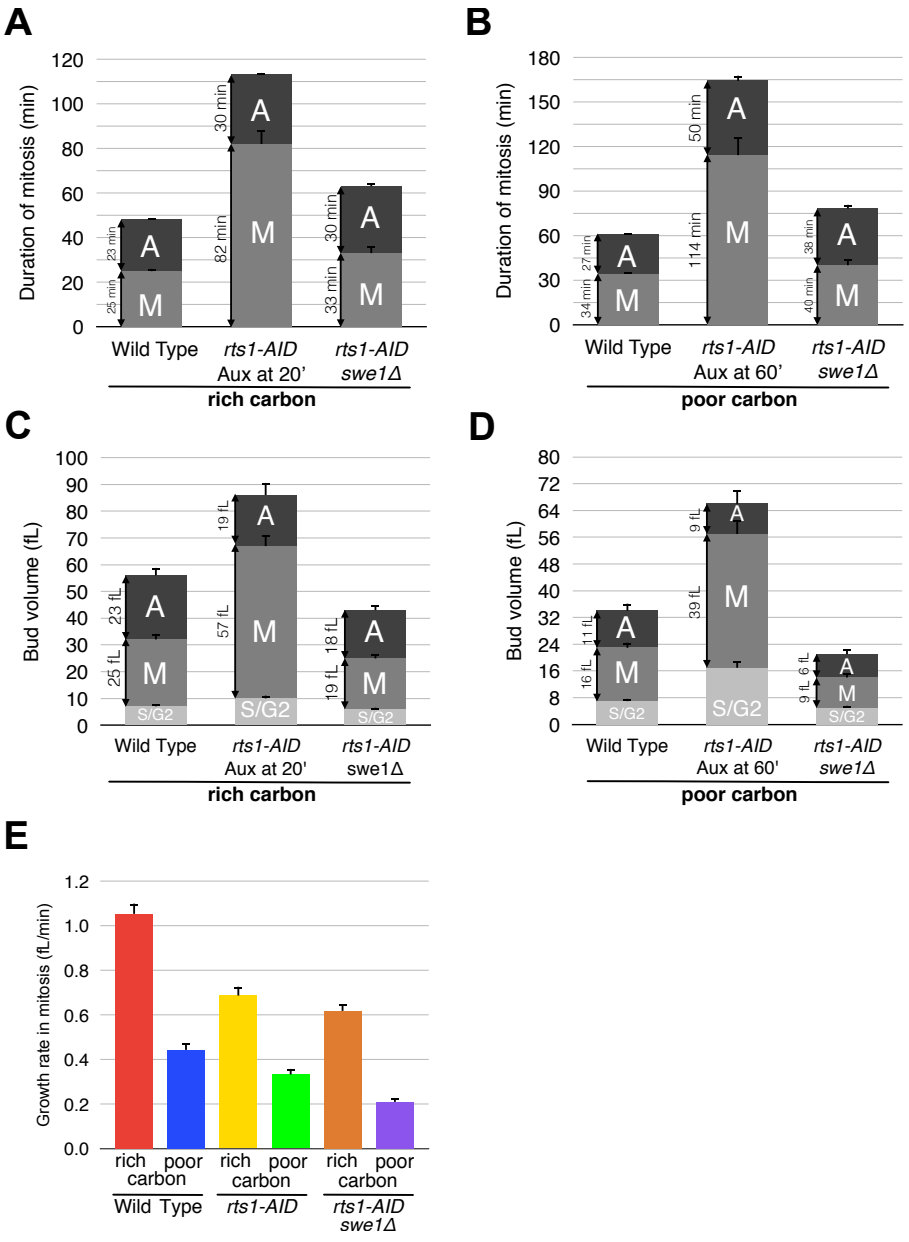

Figure 2.11. $PP2A^{Rts1}$ controls the duration of mitosis by Swe1-dependent and Swe1-independent mechanisms [microscopy]

(A) A plot showing the average durations of metaphase and anaphase for cells of the indicated genotypes growing in rich carbon. (B) A plot showing the average durations of metaphase and anaphase for cells of the indicated genotypes growing in poor carbon. (C) A plot showing the average growth in volume during metaphase and anaphase for cells of the indicated genotypes growing in rich carbon. (D) A plot showing the average growth in volume during metaphase and anaphase for cells of the indicated genotypes growing in poor carbon. (E) A plot showing the average growth rate during metaphase and anaphase in *wild type* or *swe1Δ* cells in rich or poor carbon. Error bars represent standard error of the mean.

Chapter II's Supplemental Material

Figure S2.1

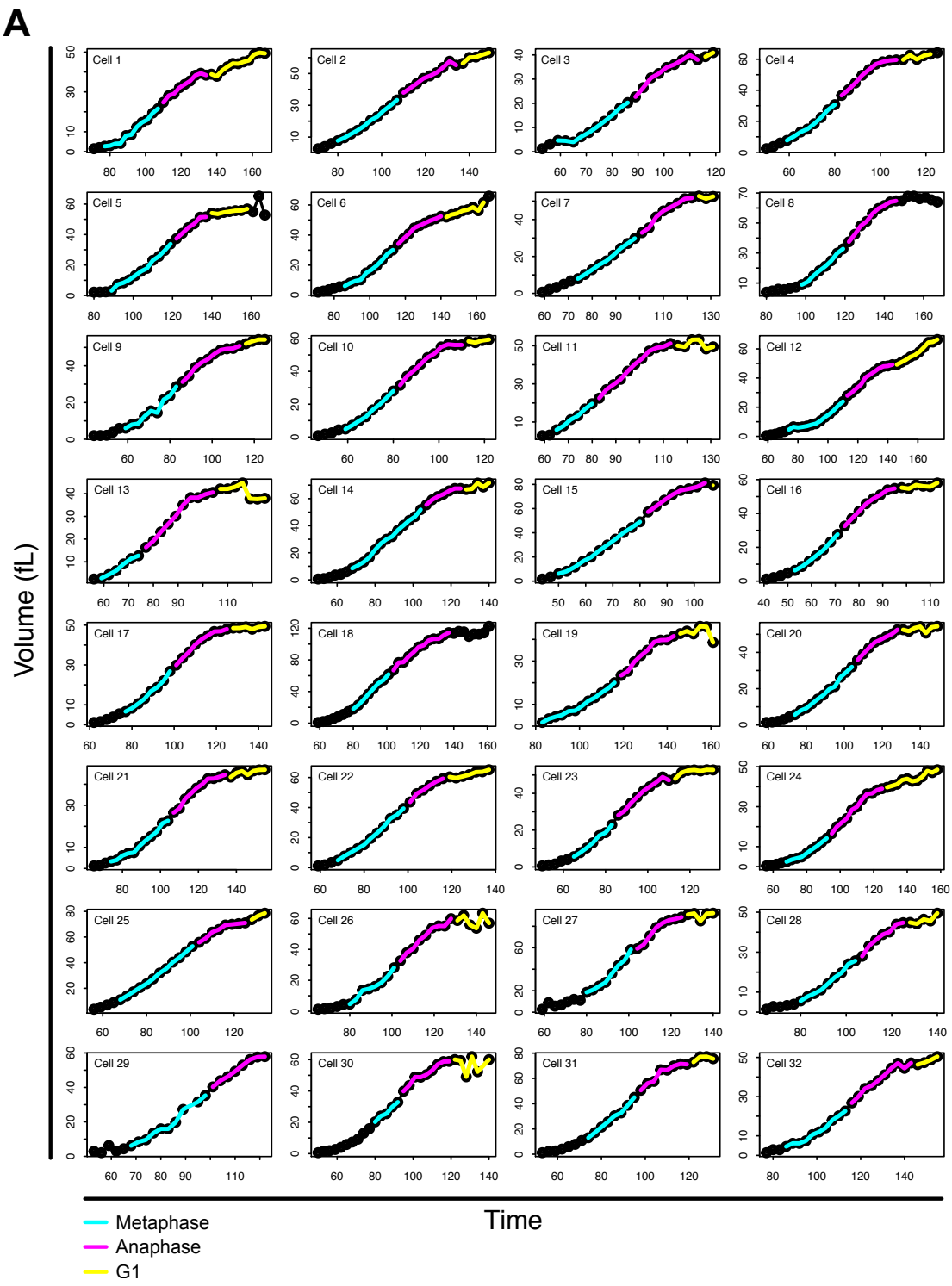
A
Cell 1
Cell 2
Cell 3
Cell 4
Cell 5
Cell 6
Cell 7
Cell 8
Cell 9
Cell 10
Cell 11
Cell 12
Cell 13
Cell 14
Cell 15
Cell 16
Cell 17
Cell 18
Cell 19
Cell 20
Cell 21
Cell 22
Cell 23
Cell 24
Cell 25
Cell 26
Cell 27
Cell 28
Cell 29
Cell 30
Cell 31
Cell 32
Volume (fL)
Time
Metaphase
Anaphase
G1

B

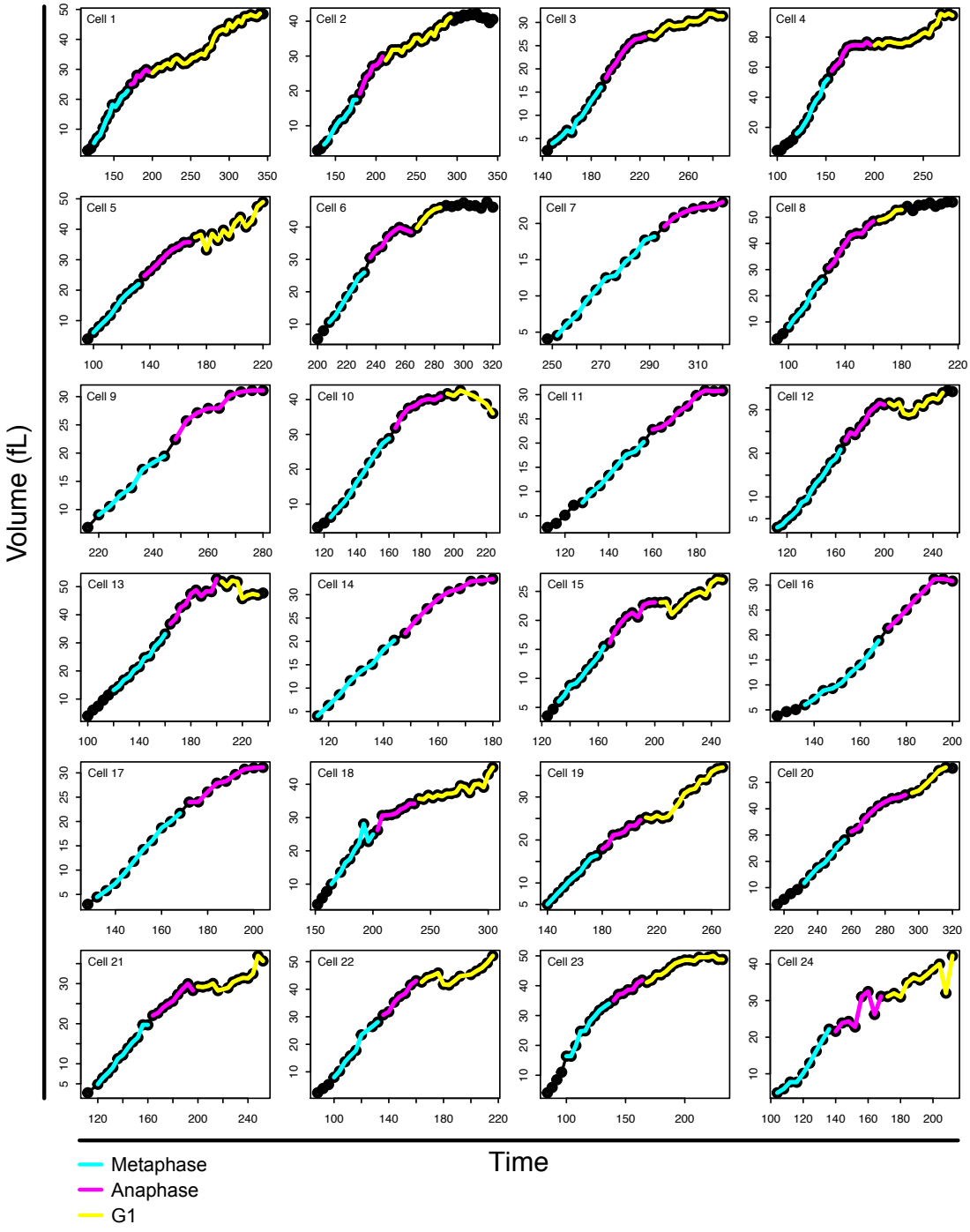
Cell 1
Cell 2
Cell 3
Cell 4
Cell 5
Cell 6
Cell 7
Cell 8
Cell 9
Cell 10
Cell 11
Cell 12
Cell 13
Cell 14
Cell 15
Cell 16
Cell 17
Cell 18
Cell 19
Cell 20
Cell 21
Cell 22
Cell 23
Cell 24
Volume (fL)
Time
Metaphase
Anaphase
G1

Figure S2.1. Growth curve data for cells growing in rich or poor carbon

Blue highlighting represents metaphase, pink represents anaphase, and yellow represents G1 phase. Curves where yellow is absent are from cells that could not be followed through a complete G1 phase or where the timing of the appearance of the daughter bud could not be determined with confidence. **(A)** Growth curves for cells growing in rich carbon. Curves for all 32 measured cells are shown. (**B**) Growth curves for cells growing in poor carbon. Several curves were omitted because they yielded clear data for one stage of mitosis, but not for others, due to imaging limitations. Data from these curves were used if they yielded high confidence data for one of the mitotic stages.

Figure S2.2

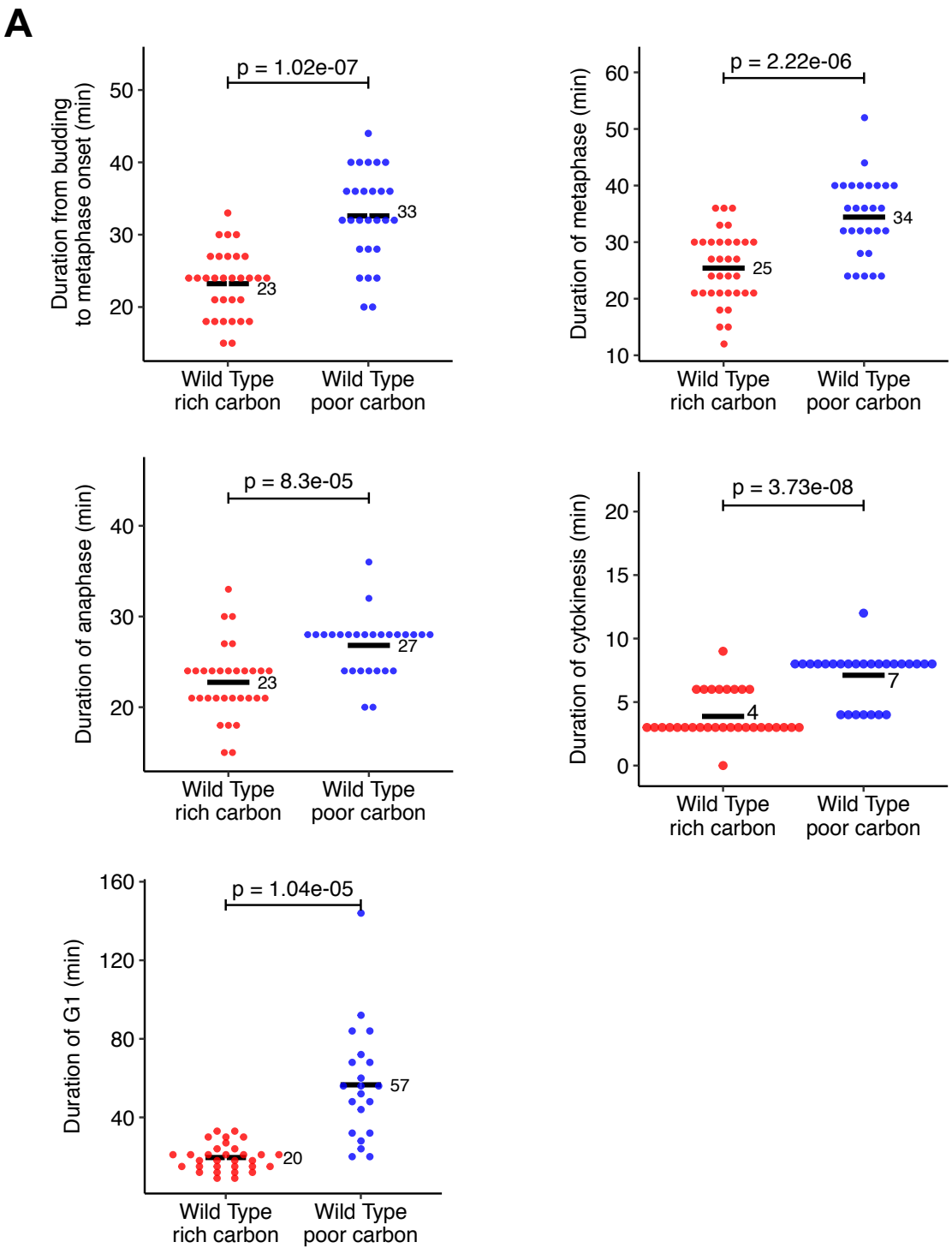
A
Duration from budding to metaphase onset (min)
p = 1.02e-07
50
40
30
20
23
33
Wild Type rich carbon
Wild Type poor carbon
Duration of metaphase (min)
p = 2.22e-06
60
50
40
30
20
10
25
34
Wild Type rich carbon
Wild Type poor carbon
Duration of anaphase (min)
p = 8.3e-05
40
30
20
23
27
Wild Type rich carbon
Wild Type poor carbon
Duration of cytokinesis (min)
p = 3.73e-08
20
15
10
5
0
4
7
Wild Type rich carbon
Wild Type poor carbon
Duration of G1 (min)
p = 1.04e-05
160
120
80
40
20
57
Wild Type rich carbon
Wild Type poor carbon

B

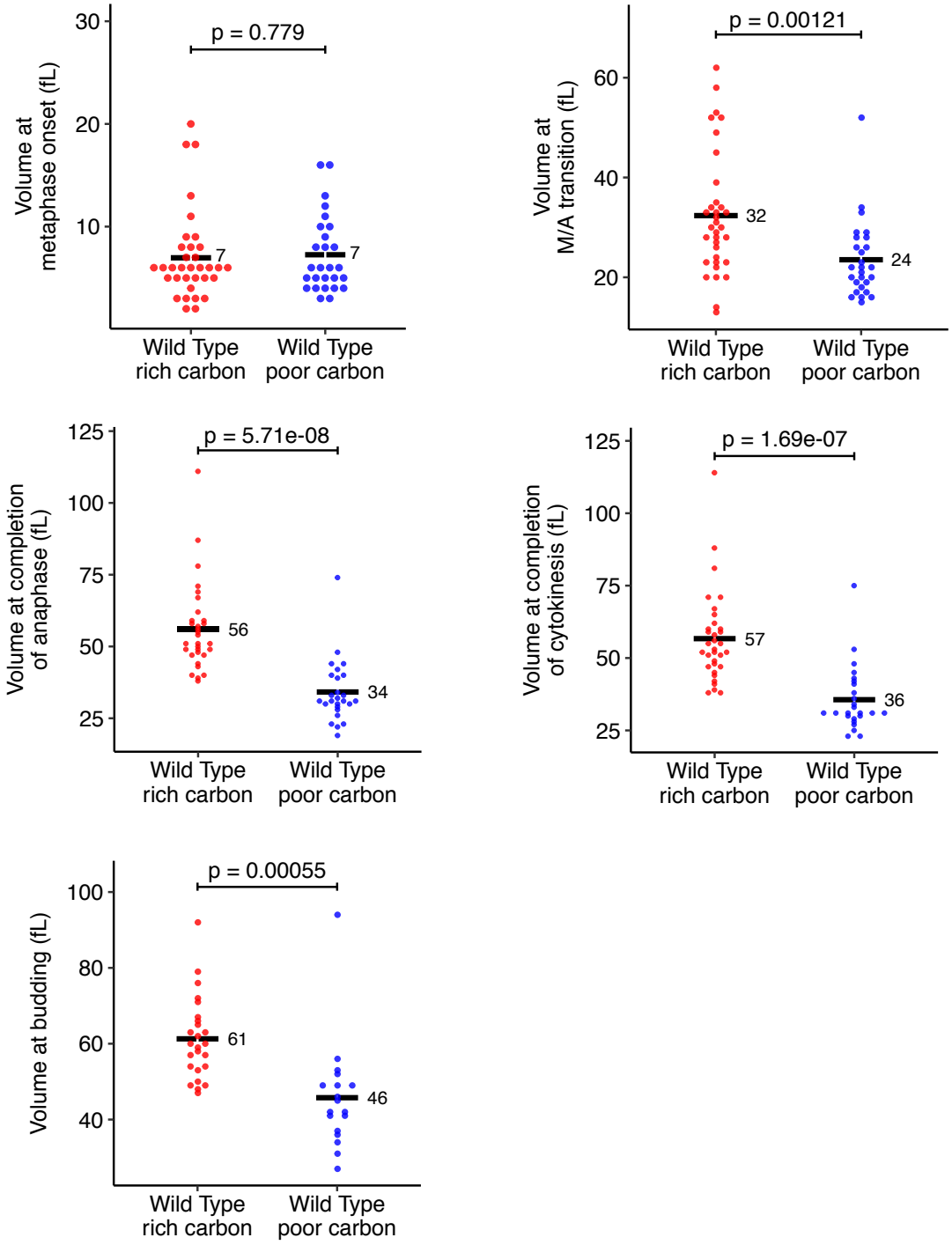
p = 0.779
Volume at metaphase onset (fL)
30
20
10
7
7
Wild Type rich carbon
Wild Type poor carbon
p = 0.00121
Volume at M/A transition (fL)
60
40
20
32
24
Wild Type rich carbon
Wild Type poor carbon
p = 5.71e-08
Volume at completion of anaphase (fL)
125
100
75
50
25
56
34
Wild Type rich carbon
Wild Type poor carbon
p = 1.69e-07
Volume at completion of cytokinesis (fL)
125
100
75
50
25
57
36
Wild Type rich carbon
Wild Type poor carbon
p = 0.00055
Volume at budding (fL)
100
80
60
40
61
46
Wild Type rich carbon
Wild Type poor carbon

Figure S2.2. Dot plot versions of the data used to generate Figure 3

Black horizontal lines and adjacent numbers represent the average value for the data in each dot plot. The significance of the difference between two conditions is given as p-values above each plot. **(A)** Dot plot version of the data used to generate Figures 3A and 3B. (**B)** Dot plot versions of the data used to generate Figure 3C.

Figure S2.3

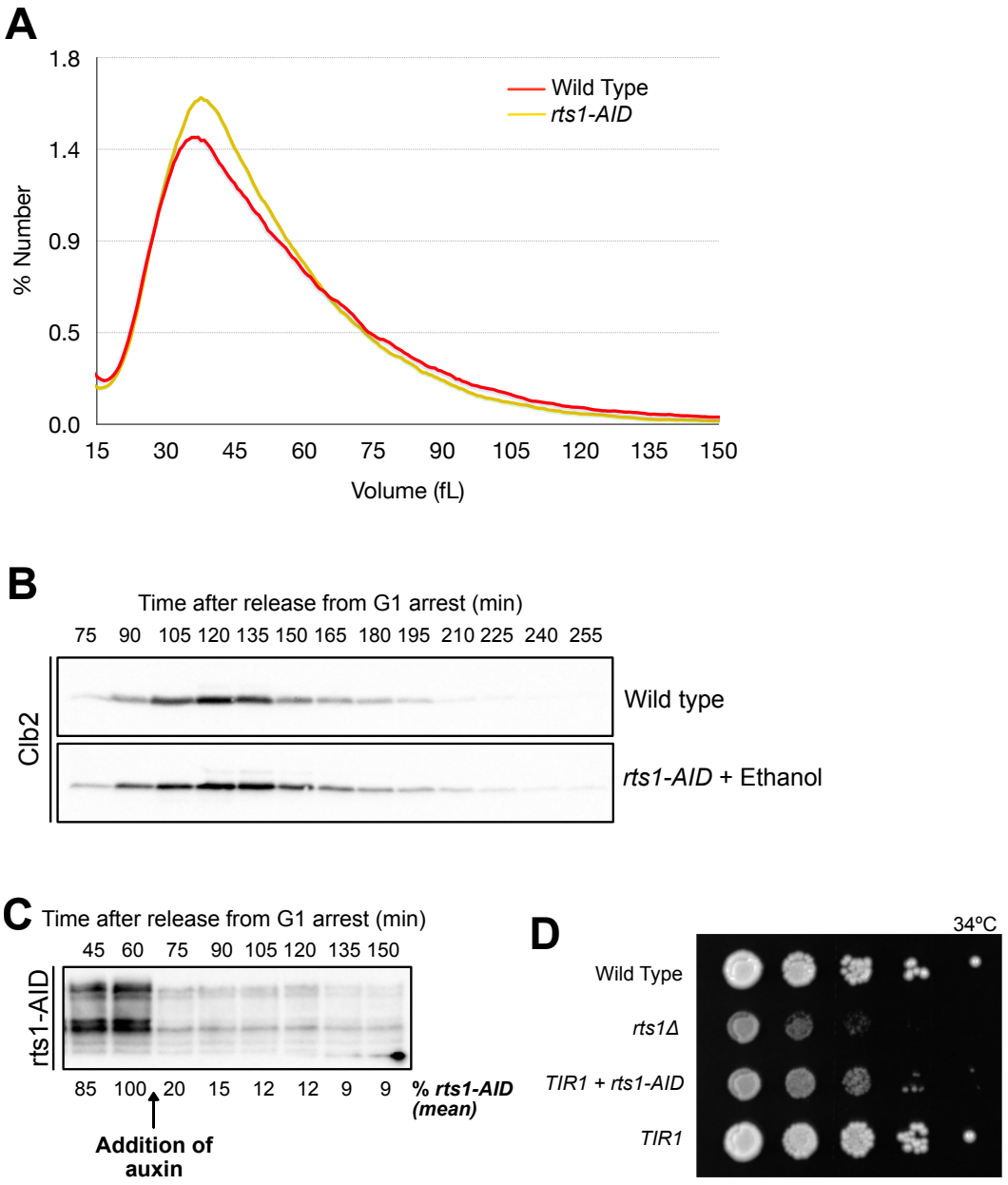
A
1.8
1.4
0.9
0.5
0.0
% Number
15 30 45 60 75 90 105 120 135 150
Volume (fL)
Wild Type
rts1-AID
B
Time after release from G1 arrest (min)
75 90 105 120 135 150 165 180 195 210 225 240 255
Clb2
Wild type
rts1-AID + Ethanol
C
Time after release from G1 arrest (min)
45 60 75 90 105 120 135 150
rts1-AID
85 100 20 15 12 12 9 9
% rts1-AID (mean)
Addition of auxin
D
34ºC
Wild Type
rts1Δ
TIR1 + rts1-AID
TIR1

Figure S2.3 Characterization of *rts1-AID* cells

(**A**) The size of *wild type* and *rts1-AID* cells grown to log phase in liquid YPD cultures was measured with a Coulter counter. (**B**) *Wild type* and *rts1-AID* cells were released from a G1 arrest in YPGE and the timing of entry into mitosis and the duration of mitosis were determined by assaying levels of the mitotic cyclin Clb2 by western blot. (**C**) rts1-AID cells were released from a G1 arrest in YPD and auxin was added at 60 minutes. Destruction of rts1-AID was assayed by western blot. The average rts1-AID signal was measured using BioRad ImagelabTM for 3 biological replicates and the mean percent of rts1-AID protein remaining at each time point is listed below each lane. (**D**) The rate of proliferation of *rts1Δ* and *rts1-AID* cells was tested by spotting a series of 10-fold dilutions of each strain on YPD+auxin at 34ºC.

Figure S2.4

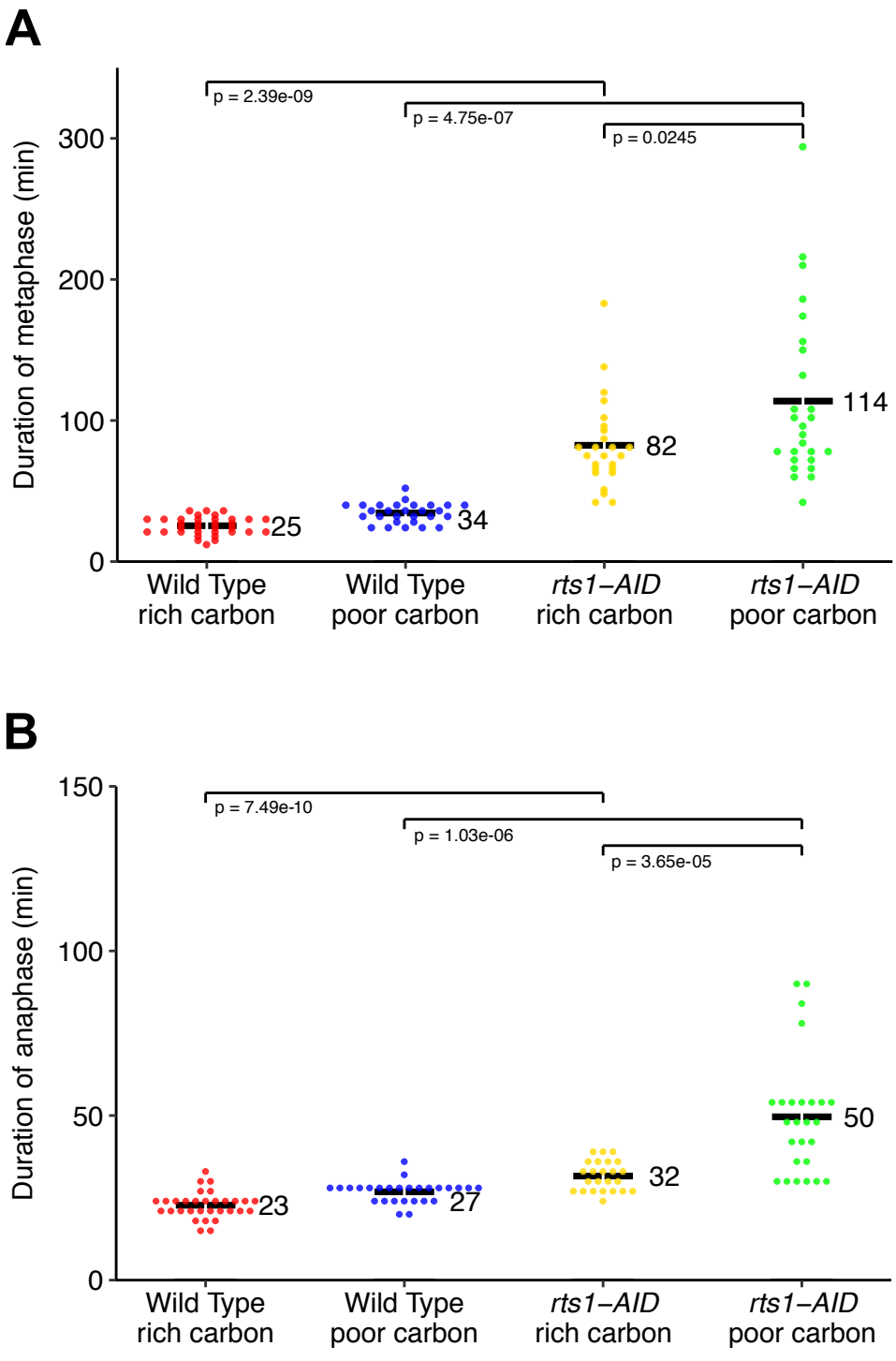
A
Duration of metaphase (min)
300
200
100
0
p = 2.39e-09
p = 4.75e-07
p = 0.0245
25
34
82
114
Wild Type
rich carbon
Wild Type
poor carbon
rts1–AID
rich carbon
rts1–AID
poor carbon
B
Duration of anaphase (min)
150
100
50
0
p = 7.49e-10
p = 1.03e-06
p = 3.65e-05
23
27
32
50
Wild Type
rich carbon
Wild Type
poor carbon
rts1–AID
rich carbon
rts1–AID
poor carbon

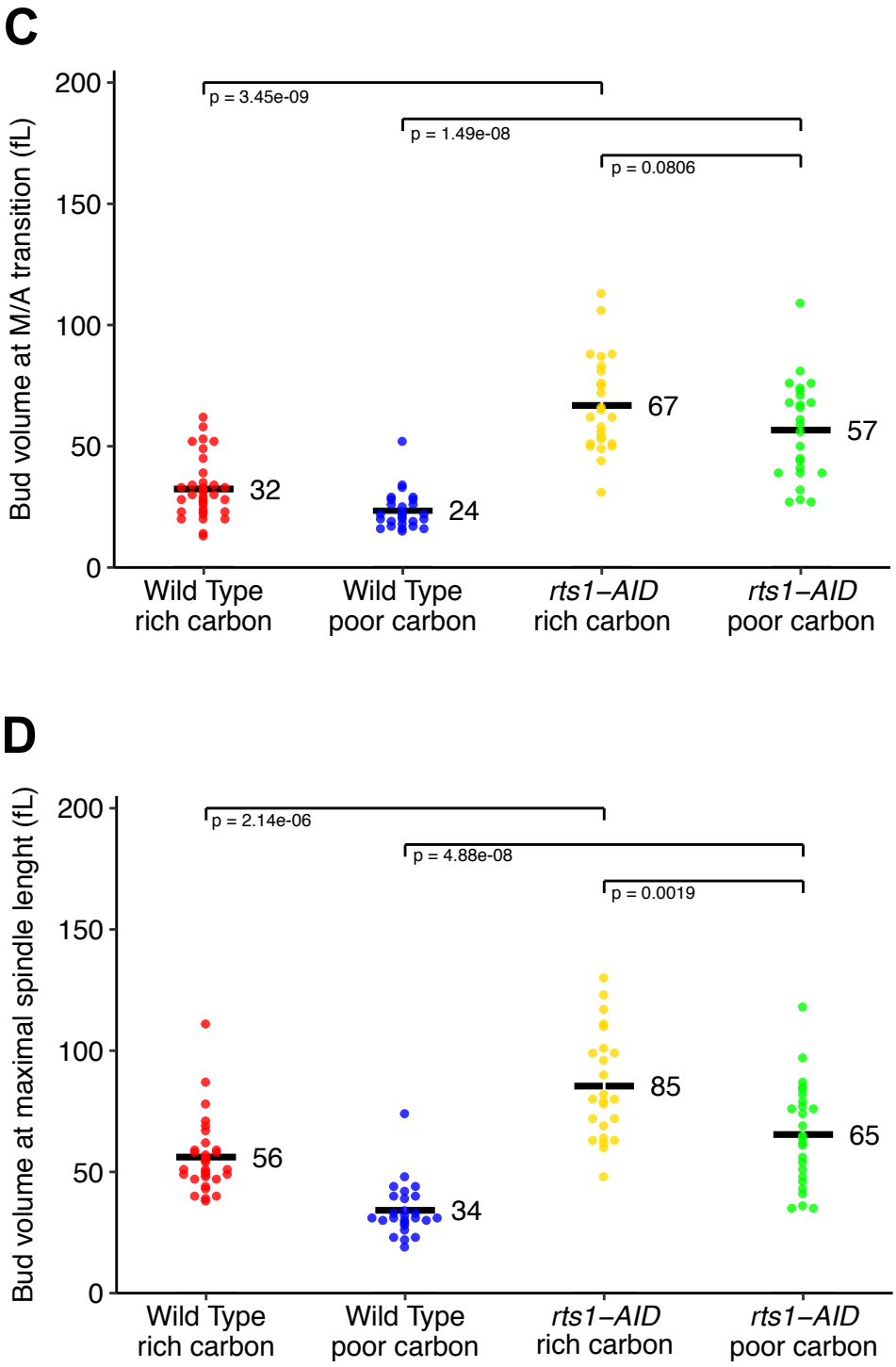
C
Bud volume at M/A transition (fL)
200
150
100
50
0
p = 3.45e-09
p = 1.49e-08
p = 0.0806
32
24
67
57
Wild Type
rich carbon
Wild Type
poor carbon
rts1–AID
rich carbon
rts1–AID
poor carbon
D
Bud volume at maximal spindle lenght (fL)
200
150
100
50
0
p = 2.14e-06
p = 4.88e-08
p = 0.0019
56
34
85
65
Wild Type
rich carbon
Wild Type
poor carbon
rts1–AID
rich carbon
rts1–AID
poor carbon

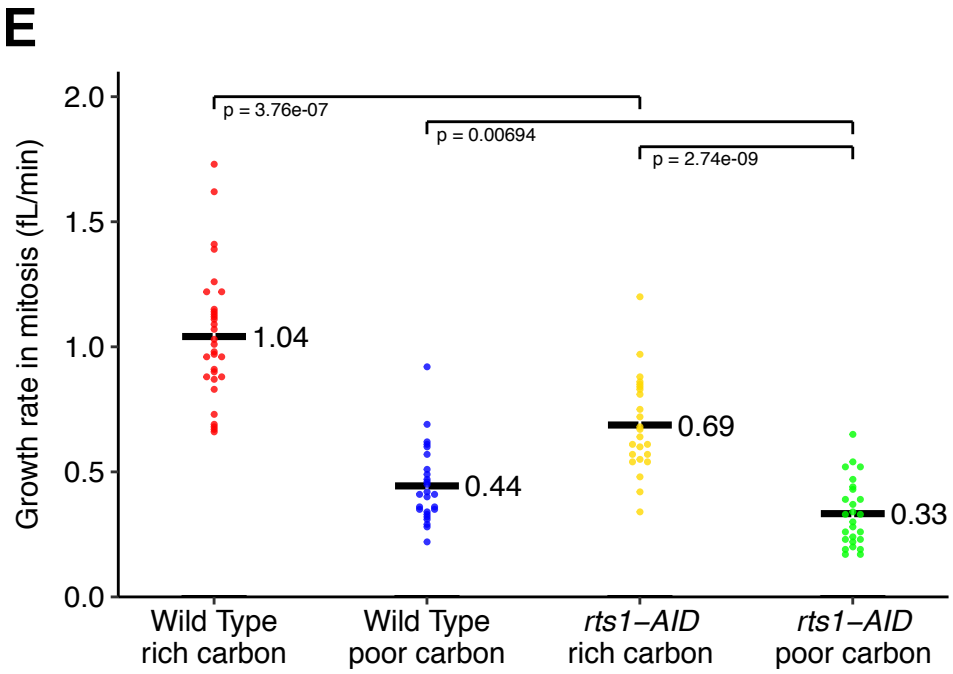
E
Growth rate in mitosis (fL/min)
2.0
1.5
1.0
0.5
0.0
p = 3.76e-07
p = 0.00694
p = 2.74e-09
1.04
0.44
0.69
0.33
Wild Type
rich carbon
Wild Type
poor carbon
rts1–AID
rich carbon
rts1–AID
poor carbon

Figure S2.4. Dot plot versions of the data used to generate Figure 7

Black horizontal lines and adjacent numbers represent the average value for the data in each dot plot. The significance of the difference between two conditions or genotypes is given as p-values below each bracket. **(A)** Dot plot versions of the data used to generate Figures 7A. **(B)** Dot plot versions of the data used to generate Figure 7B. **(C)** Dot plot versions of the data used to generate Figure 7C. **(D)** Dot plot versions of the data used to generate Figure 7D. **(E)** Dot plot versions of the data used to generate Figure 7E.

Figure S2.5

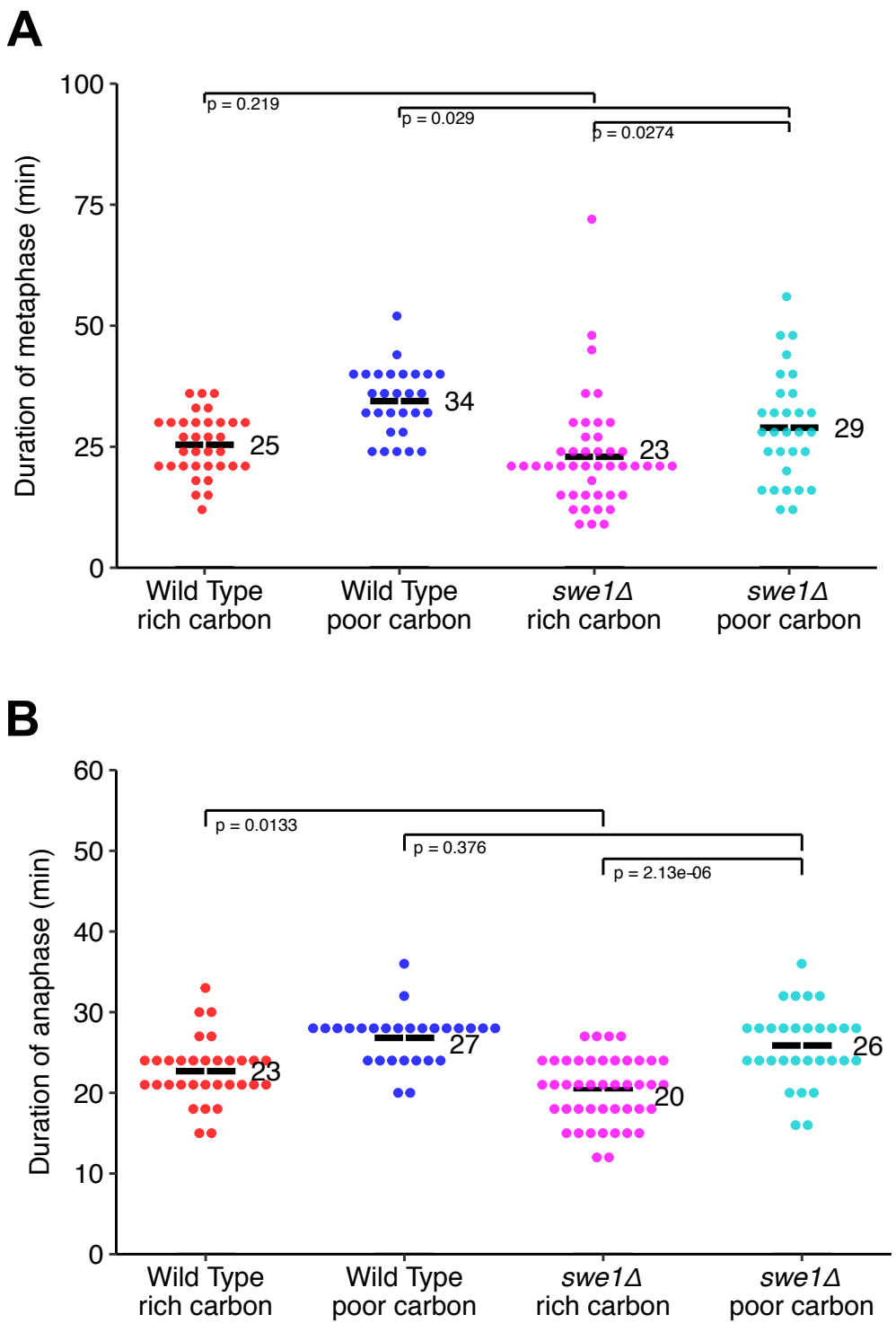
A
Duration of metaphase (min)
100
75
50
25
0
p = 0.219
p = 0.029
p = 0.0274
25
34
23
29
Wild Type rich carbon
Wild Type poor carbon
swe1Δ rich carbon
swe1Δ poor carbon
B
Duration of anaphase (min)
60
50
40
30
20
10
0
p = 0.0133
p = 0.376
p = 2.13e-06
23
27
20
26
Wild Type rich carbon
Wild Type poor carbon
swe1Δ rich carbon
swe1Δ poor carbon

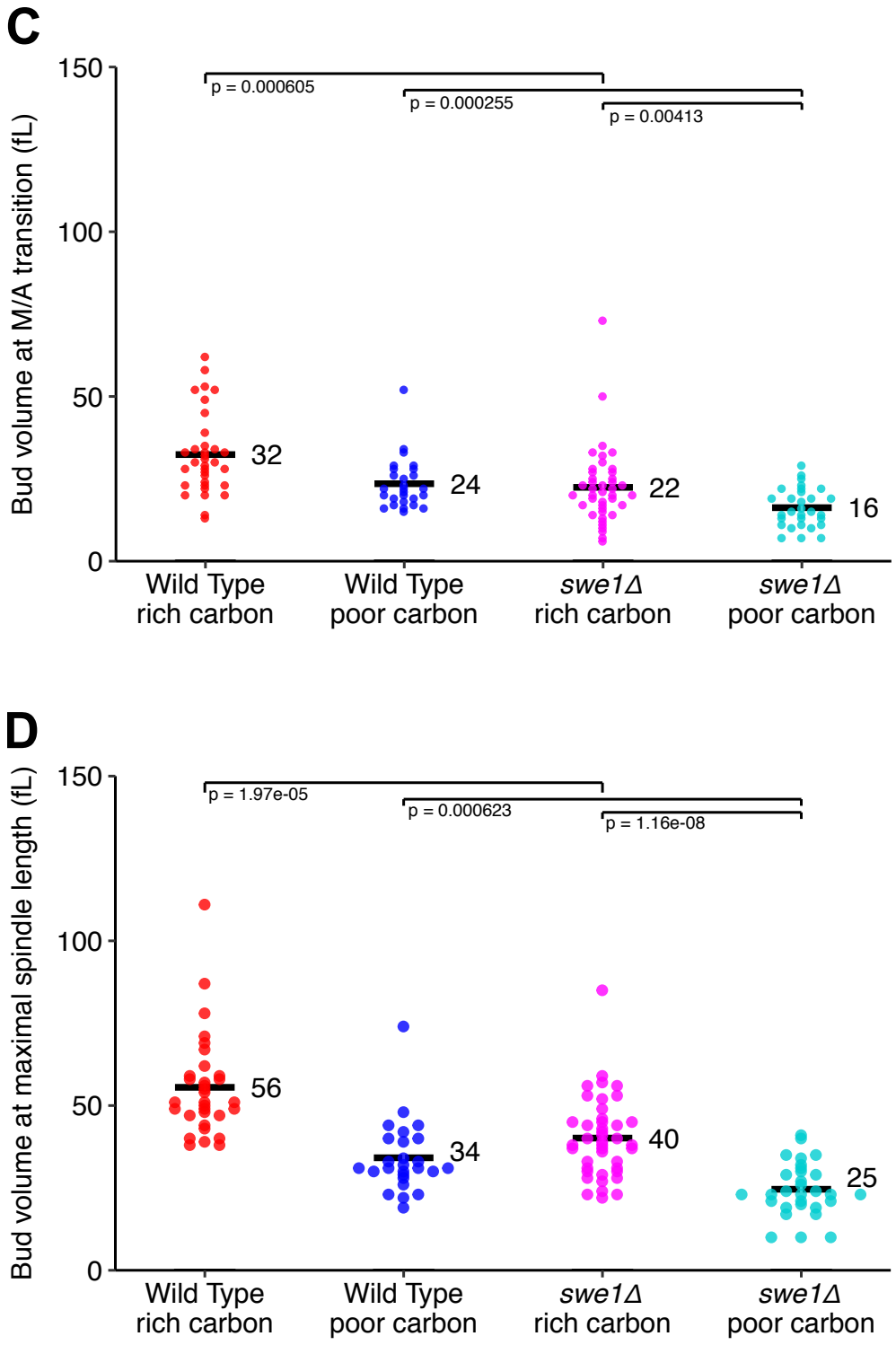
C
Bud volume at M/A transition (fL)
150
100
50
0
p = 0.000605
p = 0.000255
p = 0.00413
32
24
22
16
Wild Type
rich carbon
Wild Type
poor carbon
swe1Δ
rich carbon
swe1Δ
poor carbon
D
Bud volume at maximal spindle length (fL)
150
100
50
0
p = 1.97e-05
p = 0.000623
p = 1.16e-08
56
34
40
25
Wild Type
rich carbon
Wild Type
poor carbon
swe1Δ
rich carbon
swe1Δ
poor carbon

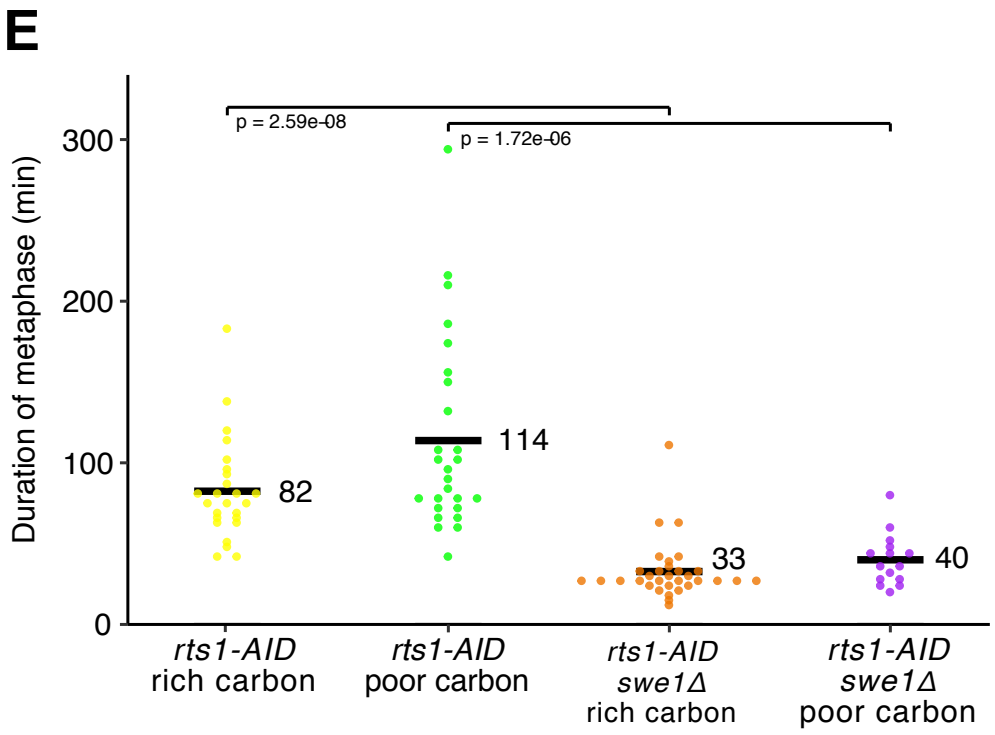
E
Duration of metaphase (min)
300
200
100
0
p = 2.59e-08
p = 1.72e-06
82
114
33
40
rts1-AID
rich carbon
rts1-AID
poor carbon
rts1-AID
swe1Δ
rich carbon
rts1-AID
swe1Δ
poor carbon

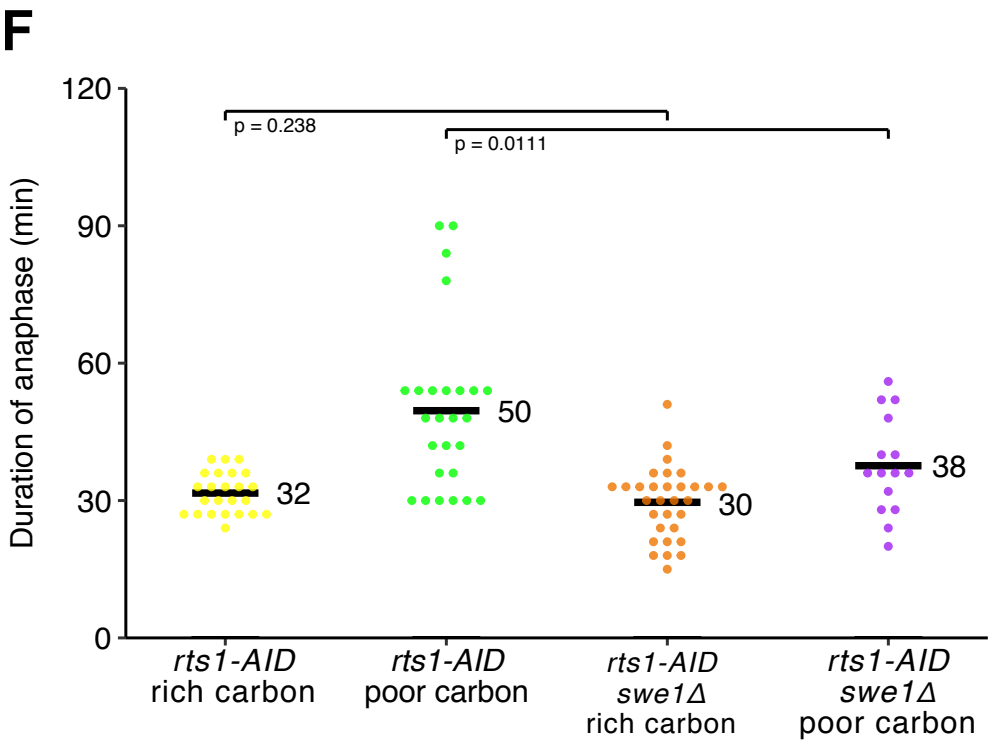
F
Duration of anaphase (min)
120
90
60
30
0
p = 0.238
p = 0.0111
32
50
30
38
rts1-AID
rich carbon
rts1-AID
poor carbon
rts1-AID
swe1Δ
rich carbon
rts1-AID
swe1Δ
poor carbon

G

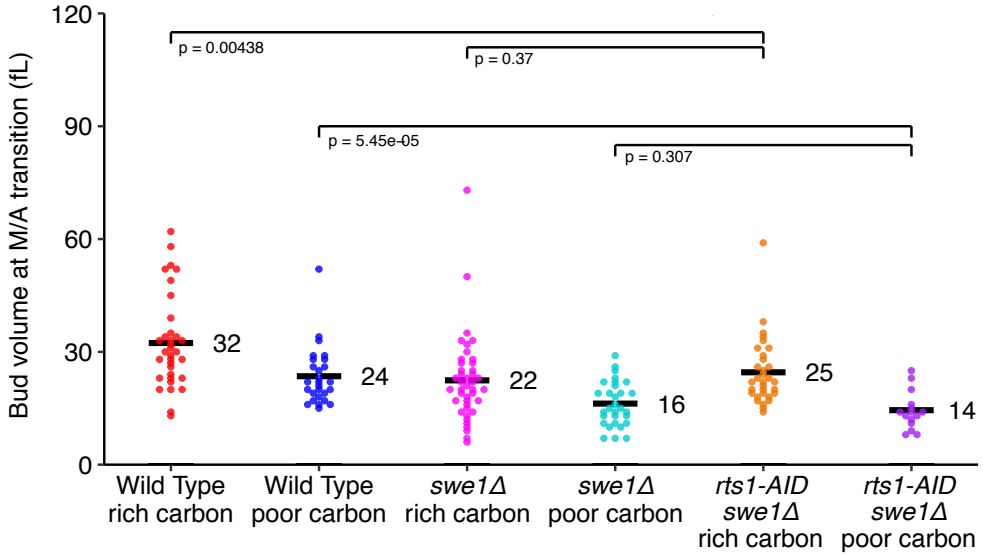
Bud volume at M/A transition (fL)
120
90
60
30
0
p = 0.00438
p = 0.37
p = 5.45e-05
p = 0.307
32
24
22
16
25
14
Wild Type rich carbon
Wild Type poor carbon
swe1Δ rich carbon
swe1Δ poor carbon
rts1-AID swe1Δ rich carbon
rts1-AID swe1Δ poor carbon

H

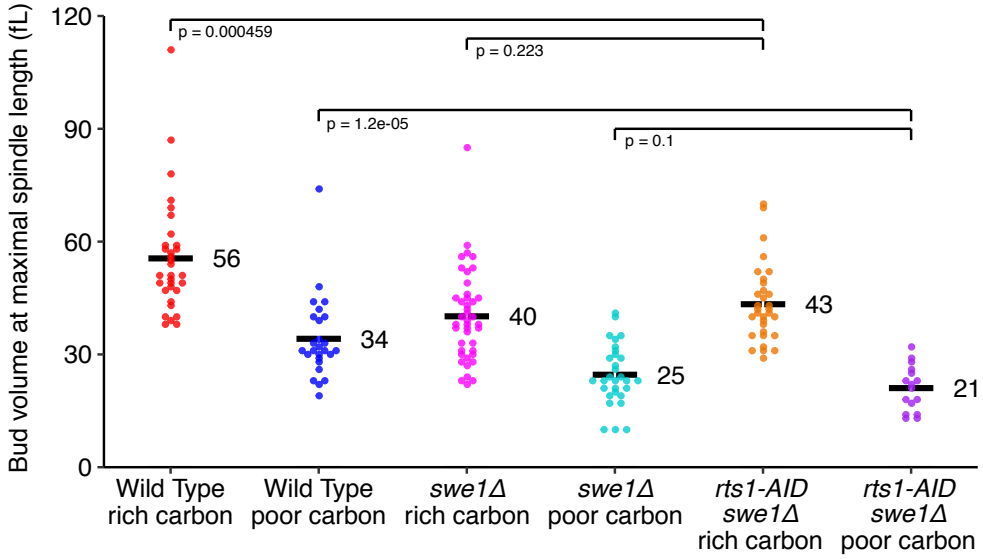
Bud volume at maximal spindle length (fL)
120
90
60
30
0
p = 0.000459
p = 0.223
p = 1.2e-05
p = 0.1
56
34
40
25
43
21
Wild Type rich carbon
Wild Type poor carbon
swe1Δ rich carbon
swe1Δ poor carbon
rts1-AID swe1Δ rich carbon
rts1-AID swe1Δ poor carbon

Figure S2.5. Dot plot versions of the data used to generate Figures 9 and 11

Black horizontal lines and adjacent numbers represent the average value for the data in each dot plot. The significance of the difference between two conditions or genotypes is given as p-values below each bracket. **(A,B)** Dot plot versions of the data used to generate Figures 9A and 9B. **(C,D)** Dot plot versions of the data used to generate Figure 9D and 9E. **(E,F)** Dot plot versions of the data used to generate Figures 11A and 11B. **(G,H)** Dot plot versions of the data used to generate Figures 11C and 11D.

CHAPTER III [ADDITIONAL EXPERIMENTS]: The duration of mitosis is controlled by $PP2A^{Rts1}$ via Swe1-dependent and Swe1-independent mechanisms

In this *Chapter I* will present additional unpublished results that, together with the results presented in *Chapter II*, provide further support for the existence of a mitotic cell size checkpoint.

Rts1 undergoes nutrient induced phosphorylation changes

In *Chapter II* I have demonstrated that shifting cells from rich to poor carbon induces a prolonged mitotic delay, with cells arresting with short spindles (a.k.a., metaphase spindles). Furthermore, I have shown that $PP2A^{Rts1}$ is required for timely progression through mitosis. Cells that lack the regulatory subunit Rts1 spend 3 times longer in metaphase when compared to *wild type* cells. Together, these data suggest that the increased duration of mitosis in poor carbon source could be the result of loss of $PP2A^{Rts1}$ activity. Protein activity is often associated with phosphorylation changes that can often be observed by western blotting. It is known that Rts1 does not suffer great changes in phosphorylation that can be seen by western blotting during an unperturbed cell cycle (Zapata, 2014). However, it has also been reported that Rts1 becomes hyperphosphorylated when cells are shifted from rich to poor carbon (Zapata, 2014). Here we test the hypothesis that nutrient shifts induce a mitotic delay that is accompanied by changes in Rts1 phosphorylation. We tested this hypothesis by growing synchronized cells in rich carbon and shifting them to poor carbon when Clb2 reached peak levels and most cells had short mitotic spindles. We then assayed for the levels of Rts1 by western

blotting. Our results indicate that Rts1 undergoes large phosphorylation changes immediately after a shift to poor carbon during mitosis (**Figure 3.1**). Furthermore, Rts1 remained hyperphosphorylated for the duration of the delay and progressively becomes dephosphorylated as the levels of Clb2 drop down. When cells complete mitosis, determined by the loss of Clb2 and lack of long anaphase spindles, Rts1 exists predominantly in a mid-phosphoform, similar to what is observed in cells continuously grown in rich carbon.

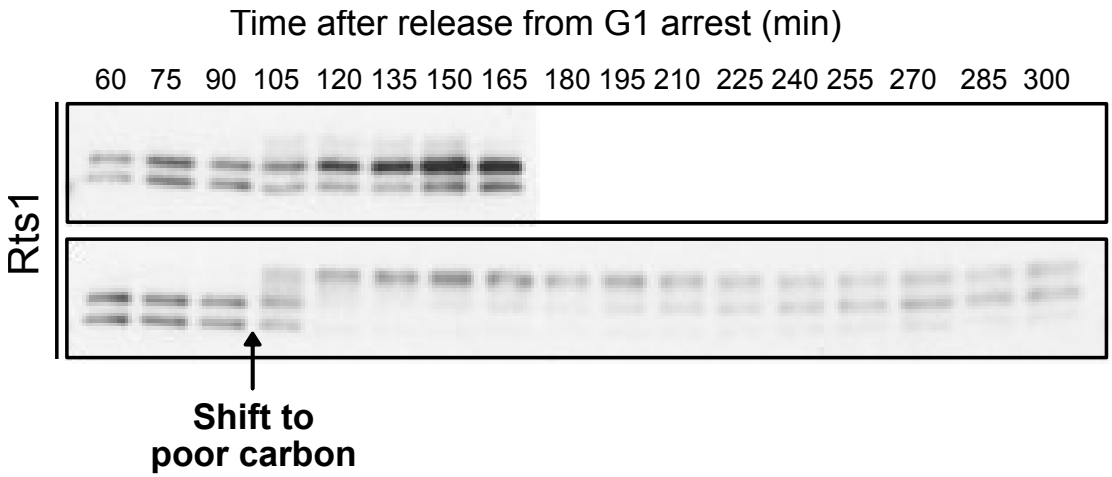

Figure 3.1. Rts1 becomes hyperphosphorylated when cells are shifted to poor carbon

Wild type cells were arrested in G1 using mating pheromone. Cells were released from the arrest, the culture was split and and samples were collected every 15min. At 90min post release both cultures were washed by centrifugation with either YPD (no shift in carbon condition) or YPge (shift to poor carbon). Samples were collected until 165min for control non-shifted cells and 300min for cells shifted to poor carbon. The samples were resolved via western blot and probed for Rts1.

Loss of Gin4 induces a prolonged Swe1 dependent mitotic delay

It has been previously proposed that Rts1 controls Swe1 via the Gin4 kinase (Zapata, 2014). This assumption has been formulated from multiple experiments that associate Rts1, Gin4 and mitotic delays, but it has never been thoroughly tested. For example, in *Chapter II* I have demonstrated that *rts1Δ* induces a mitotic delay that is dependent on Swe1. Similarly, log-phase cultures of *gin4Δ* cells are often associated with high levels of Clb2 and a high number of short mitotic spindles (Altman & Kellogg, 1997). In addition, our mass spec analysis reveals that *rts1Δ* cells not only have high levels of phosphorylated Swe1 and associated high levels of Swe1-dependent Cdk1 inhibitory phosphorylation, but also an increase in Gin4 phosphorylation. Finally, it has been previously reported that loss of Hsl1, a Gin4 related kinase, leads to accumulation of Swe1 in a partially phosphorylated form (Okuzaki, Watanabe, Tanaka, & Nojima, 2003; Shulewitz, Inouye, & Thorner, 1999). This semi-phosphorylated state of Swe1 has been described as active Swe1 (Harvey, Charlet, Haas, Gygi, & Kellogg, 2005). Together, these evidence support the hypothesis that loss of Rts1 induces a mitotic delay that is due to loss of Gin4 activity on Swe1. As a result, Swe1 would remain hyperactive and the cell cycle would delay due to persistent Cdk1 inhibitory phosphorylation.

A preliminary approach to test this hypothesis consists in determining if loss of Gin4 induces a mitotic delay that, like Rts1, is the result of Cdk1 inhibitory phosphorylation. To do so we released *gin4Δ* cells from a G1 arrest and assayed the levels of Clb2 and Cdk1-Y19 inhibitory phosphorylation (Cdk1-Y19Ⓟ) via western blot. Our results demonstrate that *gin4Δ* cells enter mitosis late and spend an increased time in mitosis, as revealed by the levels of Clb2. Appearance of Clb2 is delayed for at least 15min, in agreement with Gin4's role in controlling growth prior to mitosis. Once Clb2 is expressed it persisted at high levels for a long period of time, suggesting an increased duration of mitosis (**Figure 3.2A**). We have also tested

whether cells were indeed delaying in mitosis by analyzing mitotic spindles from the same samples used for western blotting. Our data indicates that the Clb2 delay occurs when most cells have short mitotic spindles (**Figure 3.2B**). Furthermore, this delay is accompanied by highly increased and persistent levels of Cdk1 inhibitory phosphorylation (**Figure 3.2C**), suggestive of Swe1 hyperactivity.

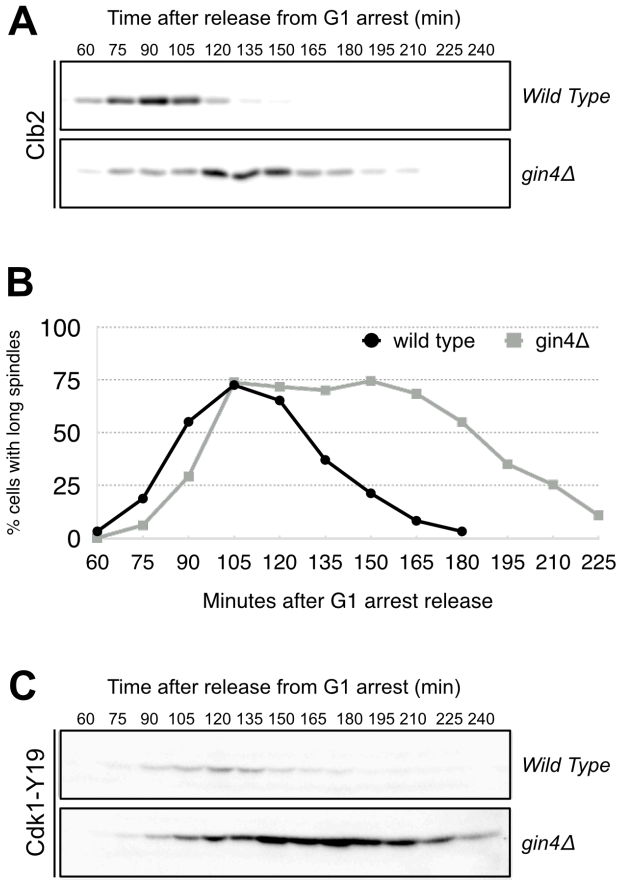

Figure 3.2. *gin4Δ* cells delay in mitosis with high levels of Cdk1 inhibitory phosphorylation

Wild Type and *gin4Δ* cells were arrested in G1 using mating pheromone. Cells were released from the arrest and samples were collected at 15min intervals for western

blotting and immunofluorescence analysis. a) cells were probed for Clb2, b) fixed cells were stained with anti-tubulin antibody and the number of short mitotic spindles analyzed, c) samples were probed for Cdk1-Y19Ⓟ.

In order to test whether the observed delay is due to Swe1 hyperactivity over Cdk1, as opposed to a failure to dephosphorylate Cdk1 by an opposing phosphatase, we probed for Swe1 protein by western blotting. The hypothesis suggests that *gin4Δ* induces Swe1 hyperactivity in a fashion similar to that of deleting the related kinase Hsl1, which can be observed by western blotting as a failure to hyperphosphorylate Swe1. Our results show that in *gin4Δ* cells Swe1 failed to become hyperphosphorylated (**Figure 3.3**) and lasted for as long as the levels of Cdk1 phosphorylation (**Figure 3.2**). Together, these data suggests that Swe1 is hyperactive in a *gin4Δ* strain.

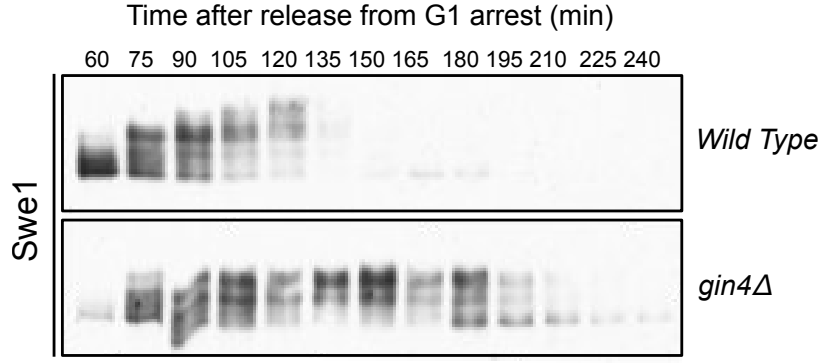

Figure 3.3. Swe1 fails to become hyperphosphorylated in *gin4Δ* cells
Wild Type and *gin4Δ* cells were arrested in G1 using mating pheromone. Cells were released from the arrest and samples were collected at 15min intervals for western blotting and probed for Swe1.

To fully demonstrate that the mitotic delay observed in *gin4Δ* is due to Swe1 hyperactivity we tested whether *swe1Δ* rescues the delay. A double mutant lacking both *Gin4* and *Swe1* spends as much time in mitosis as a *wild type* strain, judging by the levels of Clb2 protein (**Figure 3.4A**) and the number of mitotic spindles (**Figure 3.4B**). An implication derived from this result is that the increased duration of mitosis observed in poor carbon is due to a failure to inactivate Swe1 (as previously reported).

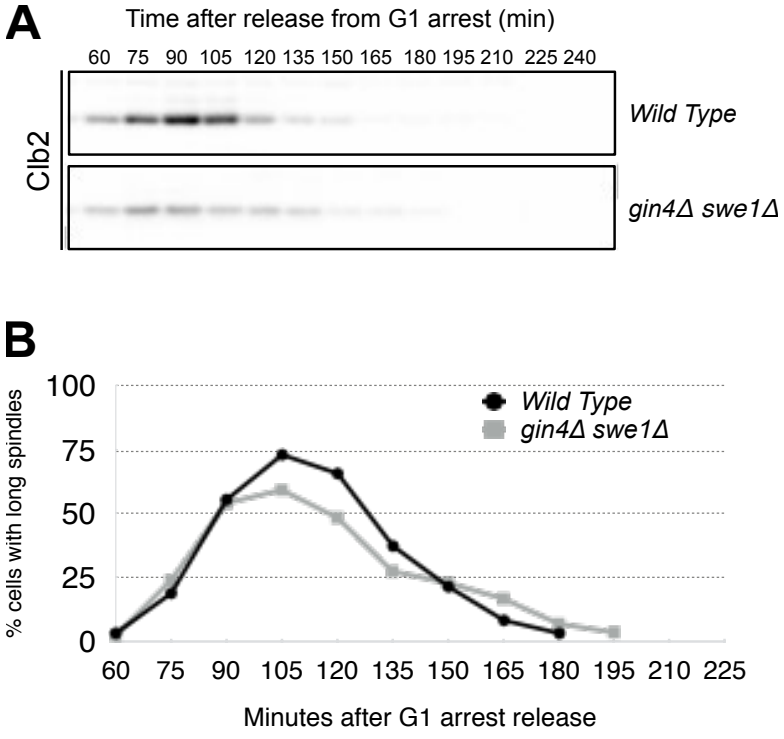

Figure 3.4. Cells lacking both *gin4* and *swe1* progress normally through mitosis

Wild type and the *gin4Δ swe1Δ* double deletion cells were arrested in G1 using mating pheromone. Cells were released from the arrest and samples were collected at 15min intervals for western blotting and immunofluorescence analysis. a) cells were probed for Clb2, b) fixed cells were stained with anti-tubulin antibody and the number of short mitotic spindles analyzed.

Because Gin4 has been previously proposed to be involved in other cell cycle related events, such as G2 and cytokinesis we decided to test for the effects of conditional loss of Gin4 protein. To do so we created a strain harboring an auxin inducible degron version of Gin4 (gin4-AID). Due to the partially redundant effects of the related kinase Hsl1 we AID-tagged Hsl1 in the same strain. Degradation of gin4-AID and hsl1-AID is robust but requires about 30min of exposure to auxin. To test its effects we synchronized cells in G1 using mating pheromone and released them from the arrest, adding auxin 30min prior to appearance of peak Clb2 levels. Loss of Gin4/Hsl1 causes cells to arrest the cell cycle with high levels of Clb2. The arrest is Swe1 dependent as cells lacking Swe1 do not delay in mitosis upon addition of auxin (**Figure 3.5**).

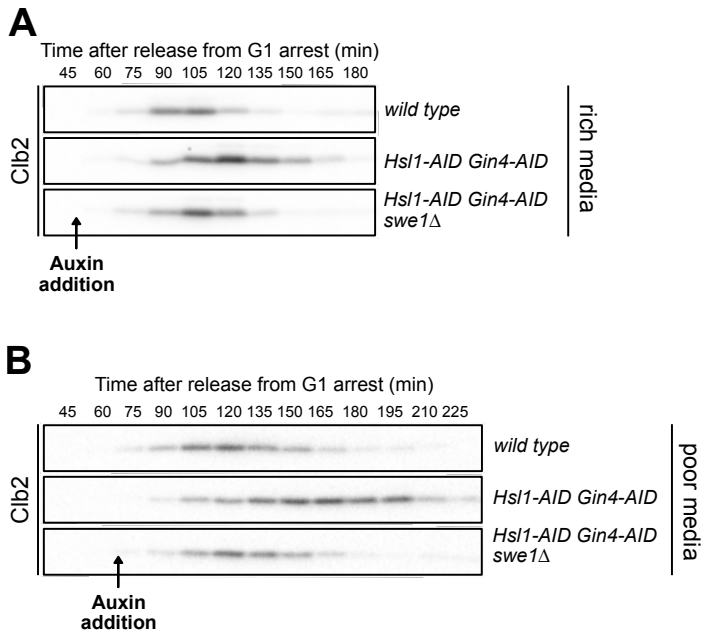

Figure 3.5. Conditional loss of Gin4/Hsl1 induces a Swe1-dependent mitotic delay

Control cells, growing in either rich (A) or poor (B) carbon sources were arrested in G1 alongside strains harboring degron versions of Gin4 and Hsl1 with and without

swe1Δ. Cells were released from the arrest and auxin was added to all flasks at 45 min (A) or 60min (B), post release. Samples were collected at 15min intervals for western blotting and probed for Clb2.

Finally, the evidence that both *rts1Δ* and *gin4Δ* cells have highly increased levels of Cdk1 inhibitory phosphorylation, and loss of Swe1 rescues both the effects of loss of Rts1 and of Gin4/Hsl1, it is arguable that Rts1 might control Swe1 activity via Gin4. We then tested whether loss of Rts1 or a shift to poor carbon has effects on Gin4. First, loss of rts1 leads to hyperphosphorylation of Gin4, as reported by the mass spectrometry data and western blotting. Second, *rts1Δ* cells fail to dephosphorylate Gin4 after a shift to poor carbon, suggesting that Gin4 dephosphorylation is $PP2A^{Rts1}$ dependent. On the other side, *wild type* cells shifted to poor carbon dephosphorylated Gin4 quickly but temporarily. After 20-30min in poor media Gin4 was, however, back to a high phosphorylation state.

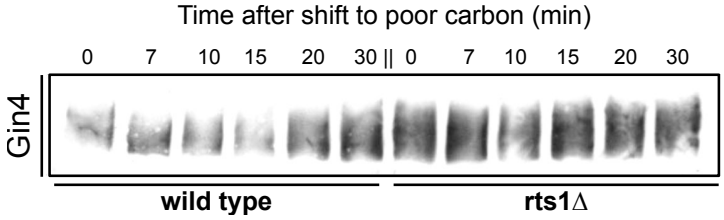

Figure 3.6. Shift to poor carbon induces Rts1-dependent Gin4 dephosphorylation

Wild type and *rts1Δ* cells grown in rich carbon were shifted to poor carbon and samples collected pr-e and post-shift, at increasing intervals, tested for Gin4 phosphorylation via western blot.

Mitotic dephosphorylation of Gin4 is delayed upon shift to poor carbon

The evidence that cells lacking Rts1 have increased phosphorylation of Gin4, as determined by mass spec, led us to speculate on the levels of Gin4 phosphorylation: is Gin4 dephosphorylation required for mitotic progression?

Cell cycle analysis of Gin4 reveals that phosphorylation of Gin4 is correlated with the increase in Clb2 levels. In addition, Gin4 remains phosphorylated for as long as the levels of Clb2 remain high. Together, these observations would suggest that Gin4 dephosphorylation would be required for cells to complete mitosis (Figure 3).

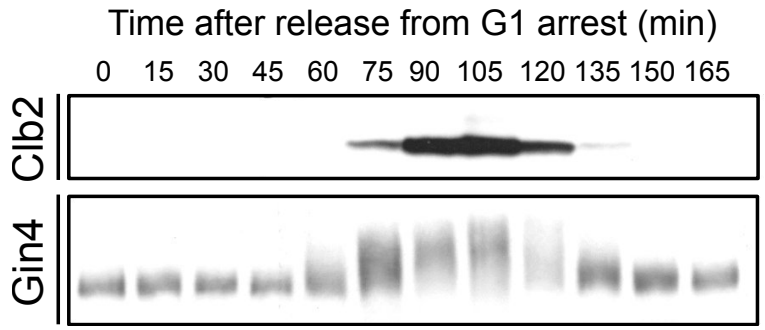

Figure 3.7. Gin4 dephosphorylation coincides with completion of mitosis
Wild type cells were arrested in G1 using mating pheromone. Cells were released from the arrest and samples were collected every 15min. The samples were resolved via western blot and probed for Clb2 and Gin4.

We next tested whether the delay observed when cells are switched to poor carbon during mitosis was accompanied by Gin4 phosphorylation changes. *Wild type* cells synchronized in G1 were released into the cell cycle and switched to poor carbon when most cells were in metaphase. Samples were collected every 15 min and probed for Gin4 via western blot. A switch to poor carbon had no noticeable

immediate effect on Gin4 phosphorylation with the exception that dephosphorylation of Gin4 was delayed. It is plausible that the large gap between time points did not allow us to observed sudden changes in Gin4 phosphorylation as observed in log-phase cells, where samples were collected more frequently. In addition, when log-phase cells are switched to poor carbon a fraction of those cells will be above the size threshold required for completion of mitosis in poor carbon. It would be expected, therefore, that in a subpopulation of cells Rts1 activity would dephosphorylate Gin4 as cells progress through mitosis. Alternatively, it is possible that the delay in mitosis is simply due to a failure to activate Gin4 towards Swe1, leading to Swe1 hyperactivity.

Figure 3.8. Mitotic dephosphorylation of Gin4 is delayed upon shift to poor carbon

Wild type cells were arrested in G1 using mating pheromone. Cells were released from the arrest, the culture was split, and samples were collected every 15min. At 90min post release both cultures were washed by centrifugation with either YPD (no shift in carbon condition) or YPge (shift to poor carbon). Samples were collected until 165min for control non-shifted cells, and 300min for cells shifted to poor carbon. The samples were resolved via western blot and probed for Gin4.

Cells shifted to poor carbon during mitosis delay in metaphase independently of Swe1

In *Chapter II* we reported that Swe1 delays mitotic progression in an unperturbed cell cycle giving cells more time for growth. Loss of Swe1, consequently, results in shorter mitosis and reduced cell size at completion of mitosis. Loss of Rts1, on the other hand, delays cell cycle progression in a pathway that is epistatic with Swe1. These results made us hypothesize that the mitotic delay observed when cells are switched from rich to poor carbon is equally due to Swe1 activity. One possible scenario predicts that when switched to poor carbon Rts1 is inactivated and Swe1 remains active for a longer period of time. Several pieces of evidence corroborate this hypothesis. First, cells shifted from rich to poor carbon delay in mitosis with increased phosphorylation of Rts1 and persistent phosphorylation of Gin4. In addition, *rts1Δ* also results in increased phosphorylation of Gin4, as observed by mass spec analysis. Together, these results suggest that a switch to poor carbon might result in a mitotic delay by mechanisms similar to those occurring in *rts1Δ* cells. For these reasons, we decided to test whether the mitotic delay observed after shift to poor nutrients is due to Swe1 hyperactivity. Because hyperphosphorylated Rts1 is likely inactive we expected to see persistent Swe1 activity after shift to poor nutrients. Swe1 activity can, in part, be analyzed from its phosphorylation state (as described in **Figure 3.3**). Here we tested the levels of Swe1 phosphorylation by western blot as we shift cells from rich to poor carbon. Shifting cells to poor carbon when Clb2 levels peak and most cells are in metaphase occurs after Swe1 full hyperphosphorylation, and its phosphorylation state remains high for the duration of the delay (**Figure 3.9**). This level of Swe1 hyper-phosphorylation is believed to represent inactive Swe1 and it is the state that commonly precedes Swe1 degradation. In stark opposition to what was previously

believed, this data suggests that the delay observed occurs at a time when Swe1 is inactive and thus the delay might be Swe1 independent.

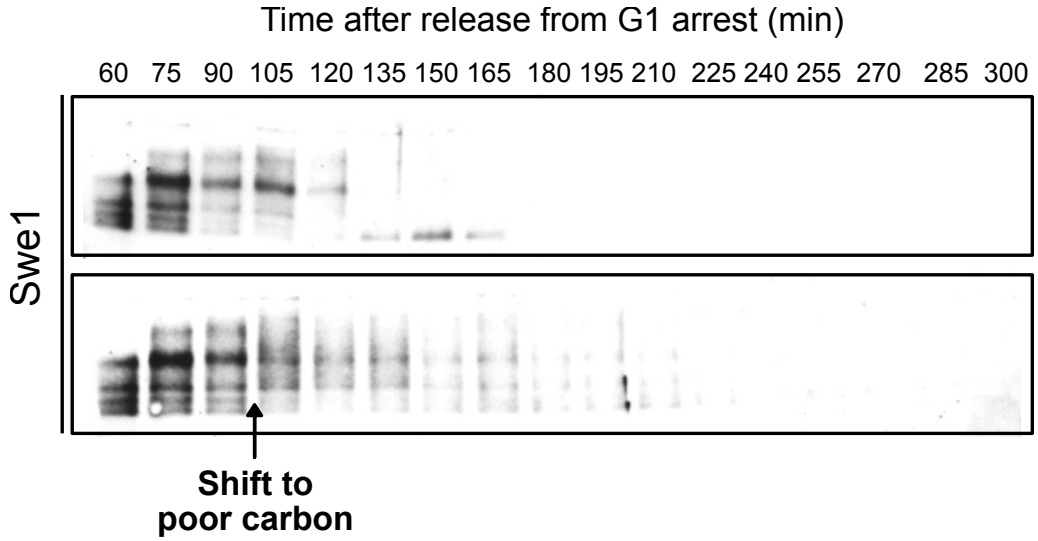

Figure 3.9. The mitotic delay upon shift to poor carbon occurs when Swe1 is hyperphosphorylated

Wild type cells were arrested in G1 using mating pheromone. Cells were released from the arrest, the culture was split, and and samples were collected every 15min. At 90min post release both cultures were washed by centrifugation with either YPD (no shift in carbon condition) or YPge (shift to poor carbon). Samples were collected until 165min for control non-shifted cells, and 300min for cells shifted to poor carbon. The samples were resolved via western blot and probed for Swe1.

An alternative interpretation is that the delay is Swe1 dependent in the sense that it occurs due to Swe1-dependent Cdk1 inhibition, but ultimately caused by a failure to remove the Cdk1 inhibitory phosphorylation. To test this hypothesis we assayed the levels of Cdk1 inhibitory phosphorylation after shifting cells to poor carbon. Our data shows that cells delay the cell cycle with high levels of Cdk1

inhibitory phosphorylation suggesting that Cdk1 inhibitory phosphorylation might be the reason of the observed delay.

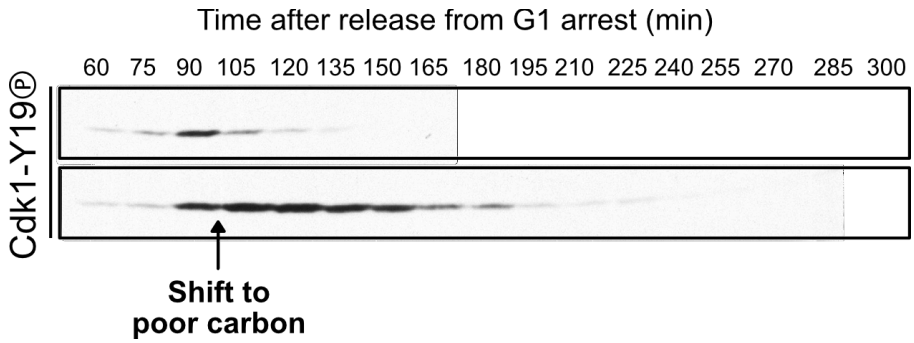

Figure 3.10. Cells shifted to poor carbon delay in mitosis with persistent Cdk1 inhibitory phosphorylation

Samples used in Figure 3.9 were resolved via western blot and probed for Swe1.

In order to test whether the delay is due to a failure to dephosphorylate and activate Cdk1 or whether it is due to an alternative pathway that controls the duration of mitosis independently of Swe1, we tested whether Swe1 is required for the delay observed upon shit to poor nutrients. Our data demonstrates that *swe1Δ* cells progress through mitosis at nearly the rate as *wild type* cells after the shift to poor carbon. This suggests that the observed delay is not solely due to delayed dephosphorylation of Cdk1 but likely controlled by mechanisms that are independent of Swe1.

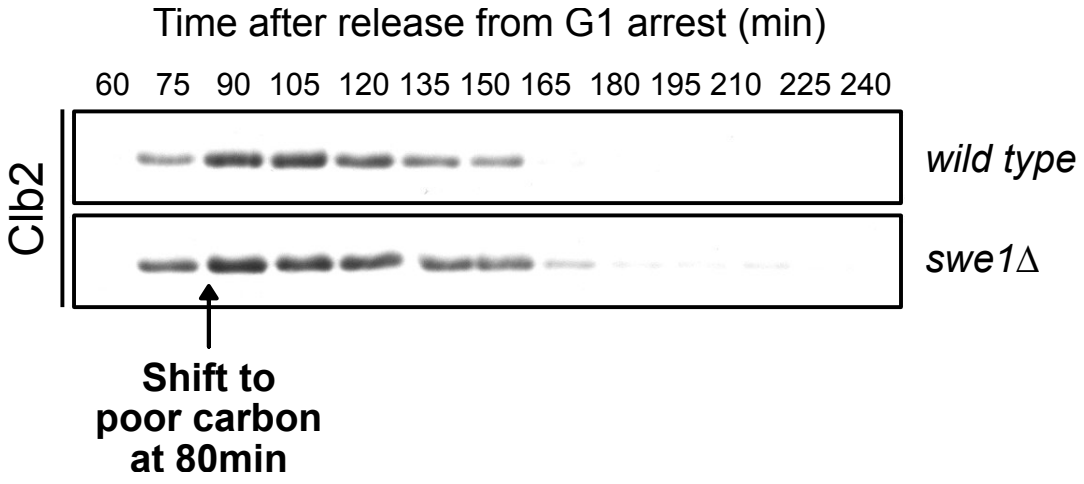

Figure 3.11. The mitotic delay induced by nutrient shifts are Swe1 independent
Wild type and *swe1Δ* cells were arrested in G1 using mating pheromone. Cells were released from the arrest and samples were collected every 15min. At 80min post release both cultures were washed by centrifugation with YPge (shift to poor carbon). The samples were resolved via western blot and probed for Clb2.

In agreement with this observation is the evidence that a switch to poor carbon does not induce an increase in Cdk1-Y19℗ levels to the same extent as loss of Gin4 (**Figure 3.2C**). It is thus fair to assume that in cells switched to poor carbon the activity of Gin4 over Swe1 remains unaltered. Furthermore, cells shifted to poor carbon arrest in mitosis when Gin4 is hyperphosphorylated and it has previously been reported that phosphorylated Gin4 has higher activity against Swe1. This data does not explain, however, why loss of Rts1 results in Gin4 hyperphosphorylation but, in stark contrast, loss of Rts1 causes cell cycle delays. One possibility is that in response to loss of Rts1 a reduced subset of sites become phosphorylated, compared to an increased phosphorylation in response to nutrient changes.

Cells shifted to poor carbon during mitosis delay in metaphase independently of Gin4

Multiple observations led us to hypothesize that the mitotic delay observed upon switch to poor carbon is independent of Gin4. First, although we have previously reported that loss of Gin4 can induce a Swe1 dependent mitotic delay, we have, however, observed that the mitotic delay upon switch to poor carbon is not Swe1 dependent. Second, a switch to poor carbon during mitosis does not reveal any abrupt change in Gin4 phosphorylation, which suggests that Gin4 activity may not be compromised by a switch to poor carbon. Here we tested whether the mitotic delay upon shift to poor carbon is Gin4 dependent by testing the effects of a carbon switch in cells lacking Gin4. For this experiment we used strains harboring a degron version of Gin4 (gin4-AID) so that cells would enter mitosis without suffering of exacerbated polar growth and pre-mitotic delays, key characteristics of *gin4Δ* mutants. Our results demonstrate that the mitotic delay induced by a nutrient shift to poor carbon is not Gin4 dependent. While it can be argued that cells depleted of Gin4 have hyperactive Swe1, we must take into account that the mitotic delay upon shift to poor carbon is not dependent on Swe1.

3

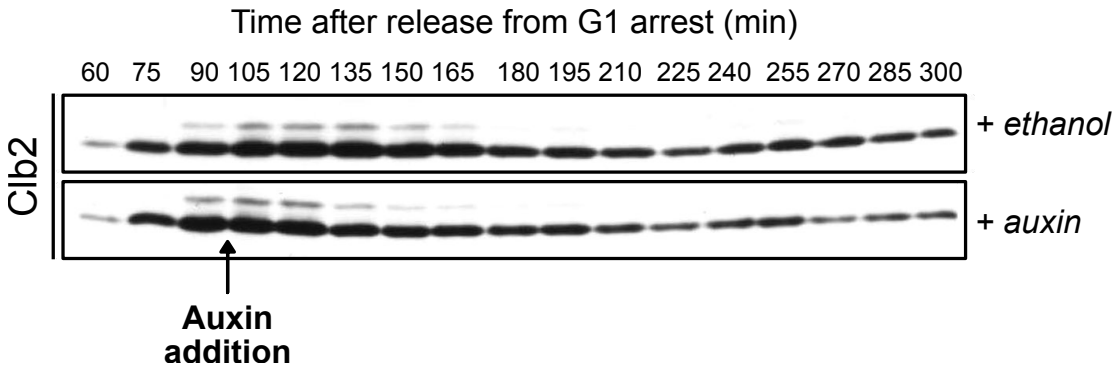

Figure 3.12. The mitotic delays induced by nutrient shifts are Gin4 independent

Wild type and *gin4-AID* cells were arrested in G1 using mating pheromone. Cells were released from the arrest and samples were collected every 15min. At 90min post release cultures were washed by centrifugation with YPge (shift to poor carbon) supplemented with either ethanol (control) or auxin. The samples were resolved via western blot and probed for Clb2.

Loss of Pds1 phosphorylation results in small size phenotype [preliminary data]

Multiple layers of evidence suggest that the duration of mitosis is controlled by Swe1 dependent and independent mechanisms. For example, loss of Rts1 or Gin4 induces a mitotic delay that is only partially rescued by Swe1 (**Figure 2.10** and **Figure 3.5**). Furthermore, while the single deletion of swe1 reduces the duration of mitosis in poor media, it does not reduce it to the duration seen in rich media. Together, these data suggest that the duration of mitosis is only partially controlled by Swe1. Furthermore, shifting cells to poor carbon induces a mitotic delay that is independent of Swe1. These observations prompted us to identify an alternative pathway controlling the duration of mitosis. Our mass spectrometry analysis of *rts1Δ* cells identified a number of additional targets of $PP2A^{Rts1}$ that could control mitotic duration (Zapata et al., 2014). Pds1, a key player involved in controlling metaphase-anaphase transition, was amongst such targets.

Pds1/securin is a highly conserved protein that represses chromosome segregation by sequestering and inactivating separase. Securin inactivation is key for the release of separase, a cystine protease required for cleaving cohesin. Upon correct chromosome bi-orientation Pds1 is dephosphorylated and is targeted for

degradation via the APC-C/cyclosome, with consequent release of separase. Anaphase onset ensues when about half of all separase is released (Agarwal & Cohen-Fix, 2002).

In addition to ensuring chromosome bi-orientation, Pds1 is also involved in delaying anaphase onset in response to DNA damage. Chk1, a serine/threonine kinase which regulates DNA damage checkpoints, phosphorylates Pds1, effectively delaying commitment into anaphase (H. Wang, Liu, Wang, Qin, & Elledge, 2001).

Our mass spectrometry analysis suggests that a similar level of regulation could occur in response to nutrient starvation. First, loss of Rts1 results in delayed mitotic progression and hyperphosphorylation of Pds1 at serine 135 and 136, according to our mass spectrometry data. Similarly, a shift to poor carbon affects Rts1 phosphorylation, induces a mitotic delay, and results in hyperphosphorylation of the same Pds1 residues. These observations led us to hypothesize that $PP2A^{Rts1}$ could play a role in controlling the duration of mitosis through dephosphorylation of Pds1. A shift to poor carbon would, on the other hand, prevent $PP2A^{Rts1}$ activity over Pds1 resulting in a delay in anaphase onset.

In order to test this hypothesis we mutated both S135 and S136 to alanines. In addition, we also mutated a cluster of two additional serines that might suffer additional phosphorylation in absence of Rts1 (S212 and S213). Phos-tag™ western blot of cells grown in rich and poor carbon confirm that Pds1 undergoes phosphorylation in poor nutrients. Pds1 response to nutrients is ablated in our phosphosite mutant, termed *pds1-4A*.

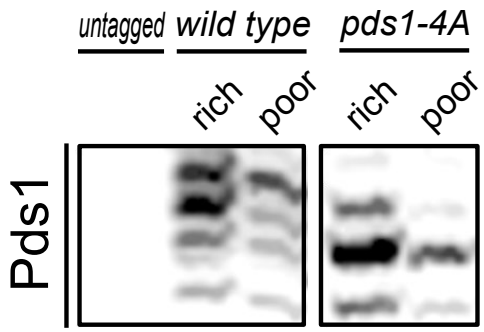

Figure 3.13. pds1-4A does not undergo nutrient dependent phosphorylation
pds1-HA and pds1-4A-HA cells were grown to log phase in rich and poor carbon. Samples were processed for western blot and probed for HA epitope.

Coulter Counter analysis of cell size of *wild type* and *pds1-4A* cells indicates that *pds1-4A* mutants are slightly smaller than *wild type*. This difference was, however, subtle (**Figure 3.14**). Two possibilities could explain such scenario. On one side loss of Pds1 phosphorylation may have little effect in an unperturbed cell cycle. Degradation of Pds1 occurs after activation of the anaphase promoting complex (APC) which, in turn, requires Cdk1 activity. It is therefore conceivable that degradation of either Pds1 or pds1-4A can only occur after full inactivation of Swe1. Dephosphorylation of Pds1 alone, without inactivation of Swe1, would not result in faster degradation of Pds1 and, therefore, faster progression through mitosis. Alternatively, it is possible that *pds1-4A* mutant cells progress through metaphase quickly and at a smaller size but undergo compensatory growth after completion of metaphase. Analysis of *swe1Δ pds1-4A* cell size via Coulter Counter revealed additional information. It has been previously described that *swe1Δ* cells are smaller than *wild type* (Harvey et al., 2005; 2011), in stark contrast, *swe1Δ pds1-4A* double mutant cells are just as big as *wild type*. In addition, the biggest cells in the population (representative of those at late mitotic stages) are, in fact, bigger than *wild*

type. While initially contradictory these results could be the consequence of compensatory growth during later phases of mitosis. While the use of *pds1Δ* strains is not an idyllic option, as Pds1 is required for efficient import of separase into the nucleus, we tested the effects of *pds1Δ swe1Δ* deletion mutants (Hornig, Knowles, McDonald, & Uhlmann, 2002). *pds1Δ swe1Δ* cells shifted from rich to poor carbon do not undergo the characteristic mitotic delay with short mitotic spindles (**Figure 3.15A**, see also **Figure 2.1C**). Instead, the data suggests a cell cycle arrest when cells have long anaphase spindles (**Figure 3.15B**). In stark opposition, both *wild type* and *pds1Δ* cells arrest in metaphase, as demonstrated by the presence of short metaphase spindles and reduced number of long anaphase spindles. Control unshifted *wild type* cells, on the other hand, did not arrest in either metaphase or anaphase.

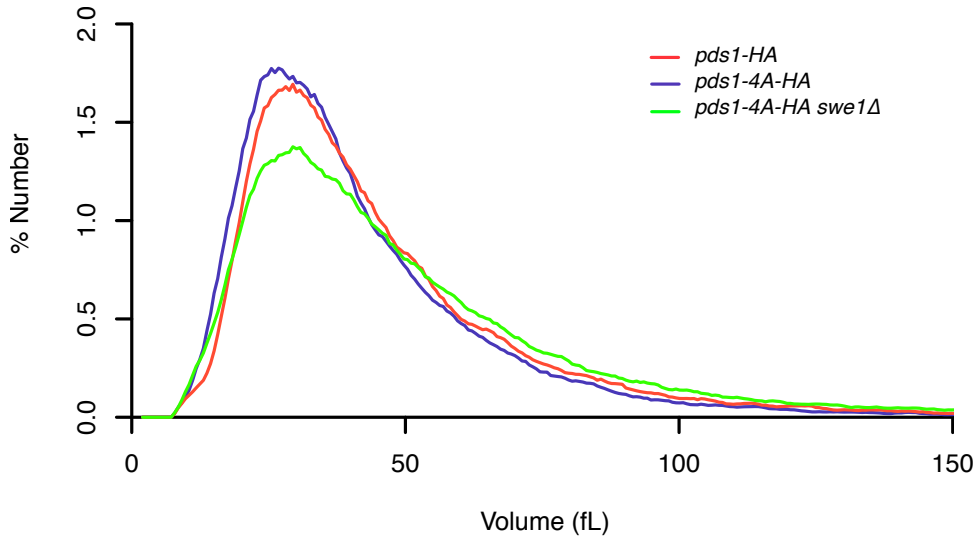

Figure 3.14. The size of *pds1-4A* cells is reduced as measured by Coulter Counter

The size of control (*pds1-HA*), *pds1-4A-HA*, and *pds1-4A-HA swe1Δ* cells grown to log phase in liquid YPD cultures was measured with a Coulter counter.

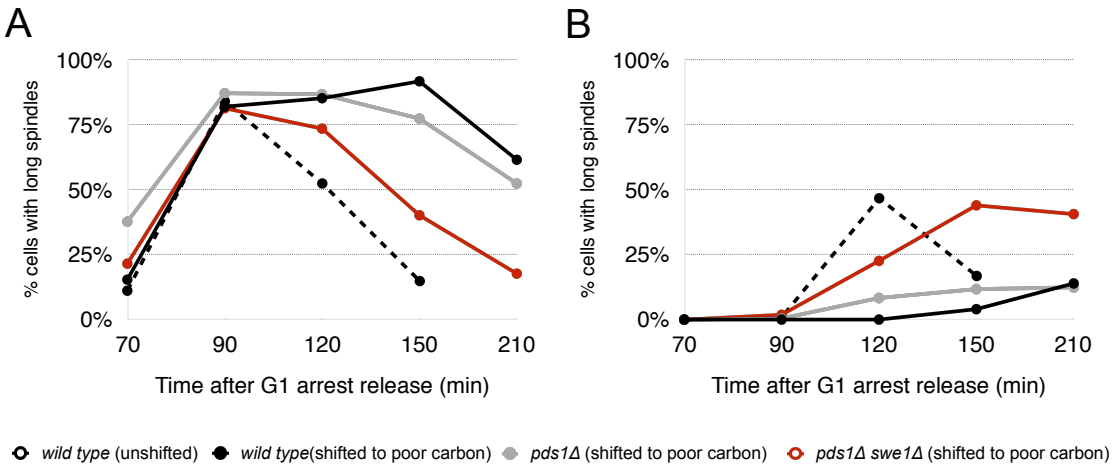

Figure 3.15. *pds1Δ swe1Δ* arrest in mitosis with long anaphase spindles
Cells of the referred genotypes were arrested in G1 using mating pheromone. 90min after release from the arrest cells were switched to poor carbon via centrifugation, with exception for the wild type unshifted control. Samples were collected at regular intervals. Fixed cells were stained with anti-tubulin antibody and the number of long mitotic spindles analyzed.

Small *swe1Δ* cells do not undergo compensatory growth in G1

The discovery of the G1 cell size checkpoint resulted from the observation that big mother cells progress through G1 rather quickly while, in contrast, their smaller daughters delay in G1 until sufficient growth has occurred. In lieu of this observation it would be expected that cells born at abnormally small sizes would delay progression through G1 in order to ensure compensatory growth. We had previously generated *swe1Δ* cells which, as shown in *Chapter II*, complete mitosis at a significantly smaller size (**Figure 2.9D,E**). Here we test whether these abnormally small cells will undergo compensatory growth during G1.

When *swe1Δ* cells were followed from cytokinesis to budding we observed no differences in G1 progression when compared to *wild type* cells: *swe1Δ* cells did not

undergo compensatory growth in G1. Both *wild type* and *swe1Δ* cells grew 6 fL in G1 when grown in rich media. When in poor media, *wild type* cells grew 10 fL, while *swe1Δ* added just 8 fL (**Figure 3.16**). This observation raises the possibility that the G1 checkpoint ensures that cells undergo a constant volume increase during G1 as opposed to reaching a critical cell size.

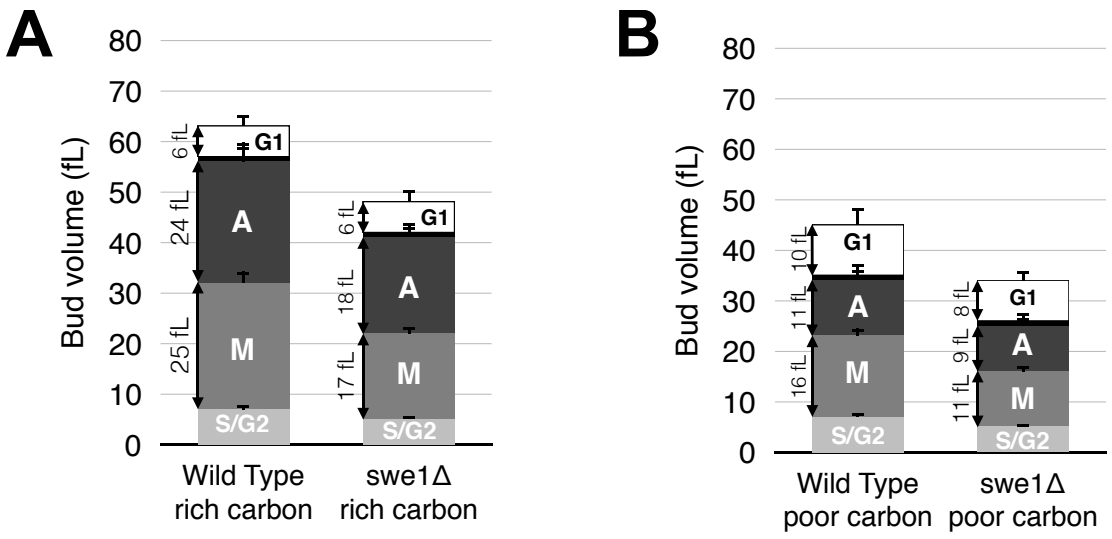

Figure 3.16. *swe1Δ* cells do not undergo compensatory growth during G1
A plot showing the average growth in volume at all stages of the cell cycle for *wild type* or *swe1Δ* cells growing in (A) rich carbon or, (B) poor carbon.

If the G1 size checkpoint ensures that a constant amount of growth is achieved during G1, as opposed to the achievement of a critical cell size, it would be expected that the size at budding is proportional to the size at cytokinesis. In order to test this hypothesis we plotted the size at budding *vs* volume at cytokinesis (**Figure 3.17A**). For all strains analyzed the volume at budding is directly proportional to the size at cytokinesis, supporting the hypothesis. This observation

held true even for cells depleted of rts1-AID, a critical regulator of the G1 cell size checkpoint. In addition our data demonstrated that the duration of G1 is inversely proportional to the size at cytokinesis (**Figure 3.17B**). Because bigger cells do support a higher growth rate it would be expected that they complete a constant amount of growth in a reduced time frame.

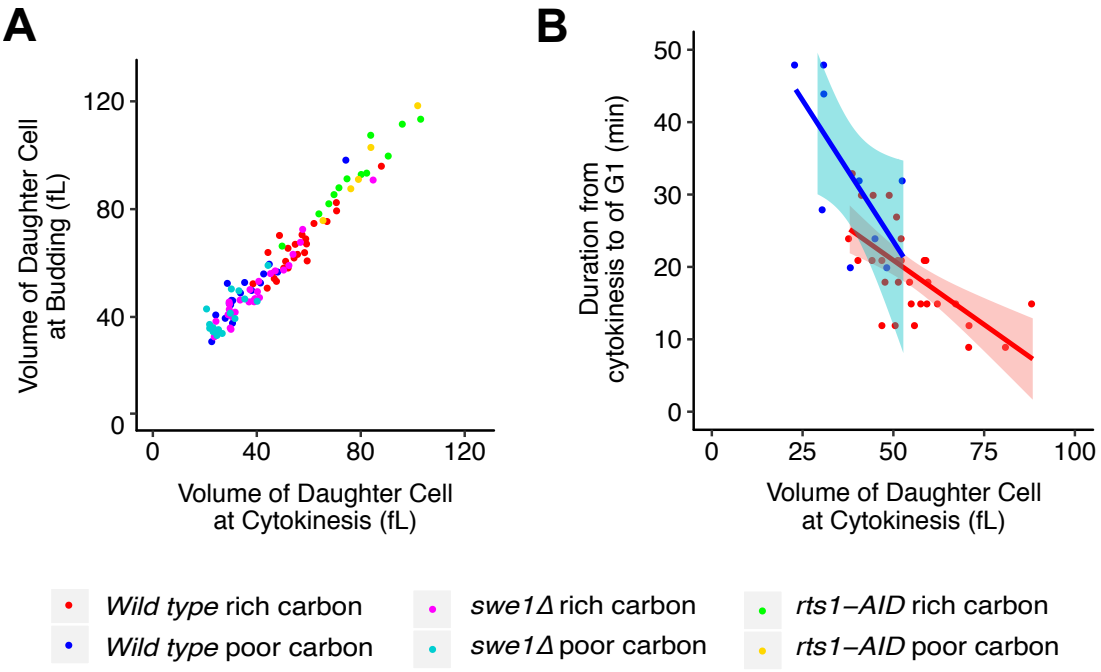

Figure 3.17. The size and duration of G1 are proportional to the volume at cytokinesis

(A) The volume of each daughter cell at budding was plotted against the volume at completion of mitosis for all strains and conditions indicated. (B) The duration of G1 was plotted against the volume of the daughter bud at cytokinesis for wild type cells in rich and poor media. Smooth lines are logistic regressions of the data. Shaded areas represent 95% confidence interval.

The G1 cyclin Cln3 regulates the duration and size at completion of mitosis

It has been previously reported that the levels of the G1 cyclin Cln3 become elevated as cells progress through mitosis (Zapata et al., 2014). Whether this phenomena is unique for cells grown in rich carbon is unknown, as the mitotic levels of Cln3 have not been previously tested in poor carbon. To address this question we collected samples through a complete cell cycle in rich and poor carbon and probed for the mitotic cyclin Clb2 and the G1 cyclin Cln3. Our data shows that Cln3 is not restricted to G1 in either carbon condition. Whether cells are grown in rich or poor carbon peak levels of Cln3 are observed to coincide with peak levels of Clb2 (**Figure 3.18**).

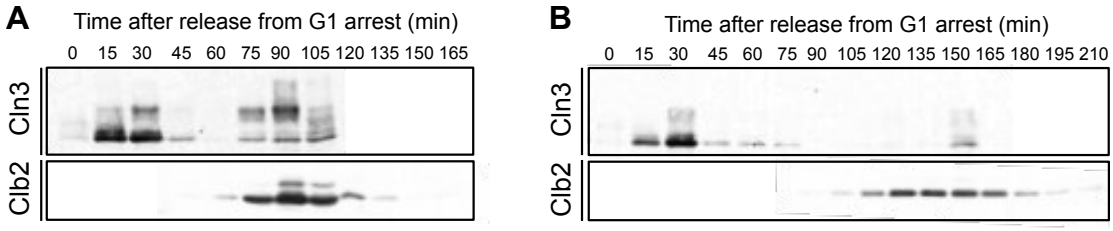

Figure 3.18. The G1 cyclin Cln3 is expressed during mitosis in rich and poor carbon

Wild type cells growing in YPD (rich carbon) or YPGE (poor carbon) were arrested in G1 phase by addition of mating pheromone. The cells were released from the arrest and samples were collected every 15min. Samples were probed for Clb2 (from 0 to 165 min in rich carbon and up to 210 min in poor carbon). A subset of these samples was also probed for Cln3 (from 0 to 105min in rich carbon, and up to 165mim in poor carbon).

Why a G1 cyclin is expressed during mitosis is unknown. Given the remarkable coincidence between the levels of Cln3 and the mitotic cyclin Clb2 we

speculated that Cln3 expression is required for normal progression through mitosis. Because shifting cells from rich to poor carbon when most cells are in mitosis causes a cell cycle delay in metaphase we tested whether the levels of Cln3 are affected during a nutrient shift. The samples used in figure 2.1B were reprobed for Cln3. Shifting cells to poor carbon when most cells were in metaphase causes a drastic reduction of the levels of Cln3 (**Figure 3.19**). The levels of Cln3 did not raise back above the detection limit for the entire duration of the time course.

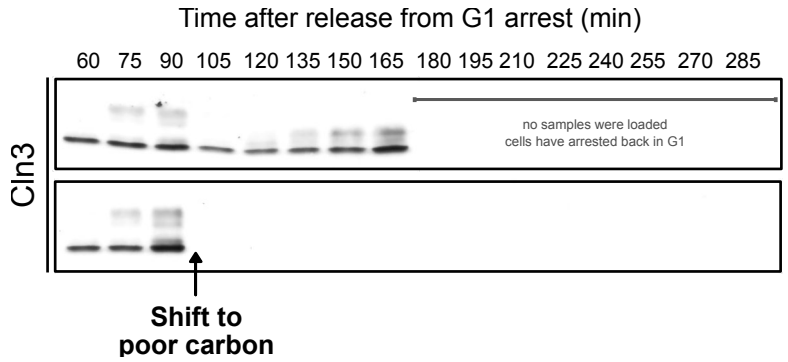

Figure 3.19. Shifting cells to poor carbon prevents reappearance of Cln3 during mitosis

Wild type cells growing in YPD (rich carbon) were arrested in G1 phase by addition of mating pheromone. The cells were released from the arrest and samples were collected every 15min. At 90 minutes the culture was split and one half was washed into YPD and the other half was washed into YPGE. Levels of the G1 cyclin Cln3 were assayed by western blot. Sample collection was terminated when most cells were in G1 (165min in rich media, 285min in poor media).

To further test our hypothesis we constructed a stabilized form of Cln3, termed cln3Δ177, and followed the behavior of this mutant with the same microscopy techniques employed in *Chapter II* (Tyers, Tokiwa, Nash, & Futcher, 1992). Imaging of *cln3Δ177* cells revealed that increased levels of Cln3 results in reduced mitotic

duration and a smaller cell size at completion of mitosis (**Figure 3.20**). As *cln3Δ177* cells fail to trigger the G1 cell size checkpoint, the reduced bud size at completion of mitosis could, in addition, be a consequence of the reduced size of their mother cells. Further analysis of how Cln3 affects mitotic progression is required to understand the cause of such phenotype.

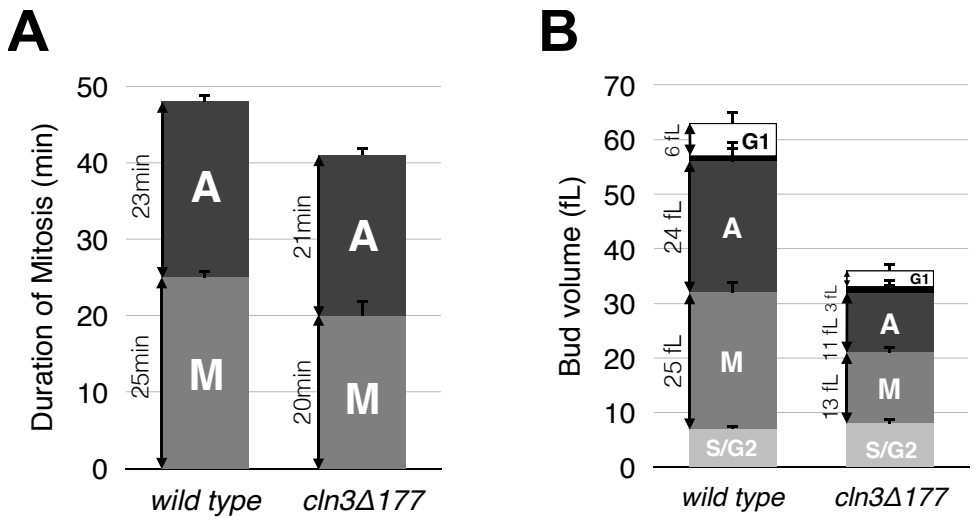

Figure 3.20. Cells containing a stabilized form of Cln3 complete mitosis at a smaller size

A plot showing the average growth in volume at all stages of the cell cycle for *wild type* or *cln3Δ177* cells growing in (A) rich carbon or, (B) poor carbon. The G1 phase of the cell cycle was omitted from the plot in poor media due to lack of sufficient data.

DISCUSSION

In this dissertation I explore the hypothesis that, in addition to a G1 size checkpoint, cell size regulation occurs during mitosis. The findings presented in *Chapter II* and *III* support this hypothesis and reveal new mechanisms for the achievement of cell size homeostasis at completion of mitosis.

In the next few pages I will discuss some of our main findings and how they fit in our current understanding of cell size control.

Daughter cell size and the duration of mitosis are modulated by nutrients

Daughter cells are born at a significantly smaller size in poor nutrients (Johnston et al., 1977). To explain this observation, it has been suggested that the average duration of bud growth is invariant, even when growth rate is reduced by poor nutrients (Johnston et al., 1977). This would suggest that the reduced size of daughter cells in poor nutrients is simply a consequence of reduced growth rate. We tested this model by simultaneously monitoring bud growth and cell cycle events, which revealed that the duration of daughter bud growth is not invariant. Rather, poor carbon causes a significant increase in the duration of daughter bud growth during mitosis. Despite the increased duration of mitosis, daughter cells growing in poor carbon are born at almost half the size of cells in rich carbon. Together, these observations suggest that cell size checkpoint mechanisms control the extent of growth during mitosis, and that the amount of growth required to pass the checkpoints is reduced in poor carbon, resulting in production of small daughter cells.

The fact that most cell growth occurs during a rapid growth phase in mitosis suggests that maintenance of a specific cell size requires tight control over the

interval of mitotic growth. For example, a 20% change in the duration of growth in mitosis would have a large effect on cell size, whereas a 20% change in the duration of growth in G1 phase would have little effect. Similarly, modulation of the duration of G1 phase seems unlikely to play a dominant role in control of cell size because so little growth occurs during G1 phase, and the rate of growth is significantly slower. Rather, since most growth in volume occurs in mitosis, it would make sense that cells control their size primarily by controlling the extent of growth during mitosis. The existence of major cell size control mechanisms in mitosis would explain why cells lacking critical regulators of the G1 size checkpoint, still show robust nutrient modulation of cell size (Jorgensen et al., 2004).

A number of observations suggest that the increased duration of mitosis in poor carbon is a response to reduced growth rate. Cells shifted from rich to poor carbon during metaphase undergo a prolonged mitotic delay, whereas cells shifted during anaphase do not. If the delay were a consequence of a reduction in ATP or other metabolites needed for mitotic spindle events, one would expect to see delays in both metaphase and anaphase. Rather, we hypothesize that a shift to poor carbon during metaphase causes a delay because the daughter bud has not yet undergone sufficient growth, whereas a shift in anaphase does not cause a delay because buds have already undergone extensive growth and have reached the threshold amount of growth needed to complete mitosis in poor carbon.

More evidence for mitotic cell size control comes from the discovery that Swe1 and $PP2A^{Rts1}$ control mitotic duration and cell size at completion of mitosis. $PP2A^{Rts1}$ was previously implicated in cell size control and is required for nutrient modulation of cell size (Artiles et al., 2009; Zapata et al., 2014). Similarly, inhibitory phosphorylation of Cdk1 by Wee1-family members has been implicated in cell size control for over three decades (Harvey & Kellogg, 2003; Jorgensen, 2002; Nurse,

1975). The involvement of Cdk1 inhibitory phosphorylation and PP2A^{Rts1} is therefore consistent with a model in which increased duration of mitosis in poor carbon is a regulated event, rather than a non-specific consequence of metabolic changes caused by poor carbon.

An alternative model could be that the duration of mitosis is controlled by a nutrient modulated timer. In rich media, the timer would be set for a short duration of growth, while in poor media it would be set for a longer interval. Because metaphase cells shifted from rich to poor carbon undergo a delay, but anaphase cells do not, the timer would have to be metaphase specific and could not account for the delay in anaphase caused by poor nutrients. A timer model could explain the correlation between growth rate and cell size, since cells with a higher growth rate should complete a growth interval at a larger size. However, the timer model does not seem consistent with the large variance in mitotic duration between individual cells growing under identical conditions.

Despite which model will prevail our data demonstrates that the duration of mitosis is not a fixed event and is controlled in response to nutritional changes

Control of mitotic duration and cell size at completion of mitosis

In previous studies, we found that PP2A^{Rts1} is required for nutrient modulation of cell size (Artiles et al., 2009). A proteome-wide search for targets of PP2A^{Rts1}-dependent regulation identified multiple potential effectors of cell size checkpoints, including proteins that control mitotic events (Zapata et al., 2014). Since known effectors of G1 cell size checkpoints are not required for nutrient modulation of cell size (Jorgensen et al., 2004), these observations led us to hypothesize that nutrient modulation of cell size occurs primarily in mitosis, and that PP2A^{Rts1} plays an important role. Here, we tested this hypothesis by analyzing how loss of PP2A^{Rts1}

affects cell growth and size throughout mitosis. This revealed that a partial loss of function of $PP2A^{Rts1}$ causes severe defects in mitotic duration and cell size at completion of mitosis. Together, these observation suggests the hypothesis that the mitotic delay in response to nutrients is likely due to temporal inactivation of Rts1. The observation that Rts1 undergoes quick but temporal hyperphosphorylation in response to a switch to poor carbon supports this hypothesis. We further established that $PP2A^{Rts1}$ influences mitotic duration, in part, by controlling Swe1-dependent Cdk1 inhibitory phosphorylation. Previous work in budding yeast, Drosophila and human cells also reached the conclusion that Cdk1 inhibitory phosphorylation controls the duration of mitotic events after mitotic entry (Z. Jin, Homola, Tiong, & Campbell, 2008; Lianga et al., 2013; Raspelli, Cassani, Chiroli, & Fraschini, 2014; Toledo et al., 2015).

Because inactivation of Swe1 requires its phosphorylation, a kinase must mediate the action of $PP2A^{Rts1}$ over Swe1. It has been previously proposed that inactivation and degradation of Swe1 requires its targeting to the bud neck via interaction with Hsl1-Hsl7 (Burton & Solomon, 2000; Cid, Shulewitz, McDonald, & Thorner, 2001; King, Jin, & Lew, 2012; King, Kang, Jin, & Lew, 2013; McMillan, Theesfeld, Harrison, Bardes, & Lew, 2002; Shulewitz et al., 1999). At the bud neck, Swe1 would be targeted by inactivating kinases that phosphorylate and prime Swe1 for degradation (Barral, Parra, Bidlingmaier, & Snyder, 1999). Gin4 has been identified as one of such kinases and our mass spec analysis has identified it as a potential target of Rts1 (Barral et al., 1999; Longtine et al., 2000; McMillan et al., 1999; Zapata, 2014). Western blot analysis of Gin4 in *rts1Δ* cells reveals that timely dephosphorylation of Gin4 requires $PP2A^{Rts1}$. In addition, analysis of *Gin4* and *Hsl1* mutants reveals that, in a fashion similar to loss of Rts1, depletion of Gin4 induces a

Swe1-dependent mitotic delay with highly elevated levels of Cdk1 inhibitory phosphorylation.

Although *swe1Δ* significantly reduced the metaphase delays caused by partial inactivation of $PP2A^{Rts1}$ or depletion of *gin4-AID*, it had little effect on anaphase delays. In addition, *swe1Δ* had no affect on the delays induced by nutrient shifts and did not reduce metaphase duration in cells growing in poor nutrients to match metaphase duration of *wild type* cells in rich nutrients. Together, these observations indicate that mitotic delays caused by poor nutrients or inactivation of $PP2A^{Rts1}$ are not due solely to Cdk1 inhibitory phosphorylation. A recent study in fission yeast also reached the conclusion that there are major Wee1-independent mechanisms for controlling cell size in mitosis (Wood & Nurse, 2013).

Pds1 phosphorylation is likely to reinforce the mitotic cell size checkpoint [preliminary data]

Our mass spectrometry analysis of *rts1Δ* cells identified a number of additional targets of $PP2A^{Rts1}$ that could control mitotic duration (Zapata et al., 2014). A particularly interesting candidate is Pds1, also referred to as securin. Pds1 binds and inhibits separase, the protease that initiates chromosome segregation via proteolytic cleavage of cohesin. Previous studies have shown that Pds1 regulation controls progression through both metaphase and anaphase in response to DNA damage (Holt, Krutchinsky, & Morgan, 2008; Tinker-Kulberg & Morgan, 1999; H. Wang et al., 2001). Thus, $PP2A^{Rts1}$-dependent control of Pds1 could play a role in controlling the duration of mitosis. Pds1 plays both positive and negative roles in controlling separase, so *pds1Δ* causes a complex phenotype (Ciosk et al., 1998; Jensen, Segal, Clarke, & Reed, 2001; Yamamoto, Guacci, & Koshland, 1996). Our mass spectrometry analysis revealed, however, key Pds1 sites that become

phosphorylated in response to poor carbon or *rts1Δ*. My preliminary data shows that mutation of such sites (*pds1-4A*) prevents Pds1 hyperphosphorylation when cells are switched to poor carbon, suggesting we might have identified all key sites that respond to nutrient changes. In addition, *pds1-4A* mutants have a slight reduction in cell volume with the smallest cells in the population (newborn cells) being smaller than control cells. We also tested the effect of deleting both Swe1 and Pds1. *pds1Δ swe1Δ* cells shifted to poor carbon do not delay in metaphase, as opposed to wild type cells. Instead the delay occurs in anaphase. This delay could be a consequence of incorrect chromosome segregation that trigger other mitotic checkpoints. Because cells grow during checkpoint arrests, triggering anaphase checkpoints would lead to increased cell size. The analysis of *swe1Δ pds1-4A* cell size via coulter counter revealed that the biggest cells in the population (late mitotic cells) are bigger than *wild type* cells. In addition, newborn double mutant cells are bigger than single *pds1-4A* mutants which could be the result of anaphase delay observed in *swe1Δ pds1Δ* cells. Finally, most cells in the population were no different from wild type cells. In contrast it has been previously described that *swe1Δ* cells are smaller than *wild type* cells. Together these observations suggest that loss of Pds1 alone or the lack of Pds1 phosphorylation are insufficient to induce a severe reduction in cell size at completion of mitosis. The inhibitory effects of Swe1 on mitotic progression are likely sufficient to regulate mitotic duration in the absence of Pds1 phosphorylation. Loss of Swe1 would make Pds1 the sole player of this checkpoint. In these circumstances loss of Pds1 or lack of its phosphorylation is likely to result in accelerated progression through metaphase, incorrect chromosome segregation and activation of corrective checkpoints. Full interpretation of the loss of Pds1 phosphorylation and how it plays a role in cell size regulation requires further work.

The rate of growth is modulated during the cell cycle

Building on previous studies, we observed dramatic changes in the rate of growth during the cell cycle. Bud growth prior to mitosis occurs at a slow rate, but once cells enter mitosis the rate of growth increases approximately 4-fold in rich carbon and 2-fold in poor carbon. As cells exit mitosis and enter G1 phase, growth slows and remains slow through G1 phase. Thus, growth cannot be considered a simple monotonic function that is independent of the cell cycle. Rather, the rate, duration, extent, and location of cell growth are all regulated during the cell cycle. Previous studies have shown that polar bud growth is dependent upon Cdk1 activity, but the signals that control bud growth at other stages of the cell cycle are unknown (McCusker et al., 2007). Moreover, the mechanisms and function of growth rate modulation during the cell cycle are unknown.

Cell size is proportional to growth rate

Previous studies found that cell size at the end of G1 phase is proportional to growth rate during G1 phase: rapidly growing cells complete G1 phase at a larger size than slow growing cells (Ferrezuelo et al., 2012; Johnston, Ehrhardt, Lorincz, & Carter, 1979). Similarly, we found that cell size at the end of mitosis is proportional to growth rate during mitosis. Thus, cell size at all key cell cycle transitions is correlated with growth rate. The correlation holds when comparing different cells growing under the same conditions, and when comparing different populations of cells growing under different nutrient conditions.

If cell size is proportional to growth rate, faster growing cells should always give rise to larger daughter cells. And since growth rate is proportional to size, larger daughter cells should have a higher growth rate, leading to ever larger daughter cells. In this case, what limits cell size? A plot of daughter cell size at cytokinesis as

a function of mother cell size revealed that daughter cell size indeed increases with mother cell size, but the ratio of mother size to daughter size is not constant across the range of mother cell sizes (**Figure 2.5B**). In other words, very large mothers produce daughters that are nearly half the size of the mother, while small mothers produce daughters of nearly equal size (Johnston et al., 1977). This relationship would correct large variations in mother cell size, which could be the result of growth during cell cycle delays induced by other checkpoints, such as the spindle checkpoint or DNA damage checkpoints. Variation in mother cell size could also be the product of noisy cell size checkpoint mechanisms. This topic is discussed later in further detail.

The strong correlation between growth rate and cell size is difficult to reconcile with a simple cell size checkpoint model in which a threshold volume must be reached to pass the checkpoint. If a specific volume must be reached to pass a checkpoint, the rate at which the cell reaches that volume should not influence the final volume at which the cell passes the checkpoint. One way to reconcile the idea of a set threshold volume with growth rate dependence would be to imagine that cell size checkpoint thresholds are noisy and imperfect. In this view, faster growing cells will overshoot the threshold size more than slow growing cells, leading to increased size. This model would not explain nutrient modulation of cell size.

Another explanation for the relationship between cell size and growth rate could be that cells measure their growth rate and set cell size checkpoint thresholds to match the current growth rate. Alternatively, the same signals that set the growth rate could also set the cell size threshold. Both models would explain nutrient modulation of cell size, since nutrients modulate growth rate. Several observations are consistent with a close functional relationship between growth rate and cell size. Inactivation of $PP2A^{Rts1}$ caused a reduced growth rate, which suggests that it

operates in signaling pathways that control growth rate. The defects in the growth rate of the bud in *rts1-AID* cells cannot be secondary consequence of defects in mother cell size, since we observed the immediate effects of loss of $PP2A^{Rts1}$ in cells with normal mother cell size. In addition, *rts1-AID* cells showed a reduced growth rate, but completed mitosis at a much larger daughter cell size. This demonstrates that the effects of *rts1-AID* are not a secondary consequence of reduced growth rate, since one would expect this to cause a reduced cell size. Most importantly, *rts1-AID* almost completely abolished the normal linear relationship between growth rate and cell size, and caused *rts1-AID* cells to complete mitosis at an abnormally wide range of bud sizes. The fact that *rts1-AID* simultaneously causes defects in growth rate, coordination of cell size with growth rate, and cell size at completion of mitosis, provides strong support for a model in which common signals coordinately set growth rate and cell size, and suggest that $PP2A^{Rts1}$ plays a central role in these signals. Further investigation of the signals that act upstream and downstream of $PP2A^{Rts1}$ should provide important clues to how cell size is controlled.

Variation in cell size at the end of mitosis could be the consequence of mitotic checkpoints that ensure DNA repair and segregation

Despite the well established notion that cells within a given tissue have remarkably little variation in size we and others have observed that cell size variation exists within a given population (Ferrezuelo et al., 2012). In addition, it has been previously observed that cell size variation is lowest at initiation of DNA synthesis and highest at completion of mitosis (Johnston et al., 1977; Killander & Zetterberg, 1965). These observations downgrade the idea of a size checkpoint that controls cell size at completion of mitosis. Alternatively, they could suggest that the mitotic checkpoint is noisy, leading to increased variation in sizes. Here I present initial

evidence of an alternative possibility: the variation of sizes at completion of mitosis results from a compensatory mechanism that ensures return to homeostasis in the event that an abnormally big cell slips through the checkpoint.

In **Figure 2.5** we demonstrated that the volume of a daughter bud at cytokinesis is, in part, proportional to the size of the mother cell: big mothers give rise to bigger daughters. We also noticed, however, that the ratio of mother size to daughter size is not constant across the range of mother cell sizes. In addition, we compared the size of mother cells to daughter cells as the daughter cells generate its own bud and, therefore, have grown to become a mother cell (**Figure 4.1**). Despite limited, our data reveals an intriguing relationship. The daughters of small mothers grow up to be nearly as big as their mother. While, on the other hand, daughters of big mothers do not reach the size of their mothers (Johnston et al., 1977). Only very sporadicly a daughter cell outgrew its mother cell.

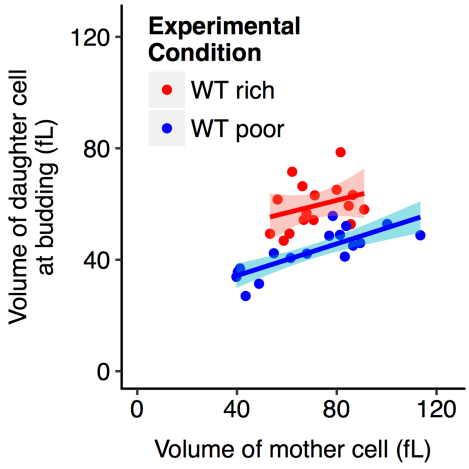

Figure 4.1. The ratio of mother volume to daughter volume increases with the size of the mother cell

The volume of each daughter bud when itself gave rise to a bud was plotted against the size of its mother. Red dots represent cells in rich carbon. Blue dots represent

cells in poor carbon. Smooth lines are logistic regressions of the data. Shaded areas represent 95% confidence interval.

One possibility could explain such scenario: metabolic capacity increases non-linearly with cell size. In other words, a mother twice the size of a small mother, does not have a growth potential twice as fast of that of the small mother. As a consequence big mothers have bigger daughters but the daughter does not grow to be the size of its own mother. If such relationship exists a big mother would have a slightly smaller daughter cell which, in turn, will generate an even smaller daughter cell. This differential would eventually cease to exist once the growth potential of a cell matches the size of the mother cell. In lieu of this scenario a single big mother cell could initiate an array of progeny that progressively would reduce in size, generating noise in the population. This hypothesis made us explore our data to understand if such scenario was ever observed. We searched for cells who, in the course of imaging, gave rise to multiple daughters and, whose daughters gave rise to new cells (a.k.a., granddaughters). In the great majority of cases the size of daughter cells never rose above the size of the mother cell. In addition, daughters of big mothers were constantly smaller then their mothers at the time of budding (i.e., when they initiated a granddaughter) (see **Figure 4.2A-D** for 4 independent cases). This pattern was repeated across multiple generations.

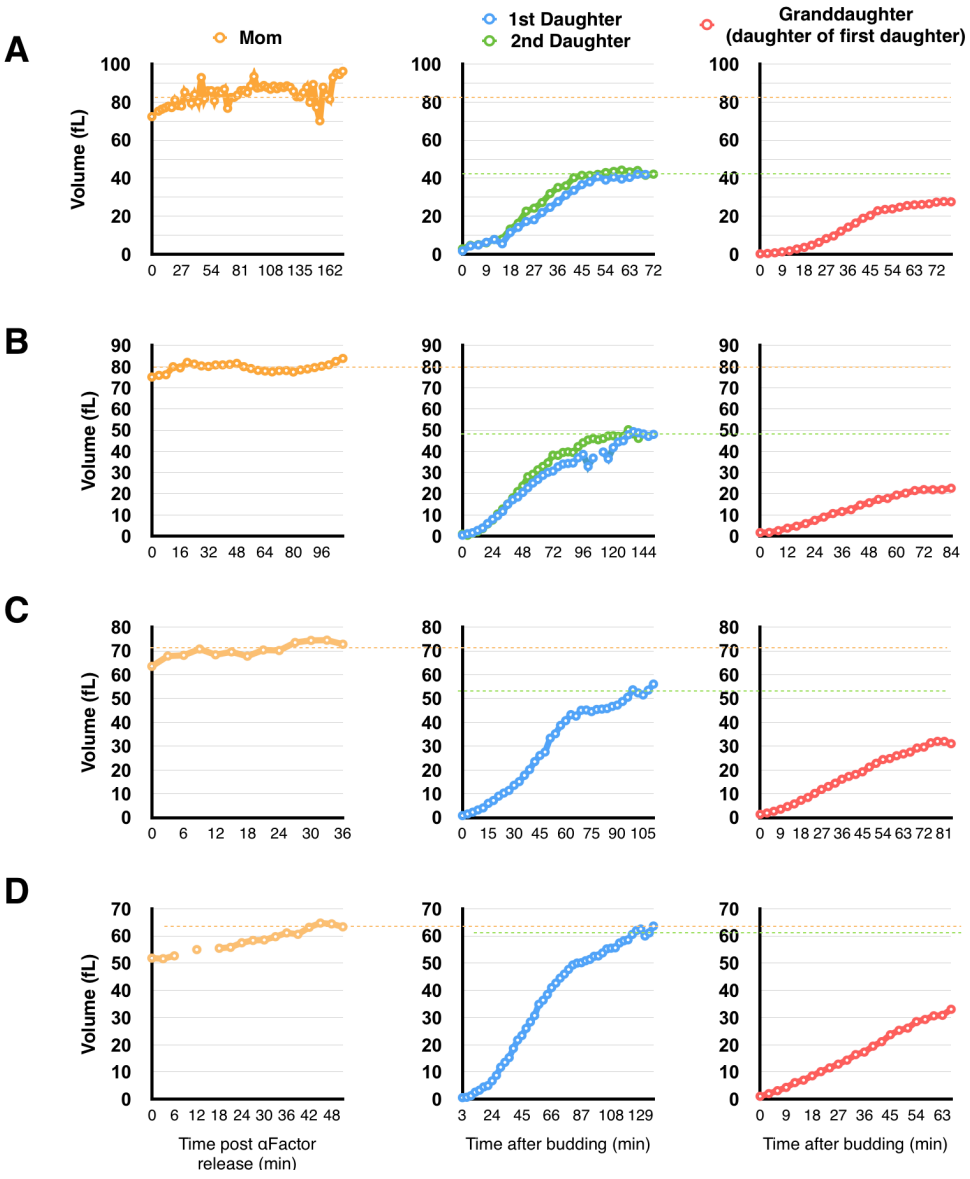

Figure 4.2. Growth curves for two succeeding generations of daughters cells

Left panels: The volume of a mother cells was plotted over time. Middle panels: Plots of volume over time for first two daughters for the cells plotted to the left. Right panels: Plot of volume over time for the first granddaughter were plotted. (A) through (D) represent 4 independent cases.

After completion of the first division, a mother cell meets the requirements to bypass the G1 size checkpoint and soon initiates a new cycle of growth. In all cases analyzed daughters of the same mother had remarkably similar growth patters and grew to become of similar sizes (see **Figure 4.2A-B** for two independent cases). Together, these evidence suggest that the growth capacity of a mother cell remains constant, at least throughout the first few generations. However, the growth potential of a big mother cell does not support the creation of an equally big cell, leading to a progressive reduction in the size of a population of cells.

Despite this intriguing possibility one question still remains: how would a cell size checkpoint allow the passage of “abnormally big” mother cells? In addition to a cell size checkpoint, progression through mitosis requires that cells overcome a myriad of other checkpoints. DNA damage checkpoints, spindle position and orientation checkpoints, chromosome bi-orientation, lagging chromosomes, all can result in a mitotic delay that is independent of cell size. During these checkpoint arrests cells continue to grow regardless of whether they would have reached their critical size for completion of mitosis. As a result, abnormally big cells could be generated before they are allowed to progress through mitosis. Because yeast cells are incapable of reducing their size, abnormally big cells would initiate a compensatory size reduction through their progeny. Similar mechanisms are known to drive size homeostasis in bacteria (Campos et al., 2014).

While much work is needed to elucidate this possibility, this line of work is beyond the scope of this thesis.

Small newborn cells do not undergo compensatory growth during G1

It is currently believed that the G1 size checkpoint ensure that cells reach a critical size before transitioning into S-phase. Our data does not support that model.

We have shown that *swe1Δ* cells complete mitosis at smaller cell size and do not undergo compensatory growth in G1. This result argues against the existence of a size checkpoint that ensures that cells reach a critical cell size. Our data suggests, on the other hand, that the G1 checkpoint is likely to require attainment of a given net growth, as opposed to a critical cell size.

Understanding G1 size checkpoints are beyond the scope of this thesis.

Working model

In order for cells grown in poor carbon to complete mitosis at a smaller cell size despite an increase in mitotic duration the threshold levels of Rts1 activity required for mitotic progression must be reduced in poor nutrients. Because cells grown in poor carbon are typically smaller and have lower protein content it is difficult to compare protein abundance between cells grown in rich and poor carbon. Here I speculate on possible scenarios. One possibility is that the activity of Swe1 is modulated by the mechanisms that control growth rate. Cells growing at slower growth rates, such as those in poor carbon, would have reduced Swe1 activity and consequently less Cdk1 inhibitory phosphorylation. As a result, complete inactivation of Swe1 could be accomplished with reduced levels of active Rts1. If the signals that activate Rts1 are proportional to growth it would require less growth to activate enough Rts1 to counteract Swe1 in poor carbon, resulting in mitotic progression at a smaller cell size. The opposite would be true in rich carbon sources. In those circumstances the levels of active Swe1 would be elevated due to the increased growth rate. It would require further growth so that enough Rts1 activity would be generated to counteract Swe1 activity. Because growth occurs at a faster pace in rich carbon sources, those cells would complete the needed amount of growth to inactivate Swe1 in a reduced time frame. This model is of interest because it could

work between nutrient conditions but would also explain the growth rate to size relationship observed within each carbon source. Another possibility is that activation of Rts1 is timed in rich and poor media, and unrelated to growth. If the timer is longer in poor media it would take longer for cells to inactivate Swe1 and therefore would have more time to grow. Due to the reduced growth rate of cells in poor media cells do not reach the same size threshold before complete activation of Rts1. This could also explain how the size at the end of mitosis is correlated with growth rate. One other possibility is that the activity of the phosphatase Cdc25 would be inversely proportional to growth rate, leading to reduced Cdk1 Y19-phosphorylation on cells grown in poor carbon. Finally it is possible that in poor nutrients phosphorylation and inactivation of Swe1 occurs at a faster rate than in rich nutrients. This could be accomplished by activation of auxiliary kinases that would contribute to full hyperphosphorylation of Swe1 in poor nutrients even at low levels of active Rts1.

The intriguing possibility that Rts1 could control Pds1 phosphorylation and prime it for degradation fits well with our model. It has been previously suggested that Pds1 phosphorylation rescues Pds1 from degradation, effectively delaying anaphase onset in response to DNA damage (H. Wang et al., 2001). Mass spec analysis reveals that a switch to poor carbon or loss of Rts1 leads to increased phosphorylation of Pds1. In addition I showed that such phosphorylation changes can be observed by Phos-tag™ western blots when cells are grown in rich *vs* poor carbon and are eliminated in phosphosite mutants. This data suggest that as cells are switched from rich to poor carbon increased phosphorylation of Pds1 ensures that cells delay in metaphase, fortifying the Swe1 dependent checkpoint. Activation of Rts1 would lead to inactivation of Swe1 and dephosphorylation of Pds1, making it a suitable target of the APC. This double checkpoint might explain why cells that

lack Swe1 are still capable of modulating the duration of mitosis in response to nutrients as those in poor carbon would phosphorylate Pds1, delaying its degradation and, therefore, anaphase onset.

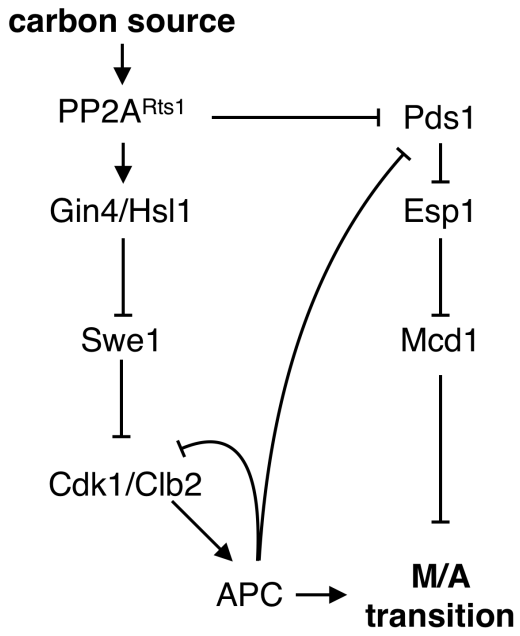

Figure 4.3. Working model: PP2A^{Rts1} controls the duration of mitosis via inactivation of Swe1 and dephosphorylation of Pds1.

MATERIALS AND METHODS

Yeast strains and media

The genotypes of the strains used in this study are listed in Table 1. All strains are in the W303 background (*leu2-3,112 ura3-1 can1-100 ade2-1 his3-11,15 trp1-1 GAL+, ssd1-d2*). Genetic alterations were carried out using one-step PCR-based integration at the endogenous locus (Longtine et al., 1998; Janke et al., 2004).

For cell cycle time courses and analysis of cell size by Coulter counter, cells were grown in YP media (1% yeast extract, 2% peptone, 8ml/L adenine) supplemented with 2% dextrose (YPD), or with 2% glycerol and 2% ethanol (YPGE). For microscopy, cells were grown in complete synthetic media (CSM) with 2% dextrose (CSM-Dex) or 2% glycerol and 2% ethanol (CSM-G/E).

Table 1 - List of used strains

Strain	MAT	Genotype*
DK186	a	*bar1*
DK1993	a	*bar1, GAL1-CDC20::NatNT2*
DK2017	a	*bar1, cln3-6xHA::HIS*
DK2019	a	*bar1, cln3-6xHA::HIS, rts1Δ::KanMX4*
DK2176	a	*bar1, GAL1-CDC20::NatNT2, rts1::KanMX4*
DK2243	a	*bar1, GAL1-CDC20::NatNT2, rts1::KanMX4, swe1::URA3*
DK2374	a	*bar1, TIR1::LEU2, TIR1::HIS3, gin4-AID::KanMX6*
DK2423	a	*bar1, TIR1::LEU2, TIR1::HIS3, rts1-AID::KanMX6*
DK2523	a	*bar1, SPC42-GFP::HIS3, MYO1-GFP::TRP*
DK2677	a	*bar1, TIR1::LEU2, TIR1::HIS3, gin4-AID::KanMX6, hsl1-AID::TRP*
DK2802	a	*bar1, TIR1::LEU2, TIR1::HIS3, gin4-AID::KanMX6, hsl1-AID::TRP, swe1Δ::URA3*
DK2879	a	*bar1, TIR1::LEU2, TIR1::HIS3, SPC42-GFP::hphNT1, MYO1-GFP:KITRP, rts1-AID::KanMX6*
DK2930	a	*bar1, SPC42-GFP::HIS3, MYO1-GFP::TRP, swe1Δ::URA3*

DK3072	a	*bar1, TIR1::LEU2, TIR1::HIS3, SPC42-GFP::hphNT1, MYO1-GFP::KITRP, rts1-AID::KanMX6, swe1Δ::URA3*
DK757	a	*bar, gin4Δ::LEU2, swe1Δ::URA3*
DK888	a	*bar, gin4::LEU2*
SH24	a	*bar1, swe1Δ::URA3*
DK3312	a	*bar1, pds1-4A-3xHA::TRP*
DK2214	a	*bar1, pds1-4A-3xHA::TRP, swe1Δ::URA3, rts1Δ::KanMX*
DK3320	a	*bar1, pds1-4A-3xHA::TRP, swe1Δ*

***** All strains are in the W303 background (*leu2-3,112 ura3-1 can1-100 ade2-1 his3-11,15 trp1-1 GAL+ ssd1-d2*)

Microscopy

Cells were grown overnight in CSM-Dex or CSM-G/E at room temperature with constant rotation to an optical density near 0.1 at λ600. 5 ml of culture were arrested with α factor at 0.5 µg/ml for 3-4 hours. Cells were released from the arrest by 3 consecutive washes with the same media and re-suspended in 500 µl of media. Approximately 200 *µ*l of cell suspension were spotted on a concanavalin A-treated glass bottom dish with a 10 mm micro-well #1.5 cover glass. Cells were adhered for 5 min and unbound cells were washed away by repeated washing with 1 ml pre-warmed media. The dish was then flooded with 3 ml of media and placed on a temperature controlled microscope stage set to 27°C (Pecon Tempcontrol 37-2 digital). The temperature of the media was monitored throughout the experiment using a MicroTemp TQ1 reader coupled to a Teflon insulated K-type thermocouple (Omega). The probe was placed in contact with the glass bottom near the contact area between the objective and the dish. Temperature was maintained at 27 $^{+}/_{-}$ 1°C; imaging sessions where the temperature varied beyond this limit were rejected from final analysis. Brightfield and fluorescent images were acquired simultaneously using a Zeiss LSM 5 Pascal microscope and a Plan-Apochromat 63x/1.4 oil

objective. 488nm light was obtained from an argon laser light source using a (488/543/633) primary dichroic beam splitter (HFT). The laser was set to 0.7% intensity. For green fluorescence images, light was collected through a long pass 505 emission filter using a 1 AU size pinhole. Brightfield images were collected using the transmitted light detector. Optical sections were taken for a total of 11 z-planes every 0.5 μm with frame averaging set to 2, to reduce noise. The total exposure was kept as low as possible to reduce photo-damage (1.60 μs dwell time per pixel, image dimension set to 512 x 512 px, and pixel size set to 0.14 x 0.14 μm). Images were acquired at 3 min intervals for rich carbon and 4 min intervals for poor carbon, with the exception of *rts1-AID* mutants in poor carbon, which were imaged every 6 min to compensate for the greatly increased cell cycle duration. Conditional degradation of rts1Δ-AID was achieved by addition of auxin to 1 mM from a 50 mM stock. Auxin was added 20 min after release from G1 arrest for rich carbon and 60 min after release for poor carbon.

Image analysis

Image analysis was performed using ImageJ (Schneider et al., 2012; Linkert et al., 2010). The ImageJ plug-ins StackReg and MultiStackReg were used for post-acquisition image-stabilization (Thevenaz et al., 1998; Busse). Stabilized bright-field images were processed using the imageJ plug-in FindFocusedSlices and the volume of growing buds was determined using BudJ, a plugin for ImageJ (Tseng; Ferrezuelo et al., 2012). Bud volumes were measured for buds whose focal plane was no more than 1.5 μm away (3 z-steps) from their mother's focal plane. Sum projections of z-stacks were treated using a 2 px mean filter, and brightness/contrast levels were adjusted to reduce background noise. The treated pseudo-colored green fluorescent

images were overlapped with the outlines of the imaged cells for reference (outlines were generated using the “find edges” command over a sum projection of all z-stacks of bright field images). Positions of spindle poles (SPBs) were determined using the crosshair tool (set to auto-measure and auto-next) and distance between the 2 SPBs was determined using the mathematical formula for the distance between 2 points. Disappearance of the Myo1 ring was determined empirically by observation of GFP signal at the bud neck.

Statistical analysis

Data acquired from ImageJ was analyzed using Apple Numbers, R (The R Core Team, 2016), RStudio (RStudio Team, 2015), and the R package ggplot2 (Wickham, 2009). p-values were calculated using a Welch Two Sample t-test and a 95% confidence interval.

Cell cycle time courses

For western blot time courses, cells were grown overnight at room temperature in liquid YPD or YPGE to an optical density of 0.5 at λ600. Because optical density is affected by cell size, we normalized cell numbers by counting cells with a Coulter counter (Beckman Coulter) when comparing cells grown in rich or poor carbon.

G1 synchronization was achieved by arresting cells with α factor at a concentration of 0.5 μg/ml until at least 90% of cells were unbudded. Cells were released from the arrest by washing 3× with fresh media. Time courses were performed at 25ºC with constant agitation. To prevent cells from re-entering the following cell cycle α factor was added back after most cells had budded. For

nutrient shift time courses a single culture was arrested and split at the moment of release from the G1 arrest. At the time of the shift both cultures were washed 3× by centrifugation with room temperature YPD (control) or YPGE (shifted cells). The volume of the culture was restored to its original volume prior to the washes and cultures were placed back at 25ºC.

To arrest cells in mitosis, *GAL1-CDC20* cells were grown overnight in YP media containing 2% raffinose and 2% galactose and arrested by washing into YP containing 2% raffinose. Cells were monitored until all cells had large buds. Cells were released from metaphase by re-addition of 2% galactose.

For western blots 1.6 ml samples were collected at regular intervals, pelleted and flash frozen in presence of 200 µl of glass beads. For immunofluorescence analysis of mitotic spindles, 800 µl of culture were collected alongside western blot samples into tubes containing 88 µl of paraformaldehyde. After fixation for 1-2 hours, cells were pelleted and washed 3× with PBS that contains 0.05%Tween-20 and 0.02% sodium azide (PBST) and stored at 4C for up to 2 days before analysis. Mitotic spindles were labelled by immunofluorescence as previously described (Pringle et al., 1991).

LogPhase nutrient shift time courses

Cells were grown overnight at room temperature in liquid YPD to an optical density of 0.5 at λ600. Cultures were washed using the EMD Millipore 47mm Glass Vacuum Filter Holder placed over nitrocellulose paper and attached to a vacuum flask. After blocking the nitrocellulose paper with YPD, 20ml of culture was flushed through the membrane using vacuum suction. Pelleted cells were resuspended using vigorous pipeting with YPge. The procedure was repeated to a total of 3 washes. Cells were finally resuspended with YPge and the optical density measured

to quantify potential losses. Western blot samples were collected pre- and post-wash.

Western blotting

Cell lysis and western blotting were carried out as previously described (Harvey et al., 2005). Briefly, cells were lysed in a Multibeater16 (BioSpec Products, Inc.) at top speed for 2 min in the presence of 165 µl of sample buffer (65 mM Tris-HCl, pH 6.8, 3% SDS, 10% glycerol, 50 mM NaF, 100 mM glycerolphosphate, 5% 2-mercaptoethanol, and bromophenol blue). For log-phase nutrient shifts the amount of sample buffer loaded to pre- and post-wash samples was adjusted to compensate for any observed loss during the washes. When samples were to be analyzed by Phos-tag™ western blots the sample buffer was prepared without phosphatase inhibitors.

PMSF was added to the sample buffer to a final concentration of 2 mM immediately before cell lysis. After lysis, samples were centrifuged for 2 min at 13,000 rpm and placed in a boiling water bath for 7 min. After boiling, the samples were centrifuged for 2 min at 13,000 rpm and loaded on an SDS polyacrylamide gel.

SDS-PAGE was performed at a constant current of 20 mA. For Clb2, Swe1, Gin4, Cln3 and Rts1 blots, electrophoresis was performed on 10% polyacrylamide gels until a 43kD pre-stained marker ran to the bottom of the gel. For Cdk1-Y19 blots 12.5% gels were used and gels were run until a 14.4-kD marker was at the bottom of the gel. For Pds1-HA analysis 10% acrylamide gels were supplemented with 50 µM Phos-tag™ and 50 µM manganese chloride, and gels were ran until the 43 kD marker was at the bottom of the gel. Proteins were transferred onto nitrocellulose membranes for either 75 min at 800 mA at 4°C in a TE22 transfer tank

(Hoeffer) in buffer containing 20 mM Tris base, 150 mM glycine, and 20% methanol, or for 7 min using Trans-Blot® Turbo™ Transfer System (Bio-Rad) using proprietary transfer buffer. Phos-Tag™ gels were pre-incubated in transfer buffer supplemented with EDTA followed by transfer buffer without EDTA, and only then transferred onto nitrocellulose.

Blots were probed overnight at 4°C with affinity-purified rabbit polyclonal antibodies raised against Clb2, Swe1, Gin4 and Rts1. Cdk1 phosphorylated at tyrosine 19 was detected using a phospho-specific antibody (Cell Signaling Technology, cat# 10A11). HA tagged Cln3 and Pds1 were probed using mouse monoclonal anti-HA antibody. Blots were probed with HRP-conjugated donkey anti-rabbit or donkey anti-mouse secondary antibody (GE Healthcare, cat# NA934) for 75 min at room temperature. Secondary antibodies were detected via chemiluminescence using WesternBright ECL or Quantum substrate (Advansta). Blots were exposed to film or imaged using a ChemiDoc™ MP System (Bio-Rad). For quantification of rts1-AID degradation, band intensity was quantified using ImageLab™.

Spindle staining and counting

Fixed cells were treated for immunofluorescence as previously described using rat anti-tubulin primary antibody followed by goat anti-rat FITC-conjugated antibody (Sigma-Aldrich, Cat# F1763) (Pringle et al., 1991). Multi-plane imaging of slides was performed using a Leica DM5500 B Widefield Microscope and a 63x/ 0.6-1.4 oil objective. Spindles were counted in ImageJ. Data was processed and plotted using Apple Numbers.

REFERENCES

Agarwal, R., & Cohen-Fix, O. (2002). Phosphorylation of the mitotic regulator Pds1/securin by Cdc28 is required for efficient nuclear localization of Esp1/separase. *Genes & Development*, *16*(11), 1371–1382. http://doi.org/10.1101/gad.971402

Altman, R., & Kellogg, D. R. (1997). Control of Mitotic Events by Nap1 and the Gin4 Kinase. *Journal of Cell Biology*, *138*(1), 119–130. http://doi.org/10.1083/jcb.138.1.119

Amin, M. B. (2004). Gleason Grading of Prostate Cancer. Lippincott Williams & Wilkins.

Artiles, K., Anastasia, S. D., McCusker, D., & Kellogg, D. R. (2009). The Rts1 Regulatory Subunit of Protein Phosphatase 2A Is Required for Control of G1 Cyclin Transcription and Nutrient Modulation of Cell Size. *PLoS Genetics*, *5*(11), e1000727 EP –. http://doi.org/10.1371/journal.pgen.1000727

Barral, Y., Parra, M., Bidlingmaier, S., & Snyder, M. (1999). Nim1-related kinases coordinate cell cycle progression with the organization of the peripheral cytoskeleton in yeast. *Genes & Development*, *13*(2), 176–187.

Basten, S. G., & Giles, R. H. (2013). Functional aspects of primary cilia in signaling, cell cycle and tumorigenesis. *Cilia*, *2*(1), 6. http://doi.org/10.1186/2046-2530-2-6

Bayne-Jones, S., & Adolph, E. F. (1932). Growth in size of micro-organisms measured from motion pictures I. Yeast, saccharomyces cerevisiae. *Journal of Cellular and Comparative Physiology*, *1*(3), 387–407. http://doi.org/10.1002/jcp.1030010306

Bernal-Mizrachi, E., Wen, W., Stahlhut, S., Welling, C. M., & Permutt, M. A. (2001). Islet beta cell expression of constitutively active Akt1/PKB alpha induces striking hypertrophy, hyperplasia, and hyperinsulinemia. *The Journal of Clinical Investigation*, *108*(11), 1631–1638. http://doi.org/10.1172/JCI13785

Boehlke, C., Kotsis, F., Patel, V., Braeg, S., Voelker, H., Bredt, S., et al. (2010). Primary cilia regulate mTORC1 activity and cell size through Lkb1. *Nature Cell Biology*, *12*(11), 1115–1122. http://doi.org/10.1038/ncb2117

Brimo, F., Montironi, R., Egevad, L., Erbersdobler, A., Lin, D. W., Nelson, J. B., et al. (2012). Contemporary Grading for Prostate Cancer: Implications for Patient Care. *European Urology*, *63*(5), 1–10. http://doi.org/10.1016/j.eururo.2012.10.015

Burton, J. L., & Solomon, M. J. (2000). Hsl1p, a Swe1p Inhibitor, Is Degraded via the Anaphase-Promoting Complex. *Molecular and Cellular Biology*, *20*(13), 4614–4625. http://doi.org/10.1128/MCB.20.13.4614-4625.2000

Campos, M., Surovtsev, I. V., Kato, S., Paintdakhi, A., Beltran, B., Ebmeier, S. E., & Jacobs-Wagner, C. (2014). A Constant Size Extension Drives Bacterial Cell Size Homeostasis. *Cell*, *159*(6), 1433–1446. http://doi.org/10.1016/j.cell.2014.11.022

Caspersson, T., Lomakka, G., Killander, D., & Foley, G. E. (1963). Cytochemical Differences Between Mammalian Cell Lines of Normal and Neoplastic Origins - Correlation with Heterotransplantability in Syrian Hamsters. *Experimental Cell Research*, *32*(3), 553–&. http://doi.org/10.1016/0014-4827(63)90193-9

Chen, J.-K., Chen, J., Neilson, E. G., & Harris, R. C. (2005). Role of mammalian target of rapamycin signaling in compensatory renal hypertrophy. *Journal of the American Society of Nephrology*, *16*(5), 1384–1391. http://doi.org/10.1681/ASN.2004100894

Chen, J.-K., Chen, J., Thomas, G., Kozma, S. C., & Harris, R. C. (2009). S6 kinase 1 knockout inhibits uninephrectomy- or diabetes-induced renal hypertrophy. *American Journal of Physiology - Renal Physiology*, *297*(3), F585–93. http://doi.org/10.1152/ajprenal.00186.2009

Cid, V. J., Shulewitz, M. J., McDonald, K. L., & Thorner, J. (2001). Dynamic Localization of the Swe1 Regulator Hsl7 During the Saccharomyces cerevisiae Cell Cycle. *Molecular Biology of the Cell*, *12*(6), 1645–1669.

Ciosk, R., Zachariae, W., Michaelis, C., Shevchenko, A., Mann, M., & Nasmyth, K. (1998). An ESP1/PDS1 Complex Regulates Loss of Sister Chromatid Cohesion at the Metaphase to Anaphase Transition in Yeast. *Cell*, *93*(6), 1067–1076. http://doi.org/10.1016/S0092-8674(00)81211-8

Cross, F. R. (1988). DAF1, a mutant gene affecting size control, pheromone arrest, and cell cycle kinetics of Saccharomyces cerevisiae. *Molecular and Cellular Biology*, *8*(11), 4675–4684. http://doi.org/10.1128/MCB.8.11.4675

Cross, F. R. (1990). Cell cycle arrest caused by CLN gene deficiency in Saccharomyces cerevisiae resembles START-I arrest and is independent of the mating-pheromone signalling pathway. *Molecular and Cellular Biology*, *10*(12), 6482–6490. http://doi.org/10.1128/MCB.10.12.6482

DF, G. (1966). Classification of prostatic carcinomas. *Cancer Chemotherapy Reports*, *50*(3), 125–128.

Dhawan, S., Georgia, S., & Bhushan, A. (2007). Formation and regeneration of the endocrine pancreas. *Current Opinion in Cell Biology VL -*, *19*(6), 634–645. http://doi.org/10.1016/j.ceb.2007.09.015

Epstein, J. I., Allsbrook, W. C., Amin, M. B., Egevad, L. L., Bastacky, S., Beltran, A. L., et al. (2005). The 2005 International Society of Urological Pathology (ISUP) Consensus Conference on Gleason Grading of Prostatic Carcinoma. *American Journal of Surgical Pathology*, *29*(9), 1228–1242.

Fankhauser, G. (1945). Maintenance of normal structure in heteroploid salamander larvae, through compensation of changes in cell size by adjustment of cell number and cell shape. *Journal of Experimental Zoology*, *100*, 445–455.

Fantes, P., & Nurse, P. (1977). Control of cell size at division in fission yeast by a growth-modulated size control over nuclear division. *Experimental Cell Research*, *107*(2), 377–386.

Ferrezuelo, F., Colomina, N., Palmisano, A., Garí, E., Gallego, C., Csikász-Nagy, A., & Aldea, M. (2012). The critical size is set at a single-cell level by growth rate to attain homeostasis and adaptation, *3*, 1012–11. http://doi.org/10.1038/ncomms2015

Francavilla, A., Ove, P., Polimeno, L., Coetzee, M., Makowka, L., Barone, M., et al. (1988). Regulation of liver size and regeneration: importance in liver transplantation. *Transplantation Proceedings*, *20*(1 Suppl 1), 494–497.

Haldane, J. (1926). On being the right size.

Hartmann, M. (1926). Über experimentelle Unsterblichkeit von Protozoen-Individuen. *Naturwissenschaften*.

Hartwell, L. H., & Unger, M. W. (1977). Unequal division in Saccharomyces cerevisiae and its implications for the control of cell division. *The Journal of Cell Biology*, *75*(2), 422–435. http://doi.org/10.1083/jcb.75.2.422

Harvey, S. L., & Kellogg, D. R. (2003). Conservation of Mechanisms Controlling Entry into Mitosis: Budding Yeast Wee1 Delays Entry into Mitosis and Is Required for Cell Size Control. *Current Biology*, *13*(4), 264–275. http://doi.org/10.1016/S0960-9822(03)00049-6

Harvey, S. L., Charlet, A., Haas, W., Gygi, S. P., & Kellogg, D. R. (2005). Cdk1-dependent regulation of the mitotic inhibitor Wee1. *Cell*, *122*(3), 407–420. http://doi.org/10.1016/j.cell.2005.05.029

Harvey, S. L., Enciso, G., Dephoure, N. E., Gygi, S. P., Gunawardena, J., & Kellogg, D. R. (2011). A phosphatase threshold sets the level of Cdk1 activity in early mitosis in budding yeast. *Molecular Biology of the Cell*, *22*(19), 3595–3608. http://doi.org/10.1091/mbc.E11-04-0340

Holt, L. J., Krutchinsky, A. N., & Morgan, D. O. (2008). Positive feedback sharpens the anaphase switch. *Nature*, *454*(7202), 353–357. http://doi.org/10.1038/nature07050

Hornig, N. C. D., Knowles, P. P., McDonald, N. Q., & Uhlmann, F. (2002). The Dual Mechanism of Separase Regulation by Securin, *12*(12), 973–982.

Jensen, S., Segal, M., Clarke, D. J., & Reed, S. I. (2001). A Novel Role of the Budding Yeast Separin Esp1 in Anaphase Spindle Elongation: Evidence That Proper Spindle Association of Esp1 Is Regulated by Pds1. *The Journal of Cell Biology*, *152*(1), 27–40. http://doi.org/10.1083/jcb.152.1.27

Jin, Z., Homola, E., Tiong, S., & Campbell, S. D. (2008). Drosophila myt1 is the major cdk1 inhibitory kinase for wing imaginal disc development. *Genetics*, *180*(4), 2123–2133. http://doi.org/10.1534/genetics.108.093195

Johnston, G. C., Ehrhardt, C. W., Lorincz, A., & Carter, B. L. A. (1979). Regulation of cell size in the yeast Saccharomyces cerevisiae. *Journal of Bacteriology*, *137*(1), 1–5.

Johnston, G. C., Pringle, J. R., & Hartwell, L. H. (1977). Coordination of growth with cell division in the yeast Saccharomyces cerevisiae. *Experimental Cell Research*, *105*(1), 79–98. http://doi.org/doi: 10.1016/0014-4827(77)90154-9

Jorgensen, P. (2002). Systematic Identification of Pathways That Couple Cell Growth and Division in Yeast. *Science (New York, N.Y.)*, *297*(5580), 395–400. http://doi.org/10.1126/science.1070850

Jorgensen, P., Rupes, I., Sharom, J. R., Schneper, L., Broach, J. R., & Tyers, M. (2004). A dynamic transcriptional network communicates growth potential to ribosome synthesis and critical cell size. *Genes & Development*, *18*(20), 2491–2505. http://doi.org/10.1101/gad.1228804

Kam, I., Lynch, S., Svanas, G., Todo, S., Polimeno, L., Francavilla, A., et al. (1987). Evidence that host size determines liver size: studies in dogs receiving orthotopic liver transplants. *Hepatology (Baltimore, Md.)*, *7*(2), 362–366.

Killander, D., & Zetterberg, A. (1965). A quantitative cytochemical investigation of the relationship between cell mass and initiation of DNA synthesis in mouse fibroblasts in vitro. *Experimental Cell Research*, *40*(1), 12–20.

Kimball, R. F., & Vogt-Köhne, L. (1961). Quantitative cytochemical studies on Paramecium aurelia. *Experimental Cell Research*, *23*(3), 479–487. http://doi.org/10.1016/0014-4827(61)90007-6

King, K., Jin, M., & Lew, D. (2012). The roles of Hsl1p and Hsl7p in Swe1p degradation: beyond septin-tethering. *Eukaryotic Cell*, *11*(12), 1496–1502. http://doi.org/10.1128/EC.00196-12

King, K., Kang, H., Jin, M., & Lew, D. J. (2013). Feedback control of Swe1p degradation in the yeast morphogenesis checkpoint. *Molecular Biology of the Cell*, *24*(7), 914–922. http://doi.org/10.1091/mbc.E12-11-0812

Kufe, D. W., & Frei, E. (2003). Cancer Medicine 6. B.C. Decker.

Laplante, M., & Sabatini, D. M. (2012). mTOR Signaling in Growth Control and Disease. *Cell*, *149*(2), 274–293. http://doi.org/10.1016/j.cell.2012.03.017

Lianga, N., Williams, E. C., Kennedy, E. K., Doré, C., Pilon, S., Girard, S. L., et al. (2013). A Wee1 checkpoint inhibits anaphase onset. *Journal of Cell Biology*, *201*(6), 843–862. http://doi.org/10.1083/jcb.201212038

Lieberthal, W., & Levine, J. S. (2012). Mammalian target of rapamycin and the kidney. II. Pathophysiology and therapeutic implications. *American Journal of Physiology - Renal Physiology*, *303*(2), F180–F191. http://doi.org/10.1152/ajprenal.00015.2012

Lingohr, M. K., Buettner, R., & Rhodes, C. J. (2002). Pancreatic β-cell growth and survival – a role in obesity-linked type 2 diabetes? *Trends in Molecular Medicine*, *8*(8), 375–384. http://doi.org/10.1016/S1471-4914(02)02377-8

Lippincott, J., & Li, R. (1998). Sequential assembly of myosin II, an IQGAP-like protein, and filamentous actin to a ring structure involved in budding yeast cytokinesis. *Journal of Cell Biology*, *140*(2), 355–366. http://doi.org/10.1083/jcb.140.2.355

Liu, B., & Preisig, P. (1999). TGF-β1-mediated hypertrophy involves inhibiting pRB phosphorylation by blocking activation of cyclin E kinase. *American Journal of Physiology - Renal Physiology*, *277*(2), F186–F194. http://doi.org/10.1016/0003-2697(76)90033-6

Longtine, M. S., Theesfeld, C. L., McMillan, J. N., Weaver, E., Pringle, J. R., & Lew, D. J. (2000). Septin-dependent assembly of a cell cycle-regulatory module in Saccharomyces cerevisiae. *Molecular and Cellular Biology*, *20*(11), 4049–4061.

Majno, G., & Joris, I. (2004). Cells, Tissues, and Disease. Oxford University Press.

McCusker, D., Denison, C., Anderson, S., Egelhofer, T. A., Yates, J. R. I., Gygi, S. P., & Kellogg, D. R. (2007). Cdk1 coordinates cell-surface growth with the cell cycle. *Nature Cell Biology*, *9*(5), 506–U45. http://doi.org/10.1038/ncb1568

McMillan, J. N., Longtine, M. S., Sia, R. A., Theesfeld, C. L., Bardes, E. S., Pringle, J. R., & Lew, D. J. (1999). The morphogenesis checkpoint in Saccharomyces cerevisiae: cell cycle control of Swe1p degradation by Hsl1p and Hsl7p. *Molecular and Cellular Biology*, *19*(10), 6929–6939.

McMillan, J. N., Theesfeld, C. L., Harrison, J. C., Bardes, E. S. G., & Lew, D. J. (2002). Determinants of Swe1p Degradation in Saccharomyces cerevisiae. *Molecular Biology of the Cell*, *13*(10), 3560–3575. http://doi.org/10.1091/mbc.E02

Menzl, I., Lebeau, L., Pandey, R., Hassounah, N. B., Li, F. W., Nagle, R., et al. (2014). Loss of primary cilia occurs early in breast cancer development. *Cilia*, *3*(1), 7. http://doi.org/10.1186/2046-2530-3-7

Mezza, T., Muscogiuri, G., Sorice, G. P., Clemente, G., Hu, J., Pontecorvi, A., et al. (2014). Insulin Resistance Alters Islet Morphology in Nondiabetic Humans. *Diabetes*, *63*(3), 994–1007. http://doi.org/10.2337/db13-1013

Montanya, E., Nacher, V., Biarnés, M., & Soler, J. (2000). Linear correlation between beta-cell mass and body weight throughout the lifespan in Lewis rats: role of

beta-cell hyperplasia and hypertrophy. *Diabetes*, *49*(8), 1341–1346. http://doi.org/10.2337/diabetes.49.8.1341

Mortimer, R. K. (1958). Radiobiological and genetic studies on a polyploid series (haploid to hexaploid) of Saccharomyces cerevisiae. *Radiation Research*, *9*(3), 312. http://doi.org/10.2307/3570795

Nash, R., Tokiwa, G., Anand, S., Erickson, K., & Futcher, A. B. (1988). The WHI1+ gene of Saccharomyces cerevisiae tethers cell division to cell size and is a cyclin homolog. *The EMBO Journal*, *7*(13), 4335–4346.

Nestel, P. J., Austin, W., & Foxman, C. (1969). Lipoprotein lipase content and triglyceride fatty acid uptake in adipose tissue of rats of differing body weights. *Journal of Lipid Research*, *10*(4), 383–387.

Nurse, P. (1975). Genetic control of cell size at cell division in yeast. *Nature*, *256*(5518), 547–551. http://doi.org/10.1038/256547a0

Okuzaki, D., Watanabe, T., Tanaka, S., & Nojima, H. (2003). The Saccharomyces cerevisiae bud-neck proteins Kcc4 and Gin4 have distinct but partially-overlapping cellular functions. *Genes & Genetic Systems*, *78*(2), 113–126. http://doi.org/10.1266/ggs.78.113

Pende, M., Kozma, S. C., Jaquet, M., Oorschot, V., Burcelin, R., Le Marchand-Brustel, Y., et al. (2000). Hypoinsulinaemia, glucose intolerance and diminished |[beta]|-cell size in S6K1-deficient mice. *Nature*, *408*(6815), 994–997. http://doi.org/10.1038/35050135

Pissadaki, E. K., & Bolam, J. P. (2013). The energy cost of action potential propagation in dopamine neurons: clues to susceptibility in Parkinson's disease. *Frontiers in Computational Neuroscience*, *7*. http://doi.org/10.3389/fncom.2013.00013

Prescott, D. M. (1956). Relation between cell growth and cell division. II. The effect of cell size on cell growth rate and generation time in Amoeba proteus. *Experimental Cell Research*, *11*(1), 94–98. http://doi.org/doi:10.1016/0014-4827(56)90193-8

Raspelli, E., Cassani, C., Chiroli, E., & Fraschini, R. (2014). Budding Yeast Swe1 is Involved in the Control of Mitotic Spindle Elongation and is Regulated by Cdc14 Phosphatase during Mitosis. *Journal of Biological Chemistry*, *290*(1), jbc.M114.590984–12. http://doi.org/10.1074/jbc.M114.590984

Richardson, H. E., Wittenberg, C., Cross, F., & Reed, S. I. (1989). An essential G1 function for cyclin-like proteins in yeast. *Cell*, *59*(6), 1127–1133. http://doi.org/10.1016/0092-8674(89)90768-X

Rieck, S., & Kaestner, K. H. (2010). Expansion of beta-cell mass in response to pregnancy. *Trends in Endocrinology and Metabolism: TEM*, *21*(3), 151–158. http://doi.org/10.1016/j.tem.2009.11.001

Rieck, S., White, P., Schug, J., Fox, A. J., Smirnova, O., Gao, N., et al. (2009). The Transcriptional Response of the Islet to Pregnancy in Mice. *Molecular Endocrinology*, *23*(10), 1702–1712. http://doi.org/10.1210/me.2009-0144

Roth, G., Blanke, J., & Wake, D. B. (1994). Cell size predicts morphological complexity in the brains of frogs and salamanders. *Proceedings of the National Academy of Sciences of the United States of America*, *91*(11), 4796–4800.

Rubin, E., & Reisner, H. M. (2009). Essentials of Rubin's pathology.

Ruvinsky, I., Sharon, N., Lerer, T., Cohen, H., Stolovich-Rain, M., Nir, T., et al. (2005). Ribosomal protein S6 phosphorylation is a determinant of cell size and glucose homeostasis. *Genes & Development*, *19*(18), 2199–2211. http://doi.org/10.1101/gad.351605

Sakaguchi, M., Isono, M., Isshiki, K., Sugimoto, T., Koya, D., & Kashiwagi, A. (2006). Inhibition of mTOR signaling with rapamycin attenuates renal hypertrophy in the early diabetic mice. *Biochemical and Biophysical Research Communications*, *340*(1), 296–301. http://doi.org/10.1016/j.bbrc.2005.12.012

Salans, L. B., Knittle, J. L., & Hirsch, J. (1968). The role of adipose cell size and adipose tissue insulin sensitivity in the carbohydrate intolerance of human obesity. *Journal of Clinical Investigation*, *47*(1), 153–165. http://doi.org/10.1172/JCI105705

Shulewitz, M. J., Inouye, C. J., & Thorner, J. (1999). Hsl7 Localizes to a Septin Ring and Serves as an Adapter in a Regulatory Pathway That Relieves Tyrosine Phosphorylation of Cdc28 Protein Kinase in Saccharomyces cerevisiae. *Molecular and Cellular Biology*, *19*(10), 7123–7137.

Silber, S. J. (1976). Growth of Baby Kidneys Transplanted Into Adults. *Archives of Surgery*, *111*(1), 75–77. http://doi.org/10.1001/archsurg.1976.01360190077014

Tinker-Kulberg, R. L., & Morgan, D. O. (1999). Pds1 and Esp1 control both anaphase and mitotic exit in normal cells and after DNA damage. *Genes & Development*, *13*(15), 1936–1949.

Toledo, C. M., Ding, Y., Hoellerbauer, P., Davis, R. J., Basom, R., Girard, E. J., et al. (2015). Genome-wide CRISPR-Cas9 Screens Reveal Loss of Redundancy between PKMYT1 and WEE1 in Glioblastoma Stem-like Cells. *CellReports*, *13*(11), 1–16. http://doi.org/10.1016/j.celrep.2015.11.021

Trpkov, K. (2015). Contemporary Gleason Grading System. In *Genitourinary Pathology* (pp. 13–32). New York, NY: Springer New York. http://doi.org/10.1007/978-1-4939-2044-0_2

Tyers, M., Tokiwa, G., Nash, R., & Futcher, B. (1992). The Cln3-Cdc28 kinase complex of S. cerevisiae is regulated by proteolysis and phosphorylation. *The EMBO Journal*, *11*(5), 1773–1784.

Wang, H., Liu, D., Wang, Y., Qin, J., & Elledge, S. J. (2001). Pds1 phosphorylation in response to DNA damage is essential for its DNA damage checkpoint function. *Genes & Development*, *15*(11), 1361–1372. http://doi.org/10.1101/gad.893201

Weisz, P. B. (1954). Morphogenesis in protozoa. *The Quarterly Review of Biology*.

Winey, M., & O'Toole, E. (2001). The spindle cycle in budding yeast. *Nature Cell Biology*, *3*(1), E23–E27. http://doi.org/10.1038/35050663

Wood, E., & Nurse, P. (2013). Pom1 and cell size homeostasis in fission yeast. *Cell Cycle (Georgetown, Tex.)*, *12*(1538-4101), 3228–3236. http://doi.org/10.4161/cc.26462

Yamamoto, A., Guacci, V., & Koshland, D. (1996). Pds1p is required for faithful execution of anaphase in the yeast, Saccharomyces cerevisiae. *Journal of Cell Biology*, *133*(1), 85–97. http://doi.org/10.1083/jcb.133.1.85

Young, P. G., & Fantes, P. A. (1987). Schizosaccharomyces pombe mutants affected in their division response to starvation. *Journal of Cell Science*, *88 (Pt 3)*, 295–304.

Zapata, J. (2014, March 5). *Regulation of PP2A-Rts1 and its Role in Cell Size and Entry into the Cell Cycle*.

Zapata, J., Dephoure, N. E., MacDonough, T., Yu, Y., Parnell, E. J., Mooring, M., et al. (2014). PP2ARts1 is a master regulator of pathways that control cell size. *Journal of Cell Biology*, *204*(3), 359–376. http://doi.org/10.1083/jcb.201309119